ANALYTICAL EXAMINATION OF PERFORMANCE LIMITS FOR SHEAR CRITICAL REINFORCED CONCRETE COLUMNS

A THESIS SUBMITTED TO
THE GRADUATE SCHOOL OF NATURAL AND APPLIED SCIENCES
OF
MIDDLE EAST TECHNICAL UNIVERSITY

BY

KAMİL ERGÜNER

IN PARTIAL FULFILLMENT OF THE REQUIREMENTS
FOR
THE DEGREE OF MASTER OF SCIENCE
IN
CIVIL ENGINEERING

OCTOBER 2009

Approval of the thesis:

ANALYTICAL EXAMINATION OF PERFORMANCE LIMITS FOR SHEAR CIRITICAL REINFORCED CONCRETE COLUMNS

submitted by **KAMİL ERGÜNER** in partial fulfillment of the requirements for the degree of **Master of Science in Civil Engineering Department, Middle East Technical University** by,

Prof. Dr. Canan Özgen
Dean, Graduate School of **Natural and Applied Sciences** _______________

Prof. Dr. Güney Özcebe
Head of Department, **Civil Engineering** _______________

Assoc. Prof. Dr. Barış Binici
Supervisor, **Civil Engineering Dept., METU** _______________

Examining Committee Members:

Prof. Dr. Haluk Sucuoğlu
Civil Engineering Dept., METU _______________

Assoc. Prof. Dr. Barış Binici
Civil Engineering Dept., METU _______________

Assoc. Prof. Dr. Ahmet Yakut
Civil Engineering Dept., METU _______________

Asst. Prof. Dr. Afşin Sarıtaş
Civil Engineering Dept., METU _______________

Yüksel İlkay Tonguç M. Sc.
General Manager, Promer Consultancy and Engineering Co. Ltd. _______________

Date: 19.10.2009

I hereby declare that all information in this document has been obtained and presented in accordance with academic rules and ethical conduct. I also declare that, as required by these rules and conduct, I have fully cited and referenced all material and results that are not original to this work.

Name, Last name : Kamil Ergüner

Signature :

ABSTRACT

ANALYTICAL EXAMINATION OF PERFORMANCE LIMITS FOR SHEAR CIRITICAL REINFORCED CONCRETE COLUMNS

Ergüner, Kamil
M.S., Department of Civil Engineering
Supervisor: Assoc. Prof. Dr. Barış Binici

October 2009, 127 pages

Most of the older reinforced concrete (RC) buildings have columns that are deficient when the current code requirements are considered. Therefore, performance of the columns determines the performance of the structure under the effects of earthquake induced lateral loads. It is recognized that no provision is proposed in TEC2007 to estimate the failure type called flexure-shear. Behavior of columns having probability of failing in flexure-shear failure mode is mostly underestimated by TEC2007 procedures. In addition, failure type classification of columns performed according to the linear and nonlinear procedures of TEC2007 needs to be examined with respect to the test results to cover all failure types including flexure-shear failure in order to lead the engineers develop economical and realistic retrofit solutions.

In this study, different methods are explored to obtain reliable estimates for the performance of code deficient shear critical RC columns. Special considerations are given to Axial-Shear-Flexure interaction (ASFI) approach due to its mechanical background.

After examination of different approaches, ASFI method with proposed modifications was selected as the most reliable model and lateral load-displacement analyses were performed on a database of shear critical columns. Findings were compared with the estimations of the nonlinear procedure given in Turkish Earthquake Code (TEC2007) for database columns. In addition, drift capacity equations and simplified safe drift capacity equations are proposed in light of statistical studies on the selected column specimens.

In the last part of the study, performance evaluation of columns according to nonlinear procedures of FEMA 356, TEC2007, ASCE/SEI 41 update supplement, and EUROCODE 8 were conducted.

Keywords: Axial-Shear-Flexure Interaction Analysis, Performance Evaluation, Acceptance Criteria, Lateral Load-Displacement, Drift Capacity

ÖZ

KESME YÖNÜNDEN KRİTİK BETONARME KOLONLARIN PERFORMANS LİMİTLERİNİN ANALİTİK OLARAK İRDELENMESİ

Ergüner, Kamil

Yüksek Lisans, İnşaat Mühendisliği Bölümü

Tez Yöneticisi: Doç. Dr. Barış Binici

Ekim 2009, 127 sayfa

Güncel yönetmelik gereksinimleri düşünüldüğünde, eski betonarme binaların çoğu yetersiz kolonlara sahiptir. Bu nedenledir ki, yapının deprem kaynaklı yatay yük etkileri altındaki performansını kolonların performansı belirler. Eğilme–kesme göçmesi olarak bilinen göçme türünü tahmin etmek için TDY2007' de herhangi bir koşul önerilmediği fark edilmiştir. Analiz sonuçlarına göre, eğilme-kesme göçmesi ihtimaline sahip olan kolonların davranışı TDY2007' ye göre genelde olduğundan az tahmin edilmektedir. Ayrıca, kolonların TDY 2007' nin doğrusal ve doğrusal olmayan yöntemlerine göre belirlenen göçme türü sınıflandırmasının test sonuçlarına göre ve mühendislerin ekonomik ve gerçekçi güçlendirme çözümleri geliştirmelerini sağlamak için bütün göçme türlerini, eğilme –kesme göçmesini de dahil, kapsayacak şekilde incelenmesi gerekmektedir.

Bu çalışmada, yönetmeliğe göre kesme yönünden yetersiz olan betonarme kolonların davranışları için güvenilir tahminler elde etmek amacıyla farklı yöntemler incelenmiştir. Mekanik temeli oluşu sebebiyle eksenel yük-kesme-eğilme etkileşimi (EKEE) yaklaşımı üzerinde özellikle durulmuştur.

Farklı yaklaşımların incelenmesinden sonra, önerilen geliştirmeler ile EKEE yöntemi en güvenilir yöntem olarak seçilmiş ve kesme yönünden kritik kolonlardan oluşan veri tabanı üzerinde yatay yük-yatay deplasman analizleri gerçekleştirilmiştir. Bulgular, veri tabanındaki kolonlar için, Türkiye Deprem Yönetmeliği'nin (TDY2007) linear olmayan yöntemi ile yapılan tahminlerle karşılaştırılmıştır. Ayrıca, seçilmiş kolon örnekleri üzerinde yapılan istatistiksel çalışmaların ışığında, yatay deplasman denklemleri ve basitleştirilmiş güvenli kat öteleme oranı limit denklemleri önerilmiştir.

Çalışmanın son bölümünde, FEMA356, TDY2007, ASCE/SEI 41 güncelleme eki ve EUROCODE 8 doğrusal olmayan yöntemlerine göre kolonların performans değerlendirmeleri yapılmıştır.

Anahtar Kelimeler: Eksenel-Kesme-Eğilme Etkileşimi, Performans Değerlendirmesi, Kabul Kriterleri, Yatay Yük-Yer Değiştirme, Yer Değiştirme Kapasitesi

To My Beloved Family

ACKNOWLEDGEMENTS

I would like to acknowledge gratefully the enthusiastic supervision of Assoc. Prof. Dr. Barış BİNİCİ. Without his inspiration and his guidance, this study would not be completed. Throughout my thesis–writing period, he provided encouragement, sound advice, good teaching, good company and many good ideas. I would like to express my sincere thanks to him.

My deepest gratitude goes to Dr. Hossein MOSTAFAEI for his kindly explanations on analytical modeling of my analysis tool.

I am indebted to my colleague Doğu BOZALİOĞLU for providing me help and insight in development of macro models for my analysis.

I am grateful to Murat BALLIOĞLU, head of the company I have worked recently, for his patience and means he provided to me to write and complete my thesis by relieving the stress of working as a design engineer.

I wish to thank my friends Bora EYCE and Arda ERDEM for helping me get through the difficult times, emotional support, camaraderie, entertainment and caring they provided.

I would like to thank my beloved one Merih AÇIKEL for his assistance throughout my study believing that I would make it to the other side. She had the incredible amount of patience with me in the last six years. It is time to start on that list of things to do “Yes, after your thesis, honey”.

I would like to thank sincerely my beloved parents and my sisters. Their constant love and encouragement was that I have relied on throughout my time at the university. Their unflinching courage and conviction will always inspire me. Their support and patience are gratefully acknowledged.

TABLE OF CONTENTS

LIST OF TABLES

TABLES

LIST OF FIGURES

FIGURES

LIST OF ABBREVIATIONS AND SYMBOLS

a: Shear span

b:Width of the column section

cc: Clear cover to transverse reinforcement

d: Flexural depth of the section

d_c: Depth of the section between the transverse reinforcement centers

f_c': Concrete compressive stregth

f_{yl}: Yield strength of the longitudinal reinforcement steel

f_{yt}: Yield strength of the transverse reinforcement steel

h: Depth of the section

n: Axial load ratio

v: Maximum shear stress

δ_a: Drift at axial failure

δ_y: Drift at first yielding of longitudinal reinforcement steel

δ_n: Drift at collapse of brittle members

ε_{cg}: Compressive strain in concrete at the transverse reinforcement boundary

ε_{cu}: Compressive strain at the outer most concrete fiber

ε_s: Strain in the longitudinal reinforcement steel

ϕ : Curvature of the end section

ϕ_y : Yield curvature of the end section

μ: Mean value

θ: Angle of the inclination of the shear crack (radians)

ρ_l: Longitudinal reinforcement ratio

ρ_s: Volumetric ratio of transverse reinforcement (TEC2007)

ρ_{sm}: Volumetric ratio of transverse reinforcement required by the code provisions(TEC2007)

ρ_v: Transverse reinforcement ratio

σ: Standart deviation

A_g: Gross cross sectional area of column (bh)

A_{sw}: Area of the transverse reinforcement

CP: Collapse prevention performance level

DR_a: Drift ratio at axial failure

DR_s: Drift ratio at shear failure

DR_{Vmax}: Drift ratio at peak lateral load

DR_y: Drift ratio at first yielding of longitudinal reinforcement

IO: Immediate occupancy performance level

L: Length of the column measured from the end section to zero moment section

L_{in}: Length of the column measured from the end section to zero moment section

L_p: Plastic hinge length

LS: Life safety performance level

M_n: Moment capacity of the column section

M_p: Moment capacity at the first yielding of longitudinal reinforcement steel

P: Applied axial load

V_{flex}: Shear force to cause formation of flexural hinging at column end (M_n/L_{in})

V_n: Shear strength of the column section

V_{test}: Peak lateral load recorded at the cyclic test

V_s: Shear strength provided by the transverse reinforcement

CHAPTER 1

INTRODUCTION

1.1. General

In Turkey, building stock is mostly composed of reinforced concrete (RC) structures, which are vulnerable to seismic damage. After the Izmit and Duzce earthquakes in 1999, a number of RC structures experienced severe damage and some of them collapsed leading to significant human and value loss. Subsequently, risk assessment of urban areas became a major concern of the community. Rapid assessment studies revealed that there are many residential and public buildings susceptible to damage and they should be assessed in detail. Current code requirements and design principles such as capacity design concept, strong column-weak beam principle, detailing requirements (for example confinement of critical end zones of members) etc. were not met in those structures. The assessment studies also show that performance estimation of columns is of vital importance for accurate estimation of damage potential and finding the most feasible retrofit solution.

Load path of an RC frame structure follows the transfer of the vertical loads (dead loads and live loads) from beams to columns and from columns to the foundation system. In case of gravity loadings, beams are mainly stressed due to bending moments and shear forces. Shear forces from beams are delivered to columns as axial loads. Gravity load system is designed such that available strength is not exceeded under the effects of the vertical loads. Columns are the most important vertical load carrying members as their inefficacy may lead to total collapse of the whole structure. Failure of a frame structure is closely related to the loss of axial load carrying capacity of one or more columns. In case of seismic loading, columns become main lateral and gravity load carrying members. In order to meet displacement demands imposed by a seismic excitation, columns should have adequate strength and must have sufficient ductility. Ductility of a column is related to its deformation capacity without loss of lateral and axial load carrying capacities. For columns that do not comply with the requirements of modern seismic codes, accurate estimation of available ductility capacity is a difficult task. However, providing the best estimate on column performance can result in the most economical retrofit solution. In order to strengthen a structure for seismic resistance, deformation capacity, ductility, and lateral and axial load capacities of columns should be evaluated by employing reliable analytical tools.

In 2007, a new chapter titled “Seismic Assessment of Existing Structures” was added in the Turkish Earthquake Code (2007) [1] to guide the engineers for assessment and retrofit design. This document contains deformation limits for code compliant and non-compliant RC columns. In this study, it is aimed to focus on deformability of deficient RC columns in light of available experimental results, analytical models, and code specified deformation limits.

1.2. Types of Column Failures

Ductile failure is aimed for earthquake resistant design and is the main requirement of performance-based earthquake engineering. To classify a member as a ductile member, its flexure and shear strength should be estimated and failure type should be identified. There are mainly three types of observed failure modes in RC columns. Those are: i) shear failure, ii) flexural failure and iii) flexure-shear failure.

Shear failure is a brittle type of undesirable and sudden failure mode. If shear strength of a column is not sufficient so that its flexural strength can develop, this column experiences a shear failure with almost no deformability. A dominating inclined crack opens and widens in the column up until sudden loss of lateral and axial capacities occur simultaneously. Experimental test results revealed that columns having shear span to depth ratio, *a/d* smaller than two or those with insufficient transverse reinforcement ratio irrespective of *a/d* ratio are susceptible to shear failure. Two columns that experienced shear failure are presented in Figure 1.1. An example of lateral load-displacement test result of a column failing in shear is shown in Figure 1.2. As it is seen in Figure 1.2 after peak strength was attained, sudden decrease in shear strength was observed with little deformation capacity.

Figure 1.1 RC Columns Failed in Shear Failure Mode (Left: World Housing Encyclopedia-Right: research.eerc.berkeley.edu)

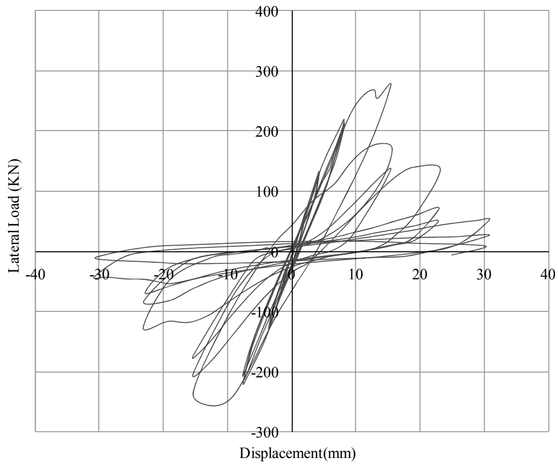

Figure 1.2 Cyclic Test Results of a Column Failed in Shear (Specimen 3CLH18 tested by Lynn, Peer Column Database)

Flexural failure mode is generally a ductile type of failure. When column has adequate shear strength, section can reach its flexural strength before it would fail under high shear demands. Column experiences inelastic deformations at its highest moment regions without significant loss of load carrying capacity under the condition that detailing of this region is appropriate. Flexural cracks are observed at regions where cracking moment is exceeded. Cracks are nearly perpendicular to member axis. Figure 1.3 shows a column, which experienced flexure failure. Load deformation plot of an RC column experiencing flexural failure is presented in Figure 1.4. As it is seen column attained its flexural strength and preserved lateral load capacity during the following load cycles. Column displayed high deformability. When test database is examined, it is seen that columns having *a/d* ratio greater than 3.5 and sufficient lateral reinforcement experienced flexure failure.

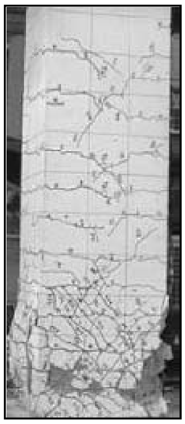

Figure 1.3 Flexure Failure of an RC Column (Specimen C20 Tested by Hattori et. al, 1998)

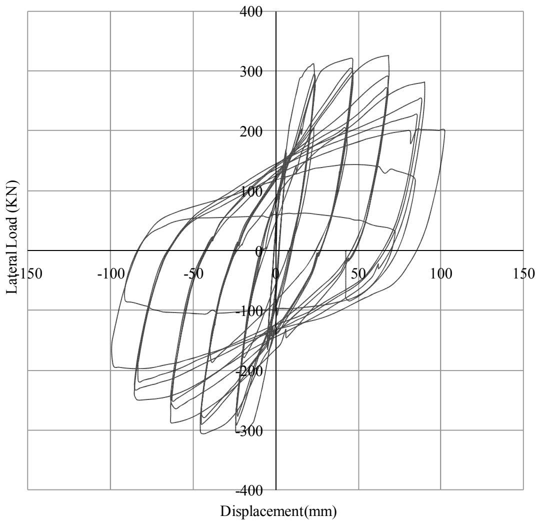

Figure 1.4 Cyclic Test Results of a Column Failed in Flexure Failure Mode (Specimen U4 Tested by Saatcioglu and Ozcebe, 1989, Peer Column Database)

Third type of the failure mode is the so-called flexure-shear failure. As it is stated by Kong [2], It is observed in the following three situations;

i.) The amount of lateral reinforcement is not sufficient to carry horizontal component of principal tensile stresses in concrete.

ii.) The vertical component of the diagonal tension force that causes web crack is greater than the compression capacity of the diagonal compression strut between the diagonal cracks.

iii.) The vertical component of the diagonal tension force that causes web crack is greater than the strength of the longitudinal reinforcement.

In this type of failure, flexural cracks occur followed by the destruction of the bond between tensile reinforcement and the surrounding concrete near the support. Additional inclined cracks are formed at about one-half of the shear span in case of single curvature columns or about one quarter of shear span in case of double curvature columns. One of these cracks widens and propagates into the compression zone of column causing failure. At the same time, flexural yielding takes place in the plastic hinge regions. This type of failure is not as brittle as shear failure. Test results show that, flexure-shear failure mostly occurs in columns having a shear span to depth ratio (*a/d*) between 2 and 3.5, volumetric transverse reinforcement ratio ranging from zero to 0.018, and an axial load level near or below the balanced load. In Figure 1.5 a column that experienced flexure-shear type of failure is presented. Flexural cracks in support regions and a dominating diagonal crack can be observed in the figure. Load deformation plot of a test column is presented in Figure 1.6. It may be observed in the load deformation plot such that, after the flexural strength was attained, lateral load capacity started to decrease with increased deformation level. Ductility observed in flexure-shear failure mode is generally in between that of flexure and shear failure.

Figure 1.5 Column Experienced Flexure-Shear Failure (Specimen C10 Tested by Hattori et al. 1998)

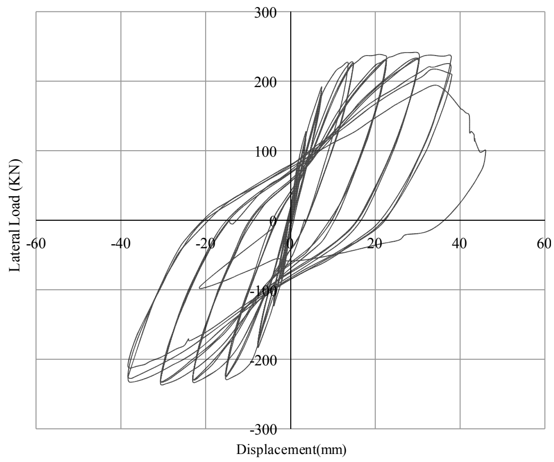

Figure 1.6 Cyclic Test Results of a Column Failed in Flexure-Shear Failure Mode (Peer Column Database, Lynn et al. 1998, specimen 2CLH18)

For the performance based design and assessment methodology, it is important to estimate the behavior and damage state of the columns for various deformation levels. For this purpose, accurate estimation of complete load deformation characteristics should be made. Afterwards, ductility, strength and stiffness properties of a column can be commented on. Complete load deformation data gives important information about the performance of columns such as drift at first yielding, ultimate strength, drift at ultimate strength, drift at shear failure (loss of lateral load capacity), and drift at loss of axial load capacity. Those properties are important for response estimation and classification of the failure modes. If individual load deformation properties are known for columns, response estimation and performance of the frame under a specified earthquake demand can be determined by combining individual responses. (E.g., Japanese Seismic Assessment Guidelines [3]). After demand is estimated, according to the performance levels of members an optimum retrofitting solution can be found. It should be kept in mind that, an economical and effective retrofit solution is possible only if behavior is estimated as close as possible to actual response as opposed to being on the overconservative side.

1.3. Literature Survey

Different modeling approaches to predict the load deformation characteristics were developed in literature. However, most of them gave little information on the failure type beforehand, and interaction of the deformations was mostly ignored. In some methods, no interaction was considered whereas in others, only shear-flexure interaction was considered. Recently, models considering axial-shear-flexure interaction have been proposed. In the literature examined, analytical models and approaches for estimating behavior of RC columns are investigated and findings are presented. Firstly, experimental studies performed to investigate the behavior of columns are briefly explained. Then, analytical models developed by different researchers were discussed. Finally, models considering the interaction of shear-flexure and axial-shear-flexure behavior are covered.

1.3.1. Studies on Lateral Load Deformation Estimation of Columns

There is a vast amount of experimental and analytical research on predicting response of columns failing in shear, flexure or flexure-shear modes. Several researchers conducted tests on determination of column performance under combined axial and lateral loads. Recently a column database for column test results was compiled [4]. This database consists of 107 rectangular and 92 circular columns failing in flexure, shear, and flexure-shear modes. Axial load ratio ranges from -0.1 to 0.9 (negative for tension and positive for compression), longitudinal reinforcement ratio ranges from 0.0046 to 0.063, and transverse reinforcement volumetric ratio ranges from 0 to 0.067 for the test columns included in database. Some of the important experimental studies about load-deformation behavior of RC columns are briefly explained below.

Wight and Sozen [5] studied the shear strength decay of reinforced concrete columns under constant axial load and lateral displacement cycles. Twelve full-scale column specimens were designed and tested. Variables were the axial load ranging from 0.071 to 0.147 and, transverse reinforcement ratio ranging from 0.003 to 0.015. Experimental data were used to examine mechanism of strength decay that is related to the crushing and spalling of the cover concrete, yielding of the transverse reinforcement and crushing of concrete along cracks. Experimental results showed that the transverse reinforcement must be proportioned to carry shear force such that column can develop ultimate moment capacity. Load deformation responses of three specimens whose failure modes are reported as flexure-shear failure tested by Wight and Sozen [5] were selected and used as a basis of comparison in this study.

Saatcioglu and Ozcebe [6] studied response of the full-scale columns under the simulated seismic loading. Full-scale columns were tested under slowly applied lateral load reversals. Both unidirectional and bidirectional loadings were included in the test program. The columns were tested with or without axial loads, including variable axial tension and compression. Test parameters were axial load ratio ranging from zero to 0.162, transverse reinforcement ratio ranging from 0.0085 to 0.0254 (A_{sv}/bs; A_{sv}: area of lateral reinforcement, b: width of the section perpendicular to applied lateral load, s: spacing of the transverse reinforcement). Directions of the lateral load application were unidirectional being parallel to one of the column axis, bidirectional along the column section diagonal and loading in two orthogonal directions. Important conclusions, drawn from the experimental studies by Saatcioglu et. al. [6], are as follows:

- Constant axial compression under cyclic loading reduced the ductility and accelerated the strength and stiffness degradation. Variable axial load yielded different behavior such that under axial tension, flexural yield strength was decreased, but strength degradation was retarded. Axial compression led to increase in flexural strength followed by rapid strength degradation.
- Application of proper confinement configuration increased the ductility of the columns loaded under combined axial compression and bending moment reversals. Columns having each longitudinal bar supported by crossties exhibited better response than those columns where longitudinal bars were not fully supported. It was also observed that, to obtain similar level of ductility, selecting a proper confinement configuration was more appropriate than reducing spacing of transverse reinforcement.
- Columns having cross ties with a 90 degree hook extending 10 bar diameters at one end responded as good as those with 135 degree hooks at both ends.
- Biaxial loading caused reduction in column capacity in both directions. If biaxial bending was generated by a lateral load following a straight-line path, overall hysteretic behavior in terms of stiffness and strength degradation was not significantly affected by biaxial bending.
- Columns subjected to simultaneously varying bidirectional loads responded differently than the ones subjected to unidirectional load reversals. Damage level in one direction adversely affected the damage level in the other direction. If the deformation in one direction was lower than the yield deformation, bidirectional effects in response in other direction were small. However, if post yield deformations were experienced in both orthogonal directions, than strength and stiffness degradation were more severe.

Lynn et al. [7] studied the seismic performance of existing RC building columns. The purpose of the research was to provide information on the behavior of the columns that were poorly detailed. In the scope of the experimental study, a total eight full-scale columns were constructed and tested. All the specimens were rectangular with a shear span to depth ratio of 3.9. They were tested in double curvature and under constant axial load. Axial load level was low (between 0.07 and 0.09) and intermediate (between 0.26 and 0.28). The columns had widely spaced transverse reinforcements with 90° bends with or without intermediate hoops and diagonal ties, and longitudinal reinforcement with or without short lap splices. Transverse reinforcement ratio ρ_v (ratio of lateral reinforcement area to spacing times the width of the section) was chosen as 0.001 and 0.0017. Longitudinal reinforcement ratio (ratio of the longitudinal reinforcement area to cross sectional area) was 0.02 and 0.03. For three of the specimens longitudinal reinforcement was spliced at the foundation level. Columns were subjected to lateral deformation cycles until the loss of axial and lateral strength occurred. Localized crushing of concrete in the plastic hinge region, reinforcement buckling, lap-splice and flexural bond splitting, shear and axial load collapse were the observed failure events. It was also observed that columns that had light transverse reinforcement developed the yield strength of longitudinal reinforcement at the splice. However, lap splice deterioration at increased displacement amplitudes caused decrease in moment capacity at the spliced end region of columns. Columns having heavy transverse reinforcement maintained the moment capacity through the increased displacement amplitudes. In all cases, splitting cracks near the splices spread into the column and eventually led to shear failure. It was seen that loss of gravity collapse occurred at or after significant loss of lateral load resistance. Axial failure occurred soon after the loss of lateral force resistance for shear critical members. In case, where lap-splice deterioration governed the response and axial load level was low, axial load resistance was maintained until eventual shear failure occurred. For Members whose response was governed by flexure, axial load capacity was maintained even at large deformation demands. Seven column specimens from that study were taken as reference of comparison in this study since they are representative for the older reinforced concrete columns that are vulnerable due to poor detailing.

Sezen [8] conducted a study on seismic behavior of the RC building columns. Shear and gravity failure of columns with insufficient and poorly detailed transverse reinforcement were investigated. Four full-scale column specimens were designed and tested under gravity and simulated seismic loadings as part of the experimental investigation. Three of them were tested under constant axial load and one under variable axial load. The behavior of columns subjected to various levels of axial loads and reversed cyclic and monotonic loads were studied. Regarding the results of experimental studies, it was concluded that response of older columns with nominally identical properties were dependent on the magnitude and history of the lateral and axial loads. Test results showed that specimens with low axial load lost their lateral strength significantly at low displacement ductility but sustained axial load at large displacements. Under the same flexural demand and very high axial load, lateral stiffness and strength increased at low displacements, on the other hand, the specimen had a sudden shear and axial failure. Another finding was that under monotonic lateral load, and under very low compressive or tensile axial loads, the lateral strength degradation was less serious. Using test results and past test data, models were proposed to determine the load deformation relations and shear strength of the columns. Three column specimens tested under constant axial load are used to investigate the model estimations in this study.

Elwood [9] studied gravity load collapse of reinforced concrete frames. He conducted shake table tests and analytical studies limited to two-dimensional frames with columns experiencing low deformation capacity and shear failure mode. Shake table test were performed to study the redistribution of forces after axial failure of a column which is not included in the content of that study. Short columns characterized by a shear failure prior to yielding of longitudinal reinforcement were not directly considered in the study.

1.3.2. Load Deformation Macro Models without Interaction of Deformations

Sezen [8] mainly focused on basic factors contributing to shear failure and gravity load collapse of lightly reinforced concrete columns. In the analytical part of the study, a shear strength model was developed for design and analyses purposes. Such different variables that can affect shear strength as effect of cross section, column aspect ratio and axial load level, longitudinal reinforcement for concrete contribution, lateral reinforcement, and displacement ductility were included in the development of the new model. Statistical analyses were performed on database including fifty shear critical columns and new shear strength model was proposed including all aforementioned variables. Results were compared with existing shear strength models. In the content of the analytical part of the study, the behavior of columns with significant stiffness and strength degradation due to shear failure after the flexural strength achieved was examined. In order to determine the load deformation response of columns, lateral load and displacement at four performance points were determined. Those are cracking, yielding, peak and loss of axial load capacity points. Based on the test results, it was shown that lateral drift stemmed from deformations due to flexure, shear, and anchorage slip of the longitudinal bars at the column ends. Analytical models were developed to model flexure, shear, and longitudinal bar slip behavior. An equation calculate shear displacement at yielding and a bar slip formulation were proposed. Contributions of individual deformation models were combined into a three spring in series model with the following response rules;

- Response before the peak point is reached: Total lateral displacement is obtained from combination of flexure, bar slip and shear displacements from three springs having similar spring forces.
- The peak strength of the column is the smaller of calculated shear strength and the lateral load corresponding to the maximum flexural capacity.
- For the post peak points, controlling behavior is estimated from the comparison of shear strength and the lateral load corresponding to the maximum flexural capacity. If post peak behavior is controlled by shear, displacement at axial failure is determined from summation of slip and flexure displacements. If behavior is controlled by flexure, total displacement at axial failure is the summation of calculated flexural and slip displacements at axial failure, and shear displacement at the peak point.

It was shown that measured cyclic response of test columns compared well with the one calculated from the proposed spring model. Interactions of deformations were not considered in that model.

Elwood [9] conducted studies on existing shear strength models. An analytical model having ability of incorporating both the shear and axial failure was developed for building frame analysis. A database composed of shear critical columns was selected. Rectangular reinforced concrete columns having axial load level ranging from 0 to 0.61, transverse reinforcement ratio ranging from 0.001 to 0.0065, and longitudinal reinforcement ratio ranging from 0.01 to 0.04 were included in the database. Two empirical models were proposed to predict drift at shear failure and drift at axial failure for columns having properties consistent with the database included in studies. Based on those models, drift at shear failure is proportional to the amount of the transverse reinforcement and inversely proportional to applied shear stress and axial load. Considering shear friction concepts and results from twelve columns tested to axial failure, a model was also developed to estimate the drift at axial failure for a shear-damaged column. According to the results of studies, it was observed that the drift at axial failure is directly proportional to the amount of transverse reinforcement and inversely proportional to the axial load ratio. Load deformation was estimated by using idealized flexure behavior and plotting drift at shear failure and drift at axial failure points as cut off point on idealized flexure response. Figure 1.7 summarizes the procedure suggested by Elwood [9]. Accuracy of the model was analyzed statistically and good agreement was observed between predicted and measured values. Details of the model are explained in Section 2.1.4.

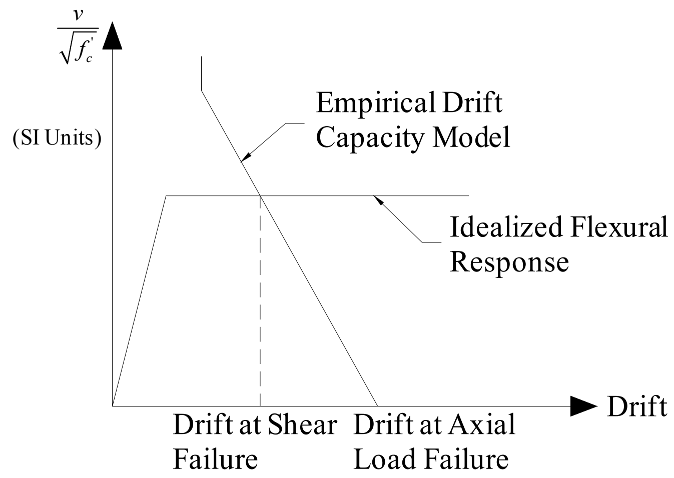

Figure 1.7 Drift Capacity Model Approach (Elwood [9])

Pincheira et. al. [10] proposed a monotonic loading backbone curve for shear critical columns. Modified compression field theory (MCFT) [11] is employed to estimate shear response. Single shear stiffness value was used to model shear deformation. Deformations due to anchorage slip, flexure and shear were combined considering a nonlinear spring model. It was concluded that response until the peak strength was well estimated and compared well with the measured response. However, due to the single shear stiffness used for the entire loading stage, stiffness degradation was not modeled accurately and leaded to wrong estimations for the post peak response. Axial failure was not considered in the model. Another drawback of the method was that residual strength, which did not exist in most of the columns failed in shear, was predicted.

Pujol et. al. [12] studied the drift capacity of the columns subjected to cyclic shear reversals and proposed two different models. Models were used to determine the drift capacity of the RC column or to determine transverse reinforcement ratio for a specific drift capacity. One of those models is developed using mechanical background. One assumption, which makes this method not applicable to this study, is that column core is confined with lateral reinforcement. This assumption does not hold for most of the older buildings. Second model was based on statistical correlation between the variables studied on column database including 94 specimens of 15 different researchers. Variables of statistical analysis were shear span to depth ratio *a/d* and the maximum drift. The proposed approach is limited to columns having maximum axial load level equal to or less than 0.2.

Hysteretic behavior is the main point of cyclic models and it is modeled considering degradation of lateral stiffness and strength with deformation amplitude and loading cycles.

Cyclic models represent complete behavior by combining the effects of different contributions. These contributions mostly are hysteretic models separately for flexure, longitudinal bar slip, and shear response. Hysteretic models for individual responses were based on some extent to available cyclic flexure, reinforcement slip, and shear models, [13], [14], [15]. After each response was determined separately, they were combined with or without interaction between components.

Pincheira et. al. [10] studied the development of a hysteretic model to evaluate the seismic performance of older non-ductile reinforced concrete columns. Main characteristics of the model included the ability to represent flexure or shear failure under cyclic loading. Stiffness degradation was also implemented in model. Model was applied to a multipurpose nonlinear analysis program. A comparison of analytical results with test results showed that the strength, failure mode and general characteristics of the measured cyclic response were well represented by the model. Combination of flexure, shear, and anchorage slip deformations were performed by constructing element flexibility matrices for individual deformation components and combining them to get total flexibility matrix for the element. After evaluation and verification of the studies, it was shown that reasonable and conservative estimates of the measured lateral strength and deformation of the columns were obtained by utilizing the analytical procedure. Furthermore, predicted failure mode was in general agreement with these test results. Based on the results of the studies, Pincheira et. al. [10] concluded that it would be unrealistic to expect to estimate cyclic response exactly due to the existence of considerable uncertainty on the structural response parameters especially for members having poorly detailed transverse reinforcement. Furthermore, it was declared that the effectiveness of column ties as shear reinforcement, confinement to the concrete core, and lateral restraint to buckling of longitudinal reinforcement was not well understood and quantified accurately. Therefore, it was suggested that reasonable response parameter values should be used in the assessment of older reinforced concrete members.

Sezen and Chowdhury [16] also suggested a cyclic model to predict the response of columns experiencing different failure modes. Three different hysteretic behavior components that were hysteretic flexure model modified from the one proposed by Takeda et al. [13], hysteretic slip model based on original Saatcioglu et al. [14] model, and hysteretic shear model proposed by Ozcebe and Saatcioglu [15] were utilized. Total cyclic response of RC columns was predicted by coupling the hysteretic flexure, slip, and shear responses as a three spring in series. Spring in series model assumes that the forces in three springs are similar and deformation of the system is the combination of three different deformation components. The combination rule proposed was that, until the peak lateral strength and during loading and unloading branches, three deformation components were added to calculate total lateral displacement. It was stated that if loading were continued beyond peak strength, total hysteretic response would be bounded by the total monotonic response that is defined considering failure mode or column classification. Proposed model was verified using the experimental data obtained from columns tested by Sezen [8], and Saatcioglu and Ozcebe [6]. As a result, it was stated that model predicted failure mode and represented the flexural and shear behavior well. Furthermore, cyclic response of columns was predicted with sufficient accuracy with limited computational effort. Interaction of deformation components was not considered in the proposed model.

Elwood [9] proposed a limit-state failure model that was developed in order to implement shear and axial failures to nonlinear analysis. In the analytical models hysteretic behavior for flexure and shear were combined. Deformation due to anchorage slip was also included in proposed models. Model was verified using full-scale column tests. Shake table tests and analytical studies were also performed on reinforced concrete frames in order to determine the accuracy of the model predictions. Based on comparisons made between model predictions and test results, it was suggested that drift capacity models can be employed to determine the response of columns whose properties match with the columns in database of the study. It was also stated that column model could be used in the assessment of reinforced concrete frames.

1.3.3. Models that Include Axial-Shear-Flexure Interaction

In order to determine the complete load deformation response of reinforced concrete columns, limited numbers of models that include axial-flexure-shear interaction were developed in literature. However, interaction of different deformation components was not taken into account in most of them. A simple combination of each deformation component was conducted in the previous studies. It is a well-known fact that deformation components are related to each other. For example, axial strain due to flexure can lead to opening of the shear crack width and cause decrease in lateral strength of column. In case of a properly designed column against lateral forces, shear deformations may not be important. However, for older reinforced concrete columns that have poor transverse reinforcement details, shear deformations are important and shall be considered in interaction with flexural deformations. Another interaction is the influence between diagonal tensile strains and concrete compressive strength. Regarding that interaction, diagonal tensile strains leads to concrete compression softening. Experiments showed that concrete compressive strength decreases as the diagonal tensile strains increases.

Petrangeli et al. [17] studied interaction of axial load, bending moment and shear behavior for beam and column elements. A new finite-beam element model was developed and it was based on fiber section discretization. Basic concept of the element was to model the shear mechanism at each fiber of the cross sections by the superposition of the classical plane section hypothesis for the longitudinal strain field with an assigned distribution over the cross section for the shear strain field. The nonlinear solution utilizes an equilibrium-based iterative solution. The resulting model was computationally demanding. It was stated that model was developed to understand the behavior of larger structures rather than the details of the members' failure mechanism. The ability of the frame finite element model to estimate axial collapse is also uncertain.

Saritas [18] studied on development of a beam finite element for the analysis of steel and concrete RC members under the interaction of axial force, shear and bending moment. Cyclic material models for steel and concrete were utilized in formulation. A 3d-plastic-damage concrete material model was utilized for the analysis of shear critical members. Perfect bond was assumed between concrete and longitudinal or transverse reinforcement steel. Buckling of longitudinal bars, dowel action of reinforcing steel and tension stiffening effect are neglected in model. Proposed beam element was validated by comparison of response of several types of RC members such as flexure yielding and shear deficient columns and beams, and flexure yielding structural walls. Two shear critical columns under low and moderate axial loads were analyzed in the study for validation purposes. Results revealed that peak lateral forces were closely captured by the model. However, significant error occurred in corresponding displacement levels. Error in results were said to be related to lack of modeling of bond failure, spalling of cover concrete and buckling of longitudinal reinforcement in the proposed beam model.

Lee et. al. [19] studied shear-flexure interaction for seismic analysis of RC bridge columns. A hysteretic model was developed accounting for interaction between flexural and shear deformations. Anchorage slip was not considered in implementation. The inelastic shear and flexure deformations of a reinforced concrete column were determined by utilizing lumped hysteretic representations. Developed model was implemented to a finite element analysis program. Proposed model was compared with test results and it was stated that good agreement between analytical results and test results was obtained. As a part of the study, specimens were analyzed without considering the interaction between shear and flexural behavior and compared with results of analysis that included interaction between shear and flexural deformations. As a result, it was concluded that if shear deformations were significant, conventional flexural models in finite element programs resulted in response information very different from the actual response.

All aforementioned models considered interaction of deformation components with each other in the frame finite element sense. However, due to the complex nature of cyclic loading behavior of both materials and members, computation process needs serious iterative solutions that are time consuming. These models cannot predict the descending regions in load deformation history and axial failure.

Mostafaei and Kabeyesawa [20] proposed a relatively practical displacement based methodology developed by considering axial- shear- flexure behavior interaction. Model was developed using section analysis combined with simultaneous MCFT [11] algorithm. To model axial-flexure behavior traditional section analysis was used. In order to model axial-shear behavior modified compression field theory developed by Vecchio and Collins [11] was utilized. Axial-shear-flexure interaction as well as satisfaction of equilibrium and compatibility was the important points of the proposed model. Method was developed to predict the response of columns for shear, flexure-shear, and flexure failure modes. Interaction of the deformation components were achieved by employing springs in series approach. Combined together with an axial spring providing the interaction, flexure, shear, and anchorage slip deformations were combined to attain total lateral displacement. By utilizing the proposed methodology, test columns were analyzed and methodology was verified using experimental data. Ultimate strength, ultimate drift, drift at loss of lateral load capacity and drift at loss of axial load capacity were obtained with a satisfactory accuracy. Verification was performed also by analyzing a one bay frame and the results were consistent with the test results.

Mostafaei and Vecchio [21] proposed a simplified model that considers axial-shear-flexure interaction in a uniaxial stress-strain field for the analysis of reinforced concrete elements. Proposed model is called as uniaxial shear-flexure model (USFM). This model has the same theory with original ASFI approach. However, modifications were made in order to simplify analysis procedure. The first level iteration process was eliminated in USFM approach by determining axial strain and principal tensile strain of a reinforced concrete column between two adjoining flexural section based on the average axial strains and average resultant concrete compression strains of the two sections. It was stated that calculation procedure was simplified and results obtained from analysis were comparable with the test results. However, from the presented comparisons it can be seen that post peak response is not estimated well and axial failure or lateral load capacity degradation is not captured.

Models mentioned above can be utilized in order to predict the lateral load-deformation response of reinforced concrete columns. Axial-shear-flexure interaction is important to predict the response of existing reinforced concrete building columns. In this study, due to their practical specialty and accuracy in response estimation, axial-shear-flexure interaction method proposed by Mostafaei et. al. [20] with some modifications and drift capacity model developed by Elwood [9] were utilized. These models explained in details in the Chapter 2.

1.3.4. Seismic Assessment Guidelines

Turkish Earthquake Code (TEC) [1] was revised in 2006 and a new part including provisions for seismic assessment and retrofit of existing buildings was added to become effective in 2007. To determine the performance level of existing reinforced concrete structures, the performance based analysis procedure, which is different from the preceding parts with force-based capacity design methodology, is suggested. In order to estimate performance level of a structure, critical sections of all its structural members are investigated for a code specified seismic demand. Afterwards, performance of structure is classified according to the damage state of the structural members. Failure types of members are defined as shear or flexural failure and no provisions are separately provided for the flexure-shear failure type. Performances of members are determined only considering the flexural deformations whereas shear and bar-slip deformations are not considered.

ASCE/SEI41 [22] is the one of the new generation documents to assist engineers with the seismic assessment and rehabilitation of existing buildings. Provisions for concrete structures given in that document are essentially the same as the FEMA356 [23]. However, it was shown that criteria given in FEMA356 [23] especially those related to deformation capacities tend to fall on the conservative side. (EERI/PEER [24]). In addition, anecdotal reports from practicing engineers revealed that most of the buildings assessed according to the criteria given in FEMA356 [23] do not pass the collapse prevention limits. Therefore, improvements to criteria are needed to realize more accurate assessments of building and to reduce the unnecessary rehabilitation costs. Recently, an update to ASCE/SEI41 update supplement tries to fill this gap. In this supplement, revisions to modeling parameters and acceptance criteria for reinforced concrete members are included based on the experimental evidence and empirical models. Failure modes of the columns are identified considering all flexure, flexure-shear and shear failure modes and acceptance criteria with numerical modeling parameters are updated for both linear and nonlinear procedures. In the development of modeling parameters and acceptance criteria, consideration is given to a fact that columns experiencing shear failure can sustain lateral deformations with a limited plastic deformation capability until the axial failure occurs. In addition, capability of flexure-shear critical columns to go under inelastic deformation is also considered.

Eurocode 8 [25] covers a section for assessment of reinforced concrete columns. Acceptance criteria are based on plastic rotations at different performance levels. Plastic chord rotations are calculated from equations presented as a function of a set of variables (Shear span, longitudinal reinforcement ratio, axial load ratio, transverse reinforcement ratio, yield strength of the transverse reinforcement steel concrete compressive strength). In order to assess performance level of a column, first, classification of failure type as “brittle” or “ductile” is made. After that, limiting plastic chord rotations are obtained using proposed plastic chord rotation formulations. Calculated plastic rotation capacities are compared with the inelastic demands obtained from incremental static lateral load analysis. For the brittle members, on the other hand, shear strength is compared with the shear force demand obtained from the analysis. If the demand is higher than the capacity, no ductility is assumed for the member. In calculation of plastic rotation limit for the so called immediate occupancy level (limit state of damage limitation in Eurocode 8), contributions of rotations from bar slip and shear deformations are also considered.

In order to determine performance of members realistically, all possible failure types should be identified and all deformations components should be taken into consideration. Otherwise, overestimations or under estimations can appear leading to unsafe and uneconomical retrofit solutions.

1.4. Objective and Scope

Literature survey revealed that new models were developed recently which were able to estimate the load deformation characteristics of a reinforced concrete column. In TEC2007 [1], a procedure is described to estimate performance level of the reinforced concrete members. It was observed that there is no rule or provision about the performance determination of columns, which can fail in flexure-shear failure mode having limited ductility. Another gap about the TEC2007 [1] is the lack of any member performance comparison studies. Following objectives are set forth in this study:

1) To investigate the accuracy of four different models on estimating the full response of RC columns, perform analyses of shear critical RC columns and compare their estimations with test results,

2) To perform statistical analyses on the results and select a model with the highest accuracy,

3) To compare the estimation of Turkish Earthquake Code (TEC2007) [1] procedure with the test results and selected model,

4) To obtain drift limits for the performance levels of shear critical including shear and flexure-shear failure expected RC columns, for shear failure and loss of axial load carrying capacity,

5) To obtain improved drift capacity equations for drift ratio at shear failure and at axial failure of shear critical RC columns considering the properties of RC columns used in older construction in Turkey.

It should be noted that the term “drift capacity” or “drift ratio” is used loosely throughout the thesis. It is known that column chord rotation is the parameter to be examined in frame structures. For single column analysis, two measures are similar. Hence, it is deemed necessary to make the appropriate correction when extrapolating the drift related results proposed in this study.

In chapter 2, information about selected database and results of different models are presented. In chapter 3, columns with typical details used in existing buildings are analyzed and their expected performance is presented. Additionally, results of parametric studies are compared and recommendations are given for the drift limits of shear critical members. Examination of acceptance criteria of nonlinear procedures of different codes such as FEMA356 [23], ASCE/SEI41 [22] update supplement, Eurocode 8 [25] and TE2007 [1] is also raised in Chapter 3 of the study. In chapter 4, conclusions derived from study are presented together with the recommendations.

CHAPTER 2

ANALYTICAL MODELLING AND EXAMINATION

In order to estimate response of columns under constant gravity load and subjected to lateral displacement increments, four different modeling approaches were used. Results obtained from analysis are compared and critically evaluated.

2.1. Utilized Models to Predict the Response of Reinforced Concrete Columns

In the scope of this study, a recent approach named as axial-shear-flexure interaction methodology [20] was employed as the first method. This methodology was chosen due to the following reasons:

i) Axial-shear-flexure deformation interaction is considered,

ii) Numerical analysis are simple compared to more involved fiber based frame finite elements,

iii) It provides information throughout the full range of member response up to collapse,

iv) Failure type can be predicted and available ductility can be estimated for all three type of failures,

v) The approach has both theoretical and mechanical background.

In order to estimate the load deformation behavior of columns, ASFI(O); original axial-shear-flexure interaction approach as proposed by Mostafaei et. al. [20], ASFI(M); axial-shear-flexure interaction with the proposed modifications for compression bar buckling as proposed by Maekawa et. al. [26], [27], HSU(M); using constitutive models proposed by Hsu et. al. [28] and compression bar buckling model of Maekawa et. al. [26], [27], are investigated. Subsequently, a simpler drift capacity model proposed by Elwood [9], named as ELWOOD, was also employed to compare the full range behavior of columns that were physically tested. All the models implemented in the course of this study are explained next.

2.1.1. Axial - Shear - Flexure Interaction Approach (ASFI(O))

Axial-shear-flexure interaction approach (ASFI) was developed as a tool for displacement based analysis of reinforced concrete members. ASFI approach can be applied to existing reinforced concrete columns to estimate different structural response properties such as ultimate strength, drift at shear failure as well as lateral drift at axial collapse. Total deformation of a column under combined action of lateral and gravity loads is calculated from contributions of shear, flexural, and anchorage slip deformations resulting in the total lateral displacement under a given lateral load. Shear behavior is modeled by using the well-known modified compression field theory (MCFT) [11] and flexural behavior is modeled using a conventional section analysis together with a lumped plastic hinge assumption. MCFT [11] is explained in Appendix A. Constitutive models used in section analysis are given in Appendix B. Shear and flexural components are coupled as springs in series considering the axial deformation interaction and concrete strength degradation, and satisfying equilibrium and compatibility relationships. Spring model is presented in Figure 2.1. Load deformation response of a single reinforced concrete column can be determined based on the sectional analysis of the plastic hinge region and in plane shear model to represent the shear behavior along the length of the column (from the end to the inflection point of the column). Modeling approach is summarized in Figure 2.2. Lateral displacement due to the end rotations stemming from anchorage slip is also modeled and considered in the numerical calculation process. Axial spring is the most important aspect of the ASFI method because it connects the axial-shear and axial-flexure behavioral aspects. Axial strains due to flexural mechanism can increase the shear crack width as well as diagonal tensile strain in the web of the column leading to lower shear capacities. This behavior is illustrated in Figure 2.3. It is a well-known fact that compressive stress on a section can increase the shear capacity if diagonal compression failure is prevented. In contrast to compressive stresses, tensile stresses can lead to increase in diagonal tensile strains and lower shear capacity.

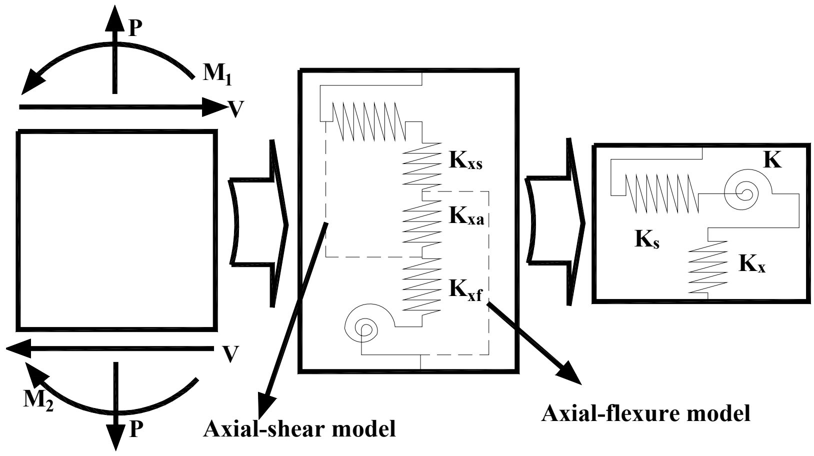

Figure 2.1 Spring Model of ASFI Approach [21]

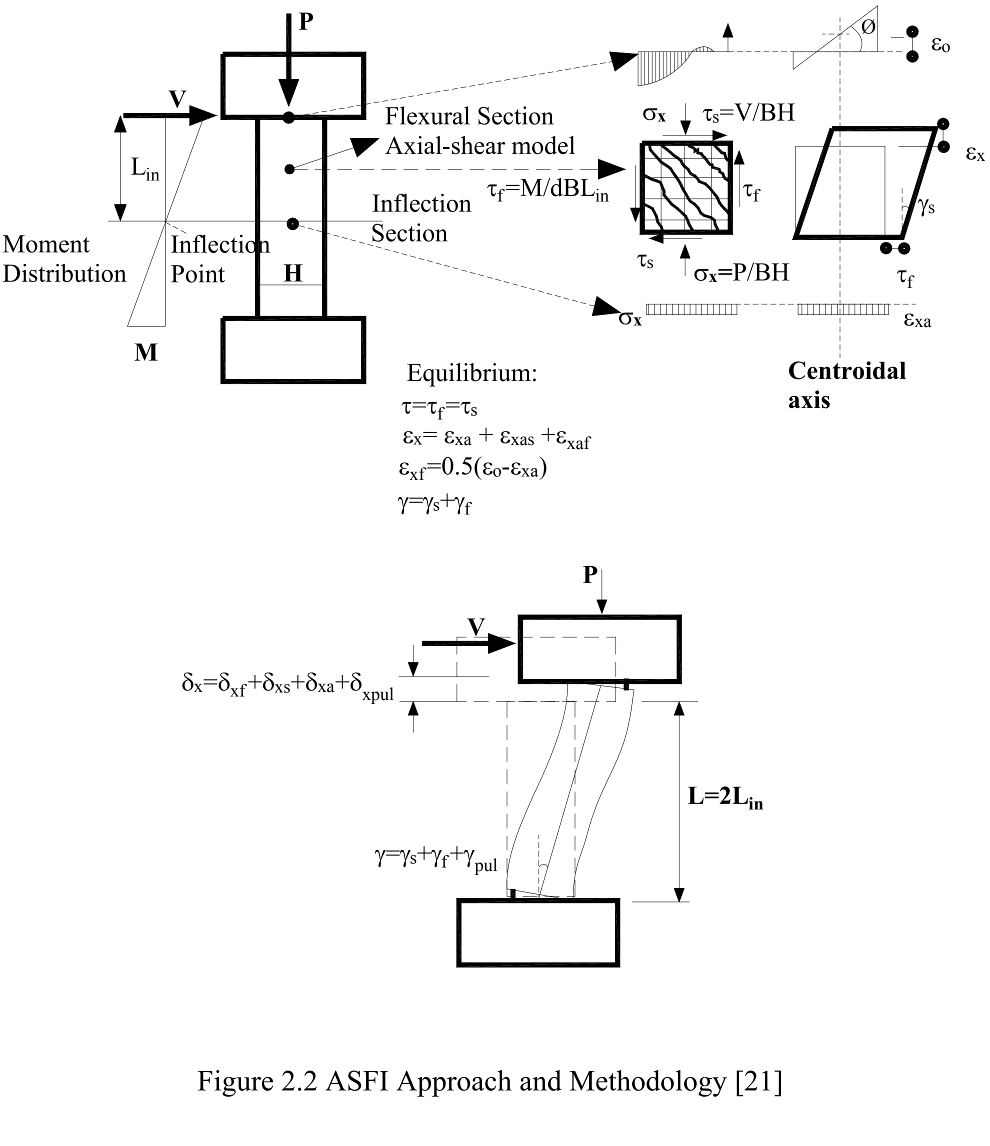

Figure 2.2 ASFI Approach and Methodology [21]

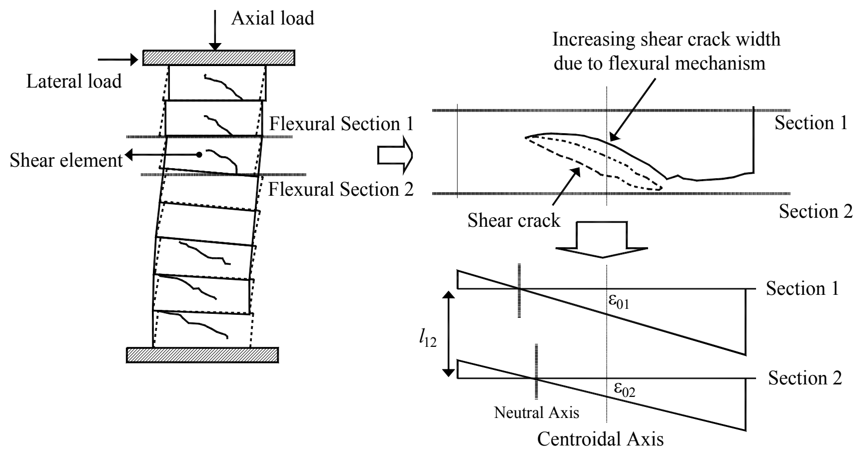

Figure 2.3 Conceptual Illustration of Effects of Flexural Deformations on Shear Deformations [20]

It is also known that concrete compressive strength softening occurs if there are tensile strains in the perpendicular direction. Therefore, axial deformations of axial-shear model and axial-flexure model shall be interconnected in the response estimation models. This is achieved in ASFI model in a way that centroidal strain of axial-flexure model is taken into account in the axial-shear model in the strength calculations and the compression softening of axial-shear model is taken into account to axial-flexure model. In other words, according to the centroidal strain value calculated in section analysis, a compression-softening factor is calculated in axial-shear model. This softening factor is applied to concrete constitutive models both in axial-shear and axial-flexure (section analysis) models. That is to say, same concrete constitutive laws are used in both deformation components.

Theory behind the ASFI method and detailed formulations are given in Appendix B. Computation process and calculation steps can be summarized as below.

1- Input geometrical properties, material properties, and applied axial load into axial-flexure model

2- Increment the drift ratio (for example 0.001)

3- Variables considered in iteration step i are centroidal strain, section curvature, axial strain along the column length, axial strain in transverse direction, and shear strain.

4- A fiber model is created to obtain centroidal strain in iteration step i+1, axial strain due to axial mechanism, axial strain due to flexure mechanism, pullout strain, drift due to pull out and flexural shear stress.

5- Compute the flexibility component for the axial deformation due to flexure, flexural stiffness and pull out stiffness.

6- Stiffness element of axial-shear element is constructed based on the MCFT [11], and then flexibility and total flexibility matrices are obtained.

7- Solving matrices axial deformations in x and y directions and shear deformation are calculated. Section curvature and centroidal strain are determined.

8- Check convergence of deformations if not converged go to step 3.

9- Determine shear force then if the desired drift ratio is reached, stop computation. Otherwise, go to step 2.

In the original ASFI method proposed by Mostafaei et. al. [20], based on test results a method was suggested to consider the buckling or slip of the compression reinforcement. According to that method, degradation of the compression strength of the longitudinal bars was initiated when strength of the unconfined-cover concrete fiber reached approximately 30% of the maximum concrete compressive strength. After that step, strength of the compression bars was linearly declined similar to the slope of the post peak confined-core concrete compression stiffness. This proposed method is completely empirical and subjective. It has also no mechanical background. Another important aspect that was declared in the method was about coupling of deformations. Since the axial-shear-flexure interaction was achieved by employing springs in series, it was important to consider the plastic offset of the three springs at the post-peak states. Hence, it was suggested that pullout stiffness should be kept constant after the peak strength. Furthermore, contribution of the axial-shear spring stiffness, K_s and concrete softening factor, β should be considered until when their values started to increase. At that stage, values of K_s and β were fixed to values at the previous stage and kept constant through the rest of the analysis. In other words, after that stage flexure component was allowed to dominate the behavior. Axial failure or gravity collapse was defined at the stage where force equilibrium in the analysis was not satisfied any more under the applied axial and loads. In other words, when columns reached their complete loss of lateral load capacity, axial failure occurred. Bond failure mechanism was not directly taken into account by the ASFI method.

2.1.2. ASFI Approach with the Proposed Modifications (ASFI(M))

Axial-shear-flexure interaction (ASFI) approach explained in Chapter 2.1.1 was utilized with a modification for the strength degradation of the compression reinforcement.

In the original ASFI method, this effect was considered and modeled based on empirical definitions to match the test results. However, as a modification, an approach based on an analytically developed model proposed by Maekawa et. al. [26] was implemented to the ASFI method. Considering the results of analytical studies, a compressive strength envelope and constitutive models were developed including the effect of slenderness ratio and yield strength of the reinforcing bars. The aim of modification was to estimate the effect of compression bar buckling realistically considering a mechanical model. Modification was applied to compressive bar stress-strain relationship in the fiber model of axial-flexure mechanism. Constitutive models and the details of the model are given in Appendix C.

Since most of the columns that are under investigation had poorly detailed lateral reinforcement with rather large spacing (approximately equal to the column size), stability of the compression bars are of great importance. Stability of the compression bars are directly related to the stiffness of the lateral reinforcement and spacing. At this point, model proposed by Maekawa et. al. [27] was preferred due to its ability of incorporating appropriate buckling mode. Once buckling mode was estimated, the slenderness value ($\frac{L}{D}$) was computed. Afterwards, stress-strain relationship of the compressive bars was computed with constitutive models defined by Maekawa et. al. [27]. Information about constitutive models is presented in Appendix C. Hence, the only difference in the ASFI computational flow is the incorporation of a realistic stress-strain model for longitudinal reinforcing bars in compression.

2.1.3. ASFI Approach Using Constitutive Models Proposed by Hsu (HSU(M))

Hsu [29] presented new constitutive models based on fixed angle softened truss model (FA-STM) soon after MCFT [11] was proposed. Proposed constitutive models can take care of important characteristics of the cracked reinforced concrete with softening effect of concrete in compression, the tension stiffening effect of concrete in tension, and average stress-strain curve of steel bars embedded in concrete. In this way, both steel and concrete constitutive models can be written in average stress-strain terms. Wang and Hsu [28] later implemented constitutive models to a finite element analysis program for reinforced concrete structures. Analyses results were unified for reinforced concrete frames shear walls, panels, and beams. Due to superior mechanical background of FA-STM over MCFT explained below, FA-STM by Wang and Hsu [28] was implemented to the ASFI analyses program in order to make a comparison of results with the results obtained from analysis utilizing constitutive models proposed by Vecchio [30]. Along with the constitutive models proposed by Hsu [28], stress-strain relationship for buckling of compression bars according to Maekawa et. al. [26], [27] was also incorporated. The reason of the implementation of the FA-STM model to ASFI is that MCFT has an important deficiency, which was severely criticized by Hsu. This deficiency is the presence of shear stress transfer check in crack in the principal shear directions. This, in fact, implies betrayal of compatibility requirement and; hence, is mechanically incorrect. Moreover, bare bar response models were utilized by Wang and Hsu [28] for steel reinforcement instead of average models. Constitutive models proposed by Hsu [28] were presented in Appendix D.

2.1.4. Drift Capacity Models (ELWOOD)

A drift capacity model was proposed by Elwood [9] based on mechanical and empirical studies employing a database consisting of cyclic test results of shear critical RC columns with the following range of properties:

- Shear span to depth ratio: $2.2 \leq \frac{a}{d} \leq 3.9$
- Concrete compressive strength: $13.1 \leq f_c{}' \leq 44.8$ Mpa
- Longitudinal reinforcement nominal yield stress: $324 \leq f_{yl} \leq 524$ Mpa
- Longitudinal reinforcement ratio: $0.01 \leq \rho_l \leq 0.08$
- Transverse reinforcement ratio: $0.001 \leq \rho_v \leq 0.0065$
- Transverse reinforcement nominal yield stress : $317 \leq f_{yl} \leq 648$ Mpa
- Maximum shear stress: $0.23 \leq \frac{v}{\sqrt{f_c{}'}} \leq 0.72$ (Mpa units).

Where;

a: Shear span (whole column length for column tested under single curvature, half of the column length for column tested under double curvature

d: Effective depth of the section considered

ρ_v: Transverse reinforcement ratio being transverse reinforcement area divided by *b.s* (*b* is the section width and *s* is the spacing of transverse reinforcement)

v: Maximum shear stress (maximum shear force divided by *b.d* where b is section width and d is effective depth)

f_{yt}: Yield stress of the transverse reinforcement

A simple model is developed to estimate the drift at shear failure and at axial failure of columns. Drift at shear failure can be calculated using Eq. (2.1).

$$\frac{\Delta_s}{L} = \frac{3}{100} + 4\rho_v - 0.0241\frac{v}{\sqrt{f_c^{'}}} - \frac{1}{40}\frac{P}{A_g f_c^{'}} \qquad \text{(MPa)} \qquad \textbf{(2.1)}$$

Where $\frac{\Delta_s}{L}$ is drift at shear failure; ρ_v, transverse reinforcement ratio $\left({}^{A_{sw}}/_{bs}\right)$; v,maximum shear stress (maximum lateral load divided by *b.d*); $f_c^{'}$, concrete cylinder compressive strength; P, applied axial load; and A_g, gross cross sectional area of column. Drift at axial failure was computed using Eq. (2.2).

$$\left(\frac{\Delta}{L}\right)_{axial} = \frac{4}{100}\frac{1+\left(\tan\theta\right)^2}{\tan\theta + P\left(\dfrac{s}{A_{st} f_{yt} d_c \tan\theta}\right)} \qquad \textbf{(2.2)}$$

Where $\left(\frac{\Delta}{L}\right)_{axial}$ is drift at axial failure, θ is the inclination of crack and is taken equal to 65°, s is the spacing of lateral reinforcement, A_{st} is the cross sectional area of the transverse reinforcement, f_{yt} is the yield stress of the transverse reinforcement steel, d_c is core dimension of column section. Eq. (2.2) was used to calculate the drift at axial failure of a shear damaged RC column. In development of Eq. (2.2) classical shear friction approach was utilized with consideration of plastic buckling of longitudinal reinforcement. Utilizing aforementioned equations, drift at shear failure and axial failure are determined and limit surfaces were found on an idealized flexural response (Figure 1.7). Axial capacity model has some deficiencies such as assumption that transverse reinforcement is fully anchored, direct bearing of concrete components is not accounted, the dependence on a distinct shear failure plane and limited database on which model was based. Therefore, it was suggested to use the model for columns whose properties resemble those of the database.

In this study, section analyses were performed on specimens selected for verification purposes and lateral load-displacement curves were obtained from proposed model. Displacements were calculated by integration of curvature along the column length and anchorage slip and shear displacement were not considered.

2.1.5. Turkish Earthquake Code Procedure

Turkish Earthquake Code [1] was edited in 2006 and it became effective in 2007. Chapter 7 of the code entitled “Assessment and Strengthening of Existing Buildings” includes provisions for assessment and rehabilitation of existing buildings. In this part of the code, elastic and inelastic methods are presented to estimate the performance level of RC structures. In the linear elastic procedure, member capacity to demand ratios are calculated and performance of the members are identified. On the other hand, in nonlinear static procedure, limit strains of materials serve as a tool to estimate the performance level for a specified demand. In the scope of this study, only nonlinear procedure was examined and used in determining performance levels of the reinforced concrete columns. In order to determine performance of an RC structure, critical regions of all its members are examined. Then member performance limits are described for three damage levels, considering the estimated failure mode and ductility capacity of each member. Performance of structure is identified according to the distribution of member damages over the building. Figure 2.4 shows the damage levels of ductile members according to the Turkish Earthquake Code 2007 (TEC 2007) [1].

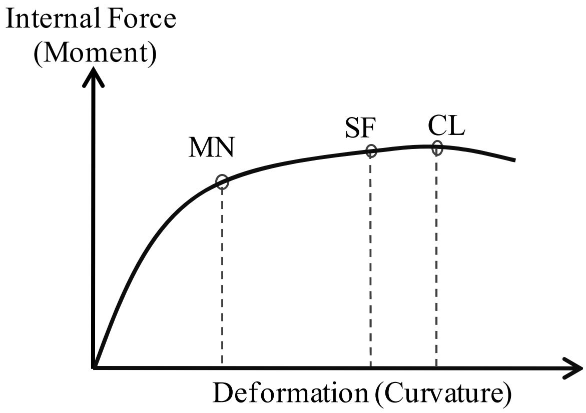

Figure 2.4 Damage Levels of a Ductile Member (TEC2007 [1])

According to the TEC2007 [1], members are classified as ductile or brittle according to their modes of failure. If a member is a shear critical member it is accepted as a “brittle member”, otherwise it is accepted as “ductile member”. In Figure 2.4, MN is the minimum damage limit and defines the onset of the significant post-elastic behavior at a critical region. Brittle members are not allowed to exceed this limit. In order to classify a member as ductile or brittle member, slightly different procedures are defined in the code for linear analysis and nonlinear analysis.

For the linear procedure, type of brittle or ductile failure is determined based on comparison of shear capacity with the capacity based on flexural strength calculated in the critical end region of column section. If shear capacity calculated according to TS500 [31] procedure is greater than the shear demand at the section, failure is classified as "ductile"; otherwise, it is classified as "brittle". Details of calculations are presented in Appendix E.

For the nonlinear procedure, ductility of the columns is determined based on shear force demand and shear capacity of the section. If shear capacity of the section determined according to the TS500 (as in the linear procedure case) is greater than shear force demand at that section, column is classified as "ductile", otherwise it is "brittle". However, if beams are stronger than the columns, classification is made as in the linear elastic procedure. Columns mostly develop their flexural capacity under lateral loads in such systems. Due to that reason, in this study it is assumed that demand is higher than the capacity of the element dictated by either shear or shear flexure.

According to the Turkish Earthquake Code provisions, nonlinear behavior of columns is investigated for ductile columns based on the plastic hinge analysis at the ends of the columns. Plastic hinge length L_p is defined as half of the section depth h ($L_p = \frac{h}{2}$). Pre-yield behavior of concrete sections is represented by flexural rigidity of cracked sections, which is $0.4EI_0$ (Where, E is the modulus of elasticity of concrete, and I_0 is the gross moment of inertia of the section.) for beams and varies between $(0.4 - 0.8)EI_0$ according to the axial stress level for columns. Damage level of a section is calculated by determination and classification of concrete fiber and reinforcement strains at plastic curvature demand considering the limit strains given as:

For minimum damage limit (MN)

$$(\varepsilon_{cu})_{MN} = 0.0035 \;\; ; (\varepsilon_s)_{MN} = 0.01 \tag{2.3}$$

For life safety damage limit (SF)

$$\left(\varepsilon_{cg}\right)_{SF} = 0.0035 + 0.01(\rho_s/\rho_{sm}) \leq 0.0135 \;\; ; (\varepsilon_s)_{SF} = 0.04 \tag{2.4}$$

For collapse damage limit (CL)

$$\left(\varepsilon_{cg}\right)_{CL} = 0.004 + 0.014(\rho_s/\rho_{sm}) \leq 0.018 \;\; ; (\varepsilon_s)_{CL} = 0.06 \tag{2.5}$$

In equations (2.3-2.5), ε_{cu} is the concrete strain at the outer fiber, ε_{cg} is the concrete strain at the outer fibre of the confined core, ε_s is the steel strain and (ρ_s/ρ_{sm}) is the volumetric ratio of existing confinement reinforcement ρ_s at the section to the confinement required by the code ρ_{sm}.

In this study, state of the column (i.e. ductile or brittle) was obtained first. For brittle columns, no deformability exists; hence, load deformation response can be assumed as linearly elastic and perfectly brittle. On the other hand, for the ductile columns lateral load displacement plot was obtained by calculating the displacement for each damage limit and for the yield curvature using Eq. (2.6) and Eq. (2.7).Up to the yield point displacement is calculated using Eq. (2.6) and after yield point to plastic curvature, it is calculated by Eq. (2.7). Curvature distribution of a column is shown in. Figure 2.5.

$$\Delta = \frac{\phi L_{in}^{2}}{3} \tag{2.6}$$

$$\Delta = \frac{\phi_y L_{in}^{2}}{3} + \left(\phi - \phi_y\right) L_p \left(L_{in} - 0.5 L_p\right) \tag{2.7}$$

In equation (2.6), Δ is the calculated tip displacement, $\emptyset$ is section curvature, and L_{in} is the shear span. In equation (2.7), L_p is the plastic hinge length and $\emptyset_y$ is the yield curvature of the section.

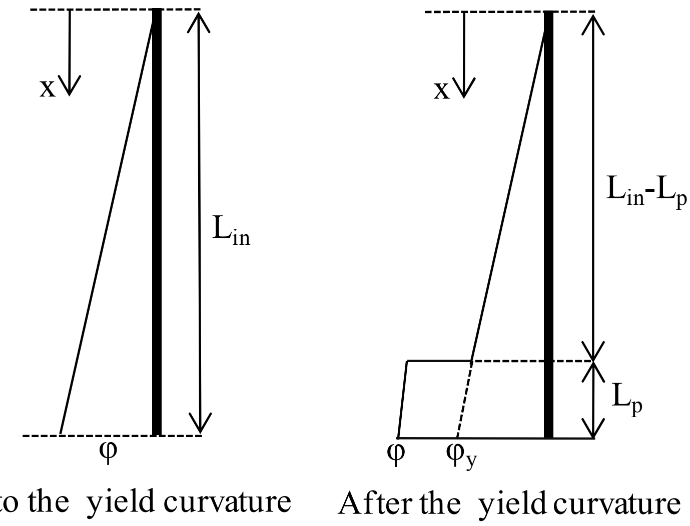

Figure 2.5 Curvature (Φ) Distribution along A Column

Calculated displacements are plotted on lateral load displacement curve as shown generically in Figure 2.6. In Figure 2.6, V_f is the shear force or lateral load obtained by dividing the moment capacity of the critical section to the shear span of the column. Calculations according to the TEC2007 [1] nonlinear procedure is presented in Appendix F.

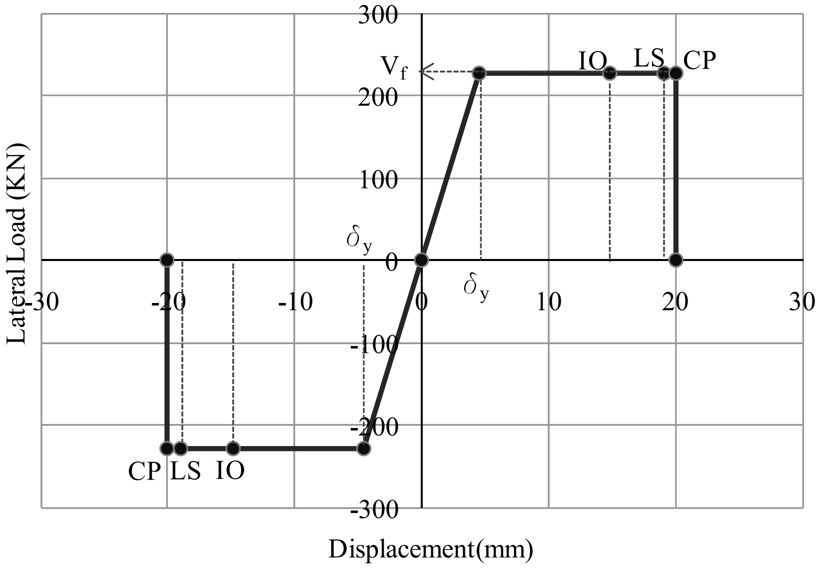

(a)

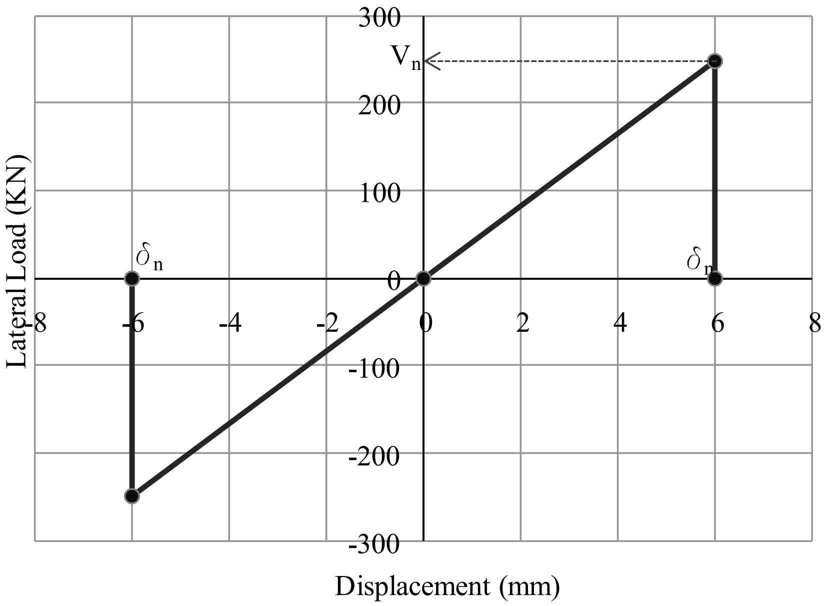

(b)

Figure 2.6 Lateral Load-Displacement Curve Obtained by TEC (2007) Procedure a) a Ductile Column b) a Brittle column

2.2. Examination of Load Deformation Prediction of Models

As explained above, five models were studied to perform analysis of columns included in the selected database of shear critical columns. Selected columns were analyzed by using five different models. Analyses were carried out and load deformation plots were obtained. Models employed for load-deformation estimation are abbreviated in the following format:

- ASFI(O): Axial-shear-flexure interaction approach as defined by Mostafaei and Kabeyesawa [20]
- ASFI(M): Axial-shear-flexure interaction approach with proposed modifications
- HSU(M): Axial-shear-flexure interaction approach with constitutive models proposed by Hsu [28] and compression bar buckling model according to Maekawa [26], [27]
- ELWOOD: Drift capacity model as defined by Elwood [9]
- TEC2007: Procedure defined in TEC [1].

2.2.1. Selected Database of Shear Critical Columns

For modeling and verification purposes, different column specimens were selected from previous studies performed on shear critical columns. Sectional properties, structural details, and cyclic test results of the selected columns were obtained from PEER structural column database [4]. Ten column specimens whose failure modes reported as flexure-shear and six column specimens failed in shear failure mode were selected from database and analyzed. While selecting column specimens, one of the important criteria was to select columns that represented the column types widely used in older building construction. Other criterion was the reliability of the test results and in depth information about sectional properties of column specimens and test results. Section properties, reinforcement ratios, axial load levels, and material properties of columns together with the ultimate moment and shear capacitiess of the sections calculated according to TS500 [31] guidelines are presented in Table 2.1. Failure types reported in Peer Column Database [4] and failure modes predicted by nonlinear procedure of TEC2007 [1] are also noted for each specimen in the same table. Maximum lateral loads reached during the tests are also shown in the Table 2.1. Load-deformation responses of all these tested columns were estimated using aforementioned procedures of five different procedures. From the estimated load-deformation responses of test specimens, ultimate lateral load, drift at ultimate capacity, drift at shear failure, and drift at axial failure were determined. Drift at shear failure was defined as the drift at which lateral load capacity decreased to 80% of its maximum value. Drift at axial failure was taken as the drift at which lateral load carrying capacity was completely lost or shear deformations excessively increased such that equilibrium could not be maintained. Determination of the drift at shear failure and drift at axial failure is explained in Figure 2.7. To determine drift at shear failure from test data; a line is drawn perpendicular to the load axis passing through 80% of maximum load until it intersects envelope curve. Drift at shear failure is projection of the intersection on drift axis. In addition, drift at first yield was determined by using the procedure defined by Sezen [8] and showed in Figure 2.7. For this purpose, a horizontal line is drawn perpendicular to load axis. Another line is drawn from origin passing through lateral load that is 70 % of the maximum lateral load and intersects the horizontal line. A line is projected from the intersection of first and second lines to the horizontal axis and value read in drift axis is accepted as drift at first yield. Calculated drifts and capacities are presented in Table 2.2.

Table 2.1 Selected Shear Critical Column Database

Specimen	b (mm	h (mm	cc (mm)	d (mm)	a (mm)	a/d	s (mm)	ρ_l	ρ_v	f_{yl} (Mpa	f_{yv} (Mpa	f_c (Mpa	P (KN)	$\frac{N}{A_g f_c}$	M_n (KN.	V_n (KN)	V_{test} (KN)	Failure Type	Failure TEC2007
Lynn (2001)																			
2CLH18	457	457	38.1	397	1473	3.71	457	0.019	0.0007	331	400	33.1	503	0.073	334.5	272.8	240.8	F-S	D
2CMH18	457	457	38.1	397	1473	3.71	457	0.019	0.0007	331	400	25.5	1512	0.284	409.0	302.0	306.0	F-S	D
3SMD12	457	457	38.1	394	1473	3.74	305	0.03	0.0017	331	400	25.5	1512	0.284	503.0	371.6	367.0	F-S	D
3CLH18	457	457	38.1	394	1473	3.74	457	0.03	0.0007	331	400	26.9	503	0.089	440.0	248.9	277.0	S	B
3CMH18	457	457	38.1	394	1473	3.74	457	0.03	0.0007	331	400	27.6	1512	0.262	518.0	309.7	328.0	S	B
3CMD12	457	457	38.1	394	1473	3.74	305	0.03	0.0017	331	400	27.6	1512	0.262	520.0	381.6	355.0	S	D
3SLH18	457	457	38.1	394	1473	3.74	457	0.03	0.0007	331	400	26.9	503	0.089	440.0	248.9	270.0	S	B
Nagasaka (1982)																			
HPRC10-63	200	200	12	176	300	1.7	35	0.013	0.0068	371	344	21.6	147	0.170	27.0	119.9	86.9	S	D
Sezen and Moehle (2002)																			
NO:1	457	457	65.1	368	1473	4	305	0.025	0.0017	434	476	21.1	667	0.151	386.0	308.4	314.8	F-S	D
NO:2	457	457	65.1	368	1473	4	305	0.025	0.0017	434	476	21.1	2669	0.605	375.0	402.8	359.0	F-S	D
NO:4	457	457	65.1	368	1473	4	305	0.025	0.0017	434	476	21.8	667	0.146	389.0	311.3	294.6	F-S	D
Umehera and Jirsa (1982)																			
CUW	410	230	25	190	455	2.4	89	0.03	0.0031	441	414	34.9	534	0.162	141.0	216.4	263.2	S	B
Wight and Sozen (1973)																			
25.033	152	305	22.3	267	876	3.28	127	0.025	0.0032	496	345	33.6	111	0.071	92.0	95.2	93.3	F-S	B
40.033a(East)	152	305	22.3	267	876	3.28	127	0.025	0.0032	496	345	34.7	189	0.117	95.0	101.1	98.8	F-S	B
40.048(East)	152	305	22.3	267	877	3.29	89	0.025	0.0046	496	345	26.1	178	0.147	91.0	112.2	104.6	F-S	D
Zhou et al. (1987)																			
223.09	160	160	12.5	138	320	2.32	40	0.022	0.018	341	559	21.1	486	0.900	20.0	264.7	67.4	F-S	D

Notation:

b: Width of the column section

h: Height of the column section

d: Distance from outer fiber of concrete section to center of tension reinforcement

a: Shear span

s: Tie spacing

ρ_l: Longitudinal reinforcement ratio (A_{sl}/bh)

ρ_v: Transverse reinforcement ratio (A_{sv}/bs)

f_{yl}: Longitudinal steel yield stress

cc: Distance from outer surface of concrete to outer edge of transverse reinforcement

f_{yv}: Transverse steel yield strength

f_c: Concrete compressive strength

P: Axial load

M_n: Moment capacity of section

V_n: Shear force capacity of the section (TS 500)

V_{test}: Maximum shear force obtained from cyclic test.

F-S: Flexure-shear failure

S: Shear failure

B: Brittle failure (TEC2007)

D: Ductile failure (TEC2007)

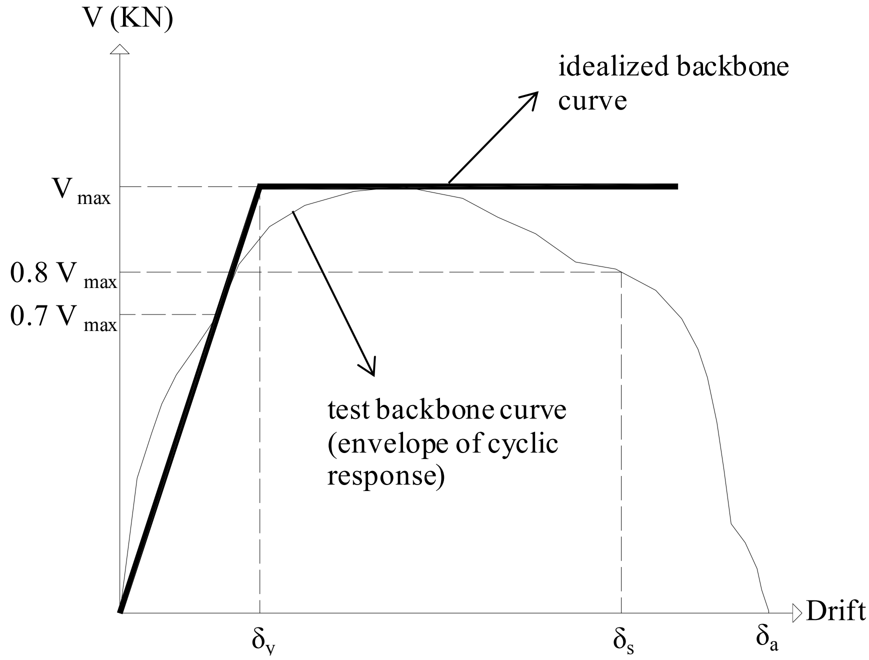

Figure 2.7 Definition of the Drift at First Yield, Drift at Shear Failure, and Drift at Axial Failure

Results of the analyses for each different column are shown in Table 2.2. Load-deformation response from four models (ASFI(O), ASFI(M), HSU(M), ELWOOD) and estimations of the TEC2007 are presented in Figures 2.8 and 2.9. Statistical analyses were performed on the data obtained from cyclic test results and analytical results in order to evaluate the accuracy of each approach qualitatively. Results obtained from four different models were normalized with test results. Comparison of calculated response and measured response were plotted for each model and presented in Figure 2.10 and Figure 2.11. Statistical analyses are summarized for columns experienced shear failure mode and flexure-shear failure in Table 2.3 and in Table 2.4 respectively.

Table 2.2 Analysis Results of Column Specimens

Specimen	Failure Type	Failure Type (NL)	Model	V_{max} (KN)	DR_y	DR_{Vmax}	DR_s	DR_a
2CLH18	Flexure-Shear	ductile	TEST	241	0.005	0.014	0.026	0.031
			ASFI (O)	255	0.005	0.011	0.027	0.032
			ASFI (M)	255	0.005	0.011	0.028	0.032
			HSU (M)	236	0.005	0.012	0.027	0.031
			ELWOOD	226	0.004	0.009	0.026	0.029
2CMH18	Flexure-Shear	ductile	TEST	306	0.006	0.010	0.010	0.010
			ASFI (O)	297	0.005	0.008	0.021	0.016
			ASFI (M)	297	0.005	0.008	0.016	0.017
			HSU (M)	263	0.004	0.007	0.019	0.019
			ELWOOD	278	0.003	0.005	0.018	0.012
3SMD12	Flexure-Shear	ductile	TEST	367	0.008	0.012	0.016	0.021
			ASFI (O)	385	0.007	0.011	0.018	0.028
			ASFI (M)	384	0.007	0.011	0.023	0.033
			HSU (M)	372	0.008	0.012	0.020	0.025
			ELWOOD	342	0.004	0.005	0.020	0.025
NO:1	Flexure-Shear	ductile	TEST	315	0.009	0.018	0.026	0.050
			ASFI (O)	307	0.010	0.019	0.026	0.050
			ASFI (M)	307	0.010	0.019	0.024	0.050
			HSU (M)	292	0.011	0.020	0.026	0.043
			ELWOOD	259	0.005	0.008	0.024	0.044
NO:2	Flexure-Shear	ductile	TEST	359	0.007	0.009	0.009	0.018
			ASFI (O)	280	0.006	0.009	0.013	0.017
			ASFI (M)	280	0.006	0.009	0.013	0.018
			HSU (M)	268	0.005	0.011	0.015	0.018
			ELWOOD	254	0.004	0.006	0.011	0.016
NO:4	Flexure-Shear	ductile	TEST	295	0.009	0.021	0.029	0.055
			ASFI (O)	309	0.010	0.019	0.026	0.052
			ASFI (M)	309	0.010	0.019	0.025	0.051
			HSU (M)	293	0.010	0.020	0.026	0.042
			ELWOOD	264	0.005	0.007	0.025	0.044
25.033	Flexure-Shear	brittle	TEST	93	0.014	0.034	0.036	0.033
			ASFI (O)	95	0.007	0.013	0.036	0.037
			ASFI (M)	95	0.007	0.012	0.050	0.050
			HSU (M)	98	0.007	0.017	0.029	0.033
			ELWOOD	94	0.005	0.011	0.031	0.064
40.033a(East)	Flexure-Shear	brittle	TEST	99	0.008	0.036	0.036	0.036
			ASFI (O)	105	0.007	0.015	0.029	0.029
			ASFI (M)	105	0.007	0.015	0.041	0.041
			HSU (M)	106	0.007	0.016	0.025	0.027
			ELWOOD	104	0.006	0.008	0.030	0.051

Notification: ASFI (O); Original ASFI procedure without modification, ASFI (M): ASFI procedure model with modification; HSU (M); ASFI procedure with constitutive models proposed by Hsu [28], ELWOOD: Procedure proposed by Elwood [9]. NA: Not applicable (Column has properties not compatible with the properties included in database.). DR_y; Drift ratio at first yielding of longitudinal reinforcement, V_{max}; Peak lateral load, DR_{Vmax}: Drift ratio at the peak lateral load, DR_s; Drift ratio at the shear failure, DR_a; Drift ratio at the axial failure, NL: Failure type determined according to the TEC2007 using precise calculation.

Table 2.2 continued

Specimen	Failure Type	Failure Type (NL)	Model	V_{max} (KN)	DR_y	DR_{Vmax}	DR_s	DR_a
40.048(East)	Flexure-Shear	ductile	TEST	105	0.014	0.028	0.055	0.049
			ASFI (O)	103	0.008	0.019	0.030	0.034
			ASFI (M)	103	0.008	0.019	0.040	0.042
			HSU (M)	105	0.008	0.017	0.029	0.029
			ELWOOD	101	0.006	0.013	0.035	0.061
223.09	Flexure-Shear	ductile	TEST	67	0.006	0.019	0.038	0.038
			ASFI (O)	67	0.006	0.012	0.042	0.047
			ASFI (M)	67	0.006	0.024	0.040	0.044
			HSU (M)	56	0.003	0.009	0.012	0.012
			ELWOOD	NA	NA	NA	NA	NA
3CLH18	Shear	brittle	TEST	277	0.007	0.010	0.010	0.021
			ASFI (O)	338	0.008	0.015	0.025	0.026
			ASFI (M)	338	0.008	0.015	0.024	0.024
			HSU (M)	310	0.007	0.013	0.023	0.025
			ELWOOD	299	0.004	0.007	0.024	0.029
3CMH18	Shear	brittle	TEST	328	0.008	0.009	0.010	0.021
			ASFI (O)	384	0.007	0.012	0.014	0.019
			ASFI (M)	360	0.005	0.008	0.017	0.018
			HSU (M)	379	0.007	0.012	0.017	0.021
			ELWOOD	351	0.004	0.005	0.019	0.012
3CMD12	Shear	ductile	TEST	355	0.007	0.011	0.016	0.021
			ASFI (O)	360	0.008	0.011	0.018	0.028
			ASFI (M)	360	0.008	0.011	0.020	0.032
			HSU (M)	344	0.005	0.014	0.022	0.028
			ELWOOD	354	0.004	0.005	0.021	0.025
3SLH18	Shear	brittle	TEST	270	0.005	0.008	0.010	0.031
			ASFI (O)	304	0.008	0.015	0.025	0.026
			ASFI (M)	304	0.008	0.015	0.024	0.025
			HSU (M)	280	0.008	0.013	0.023	0.026
			ELWOOD	300	0.004	0.007	0.024	0.028
CUW	Shear	brittle	TEST	263	0.008	0.014	0.021	0.031
			ASFI (O)	265	0.004	0.007	0.018	0.019
			ASFI (M)	253	0.004	0.014	0.018	0.024
			HSU (M)	296	0.008	0.018	0.019	0.022
			ELWOOD	310	0.003	0.006	0.021	0.039
HPRC10-63	Shear	ductile	TEST	87	0.004	0.013	0.017	0.026
			ASFI (O)	88	0.004	0.014	0.030	0.030
			ASFI (M)	88	0.004	0.014	0.030	0.030
			HSU (M)	86	0.005	0.020	0.029	0.029
			ELWOOD	NA	NA	NA	NA	NA

Notification: ASFI (O); Original ASFI procedure without modification, ASFI (M): ASFI procedure with modification model; HSU (M); ASFI procedure with constitutive models proposed by Hsu [28, ELWOOD: Procedure proposed by Elwood [9]. NA: Not applicable (Column has properties not compatible with the properties included in database.). DR_y; Drift ratio at first yielding of longitudinal reinforcement, V_{max}; Peak lateral load, DR_{Vmax}: Drift ratio at the peak lateral load, DR_s; Drift ratio at the shear failure, DR_a; Drift ratio at the axial failure, NL: Failure type determined according to the TEC2007 using precise calculation.

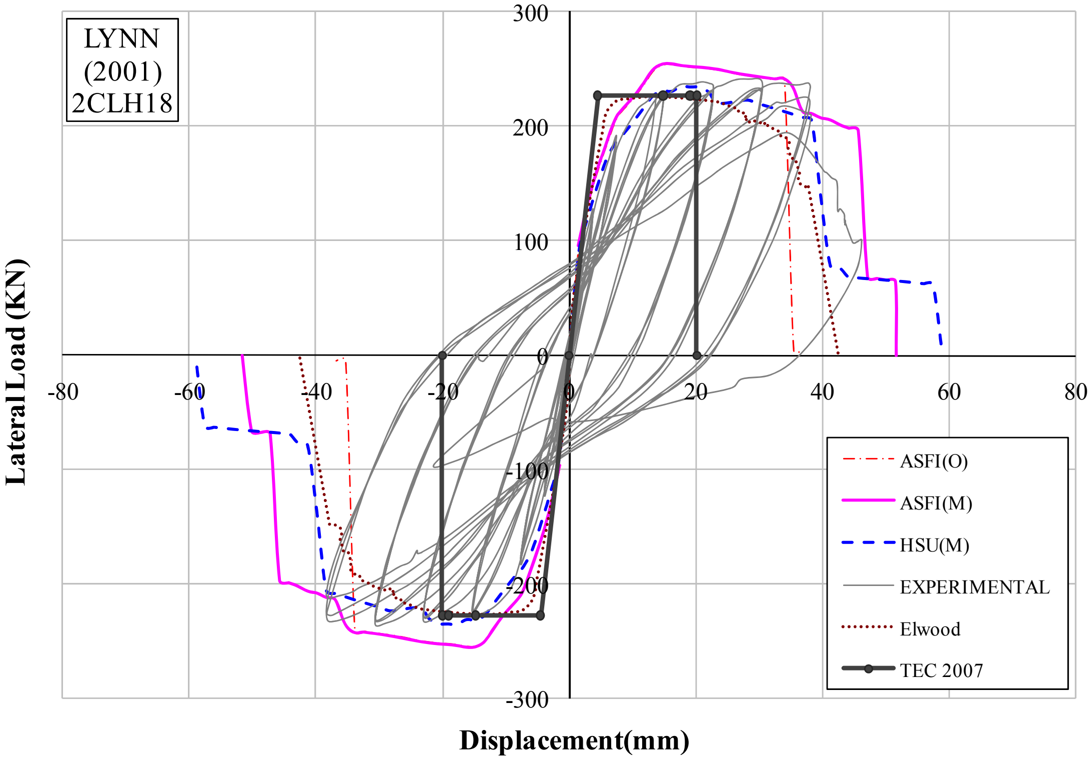

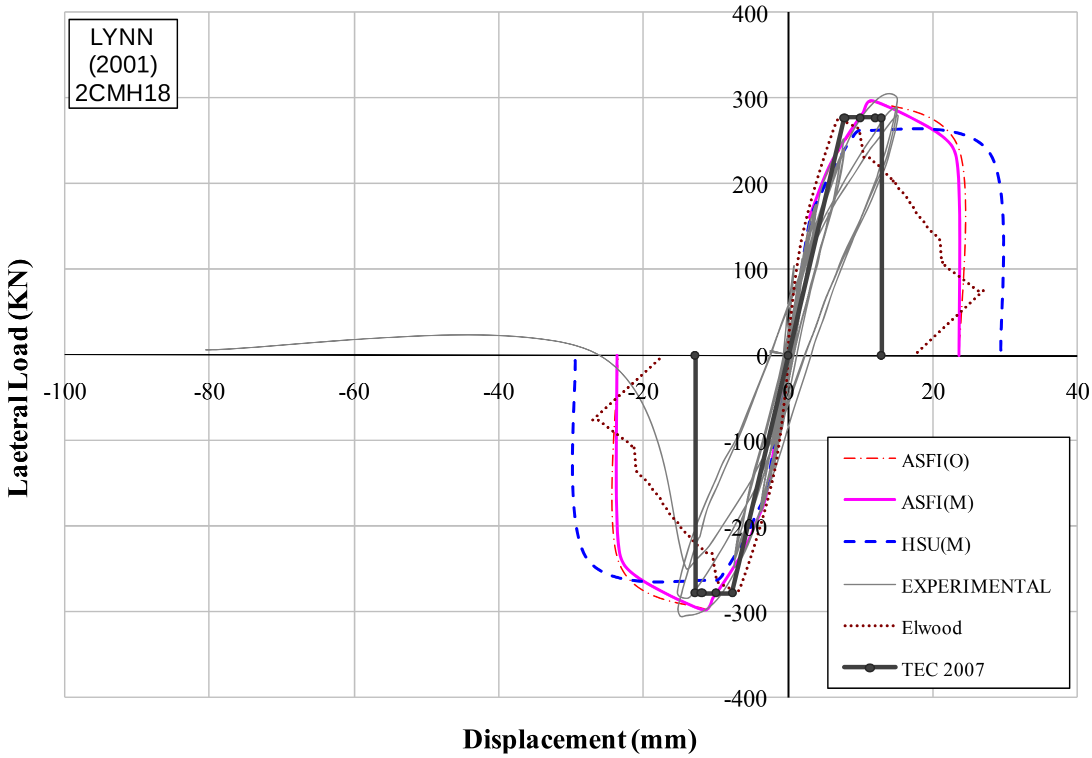

Figure 2.8 Lateral Load Displacement Curves of Flexure-Shear Failure Specimens Estimated by Use of Different Models and TEC2007 Nonlinear Procedure together with the Experimental One.

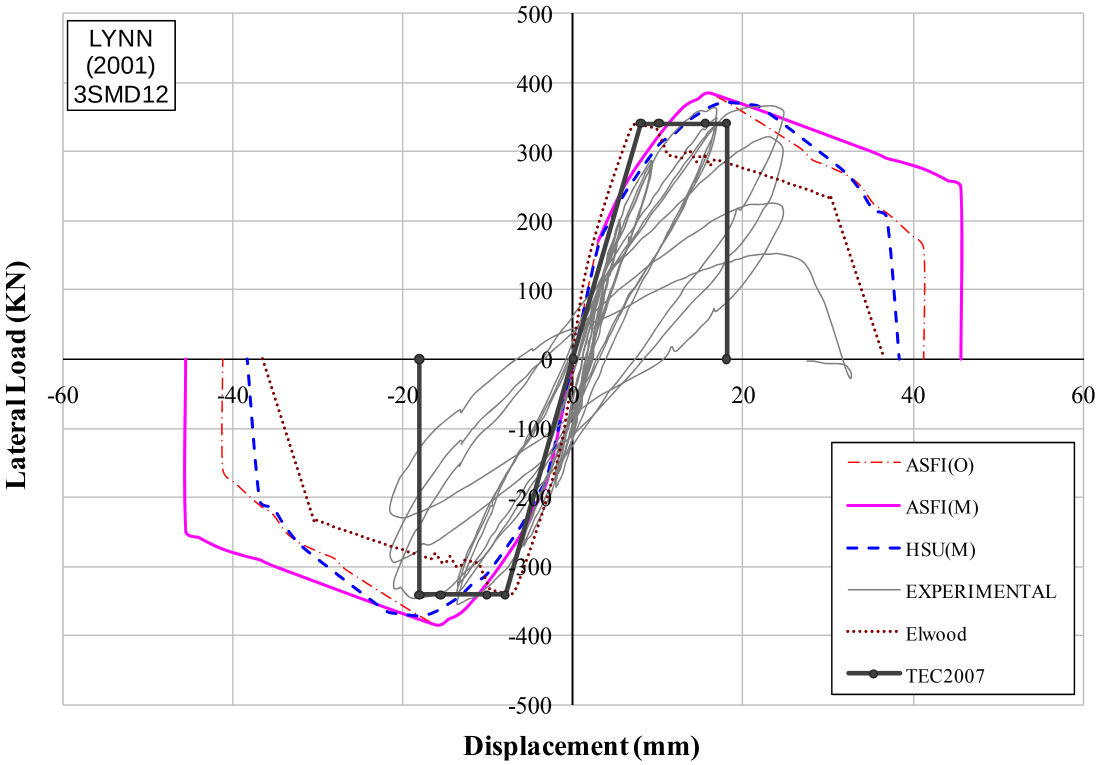

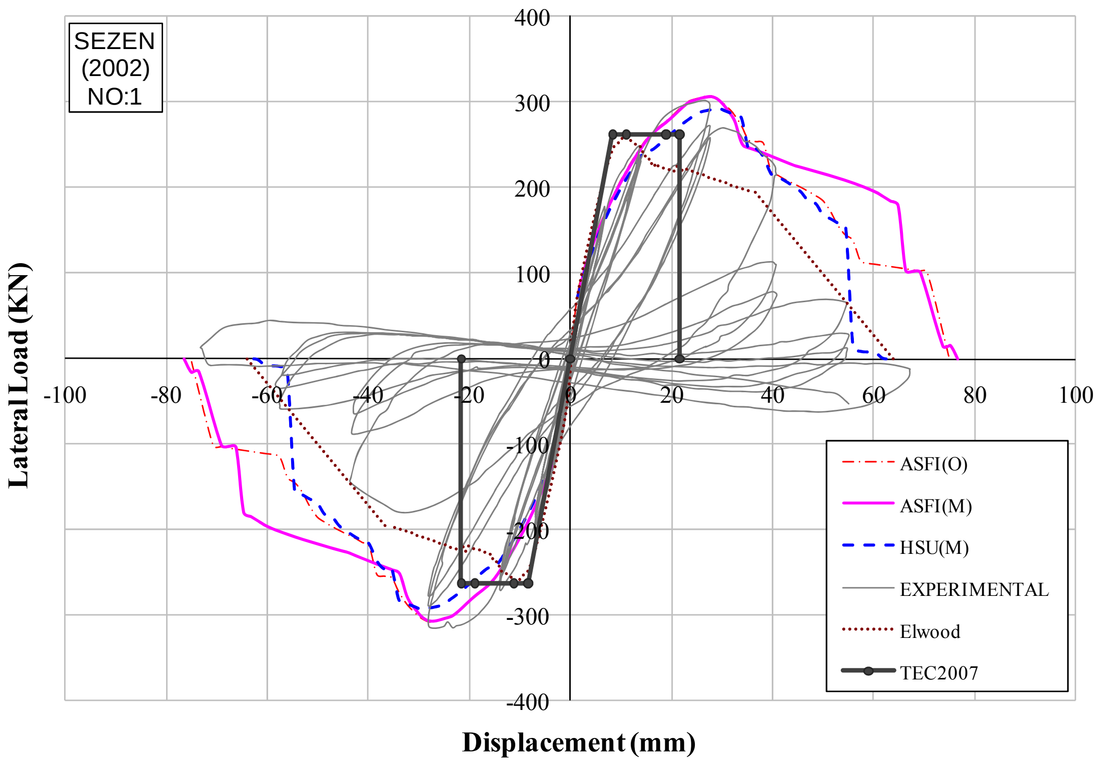

Figure 2.8 (Cont'd) Lateral Load Displacement Curves of Flexure-Shear Failure Specimens Estimated by Use of Different Models and TEC2007 Nonlinear Procedure together with the Experimental One.

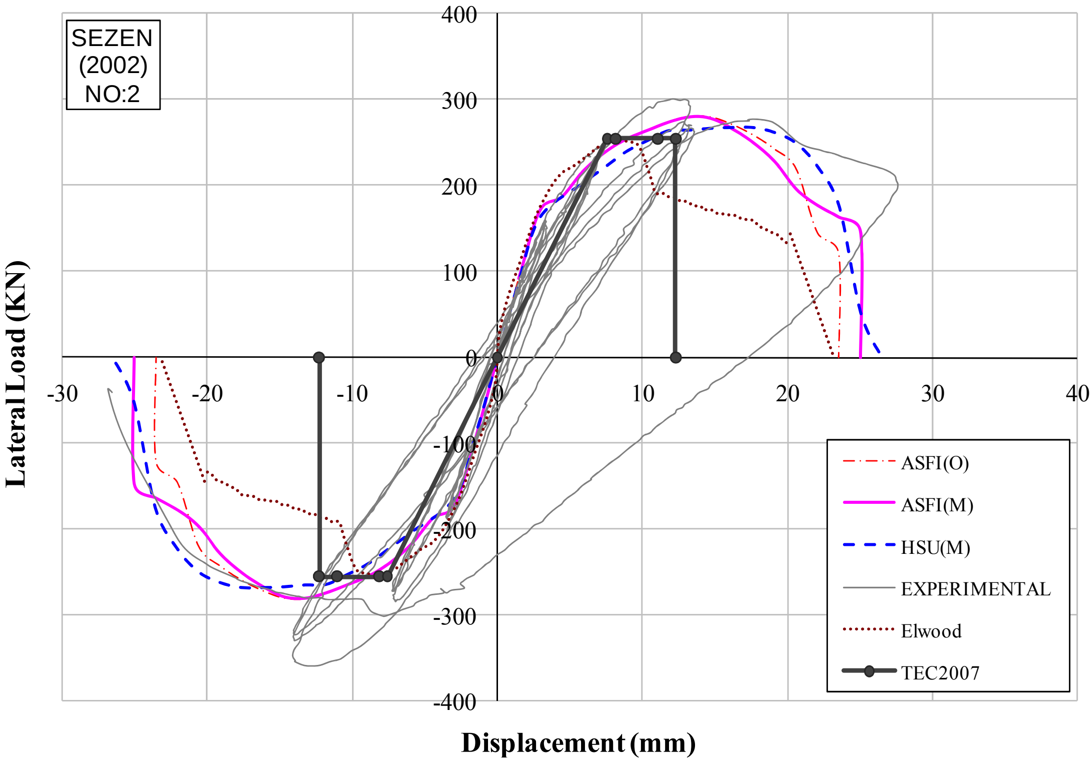

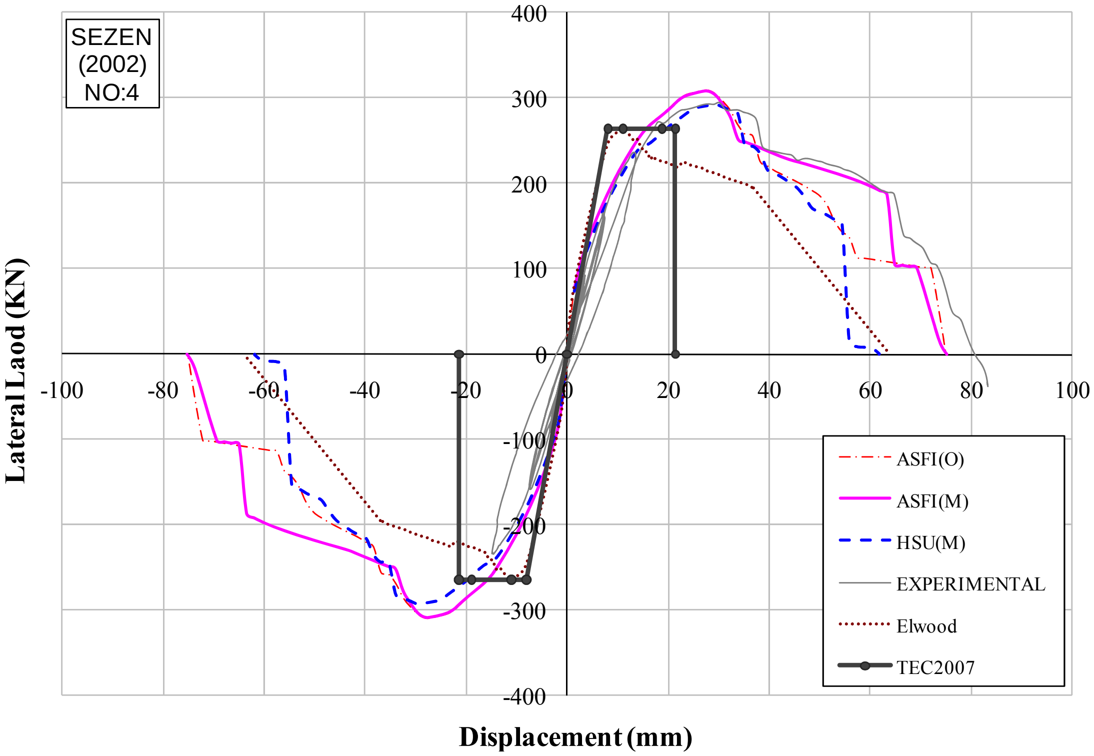

Figure 2.8 (Cont'd) Lateral Load Displacement Curves of Flexure-Shear Failure Specimens Estimated by Use of Different Models and TEC2007 Nonlinear Procedure together with the Experimental One.

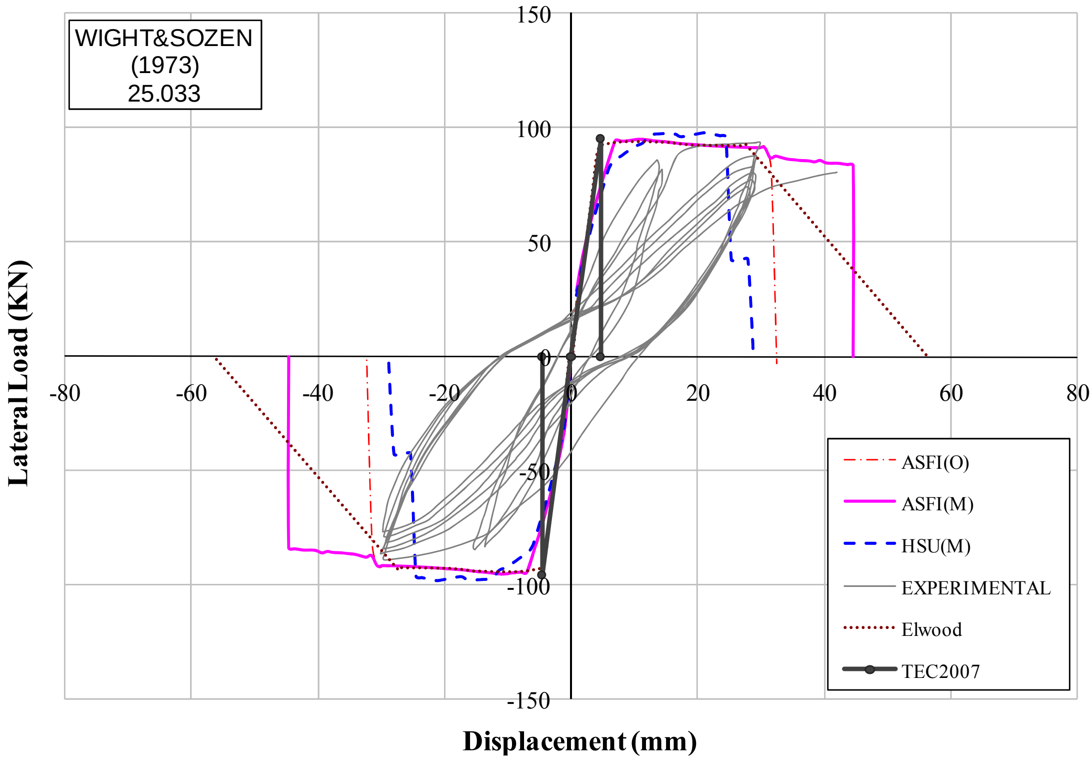

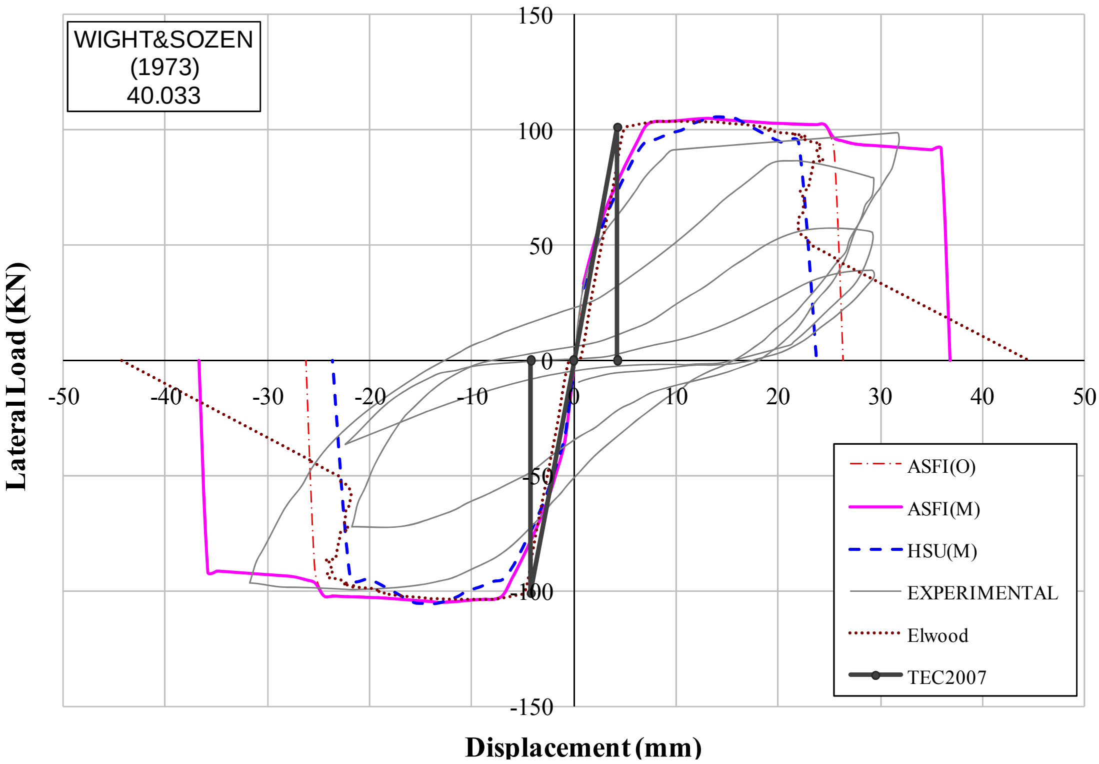

Figure 2.8 (Cont'd) Lateral Load Displacement Curves of Flexure-Shear Failure Specimens Estimated by Use of Different Models and TEC2007 Nonlinear Procedure together with the Experimental One.

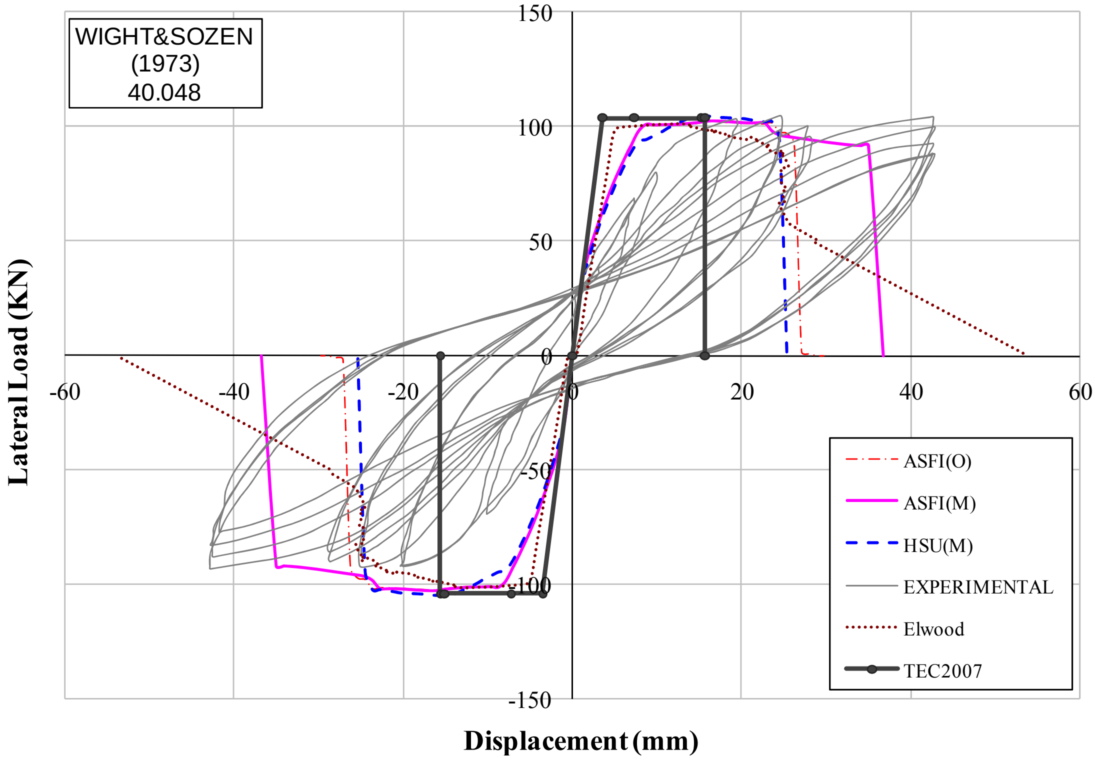

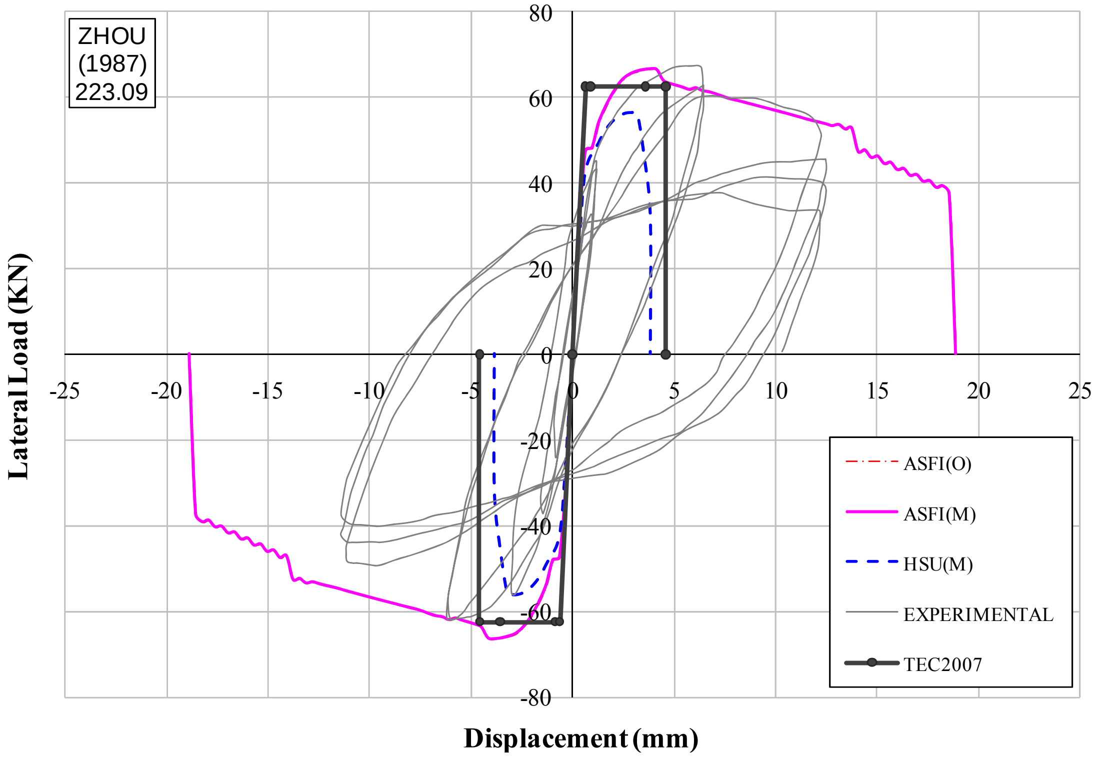

Figure 2.8 (Cont'd) Lateral Load Displacement Curves of Flexure-Shear Failure Specimens Estimated by Use of Different Models and TEC2007 Nonlinear Procedure together with the Experimental One.

When the graphs presented in Figure 2.8 are examined, following conclusions can be drawn.

- All models predicted the lateral load capacity satisfactorily.
- Estimations of HSU(M) model for lateral load capacity is generally conservative. However stiffness until the peak point is accurately estimated by HSU(M) model.
- ASFI(M) and ASFI(O) yielded similar load deformation response for all columns. Drift at shear failure is better estimated by ASFI(M) model on the other hand ASFI(O) predicted the drift at axial failure better.
- Since only flexural deformations are included in ELWOOD model until the drift at shear failure, drift estimations are conservative before shear failure. Inclusion of slip and shear deformations can improve the drift estimations.
- All models predicted the pre-peak response with high accuracy.
- TEC2007 nonlinear procedure is conservative for post peak response. In addition, it yielded wrong failure type for some of the columns especially for those having shear strength close to lateral load causing plastic hinging at column ends.
- Increase in axial load level caused decrease in drift capacity of columns and increase in lateral load capacity. Estimations follow a similar trend.
- Decrease in transverse reinforcement spacing is observed to improve drift capacities obviously.

When the response estimation presented in Figure 2.9 is studied following conclusions can be made;

- Estimations of TEC2007 are conservative. It estimated wrong failure type for some of the columns.
- Especially for specimens having transverse reinforcement ratio smaller than 0.001, models resulted in higher deformation capacities and strength when compared to test results. It can be said that for columns having transverse reinforcement ratio smaller than 0.001, use of models is not appropriate.
- ASFI (M) and ASFI (O) models yielded similar load deformation response. Axial failure drifts are better estimated by ASFI(M) models when compared to other models.
- For intermediate axial load levels (around 0.25) axial load and lateral load capacities were lost around same drift.
- For columns having closely spaced transverse reinforcement (HPRC1063), predictions of TEC2007 may fall into un safe side.

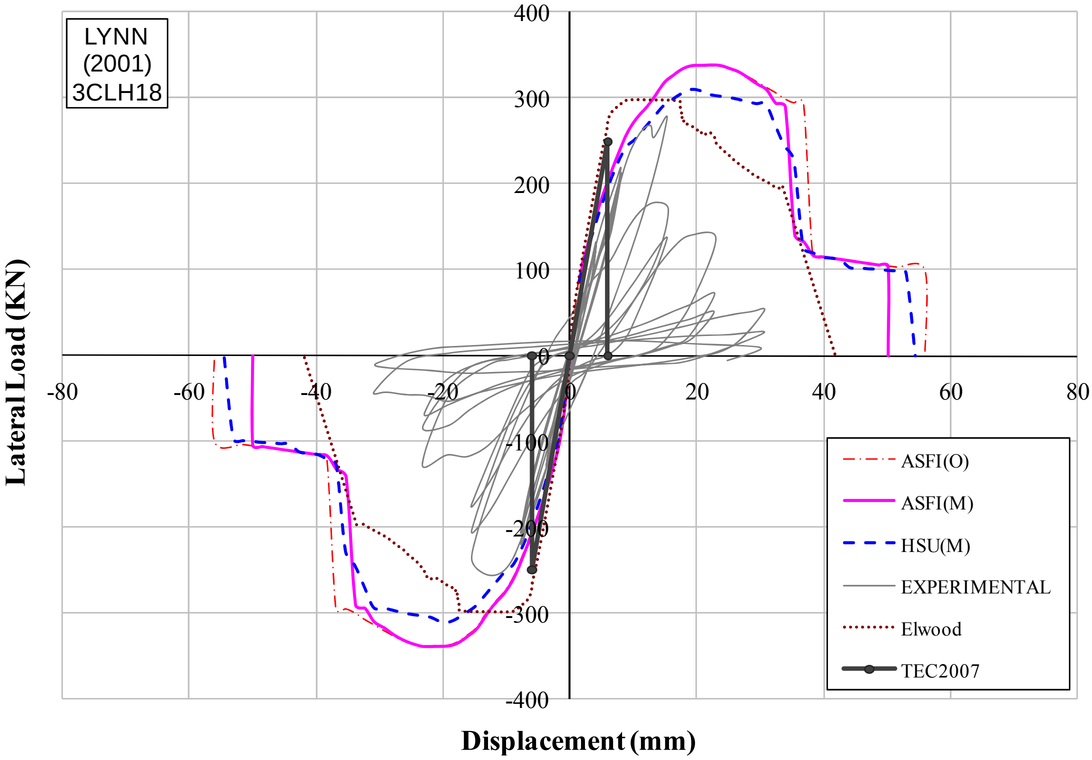

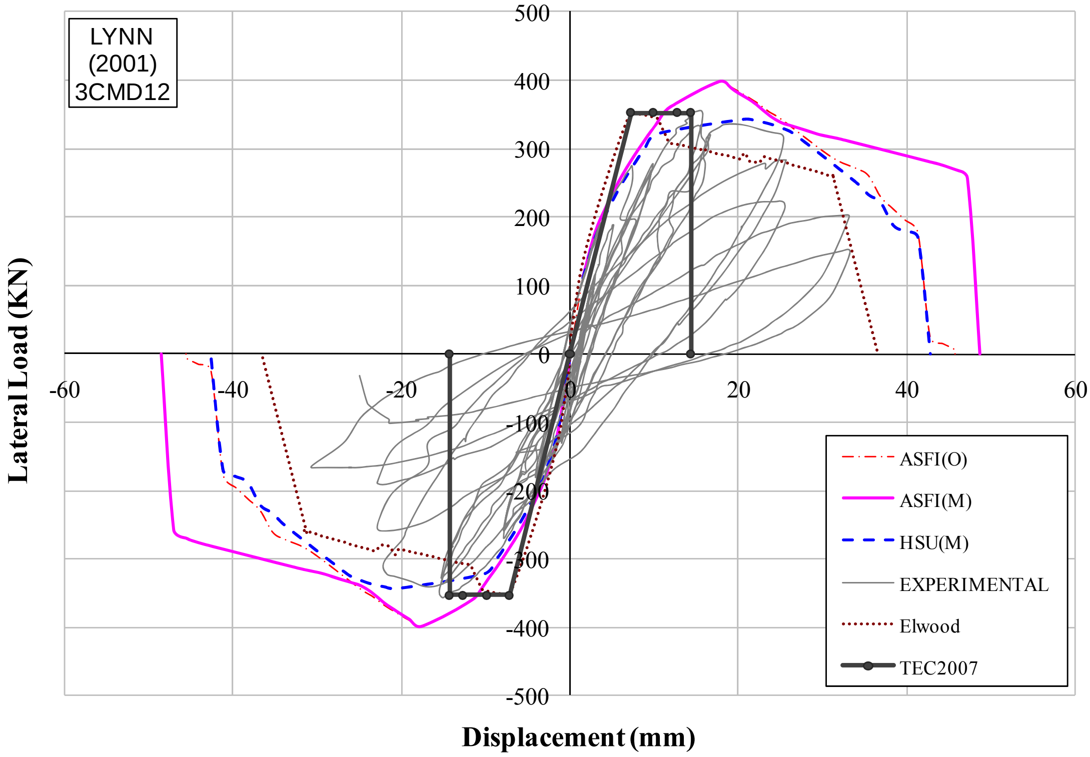

Figure 2.9 Lateral Load Displacement Curves of Shear Failure Specimens Estimated by Use of Different Models and TEC2007 Nonlinear Procedure together with the Experimental One.

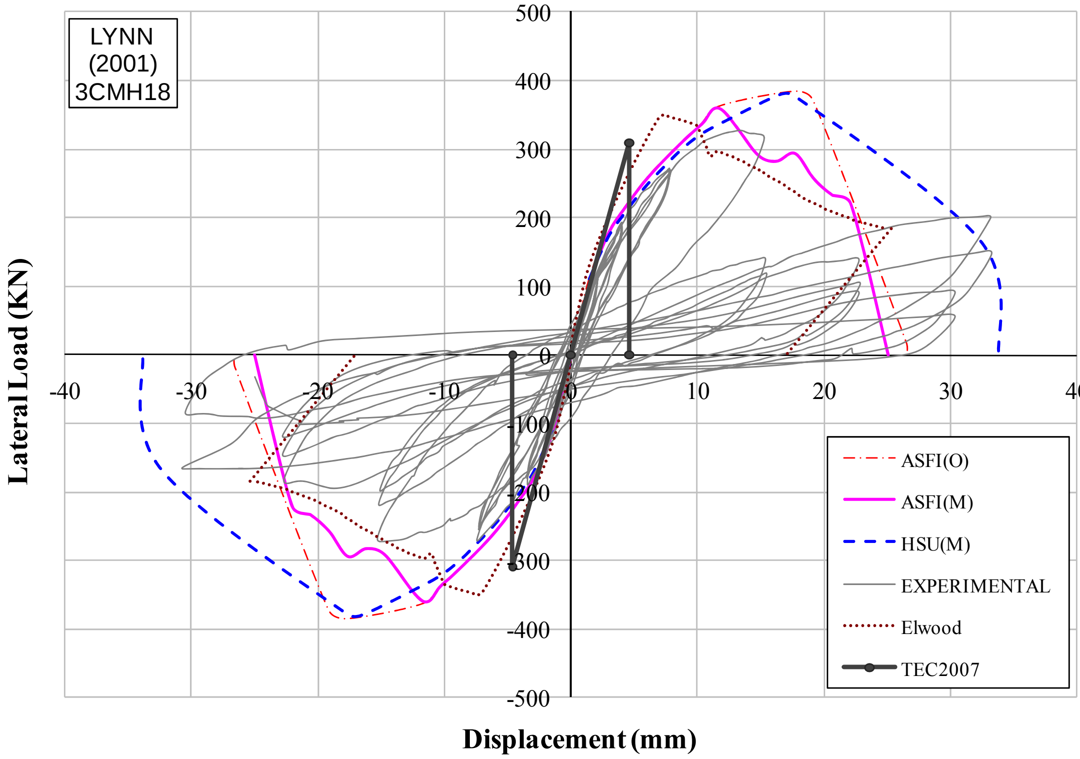

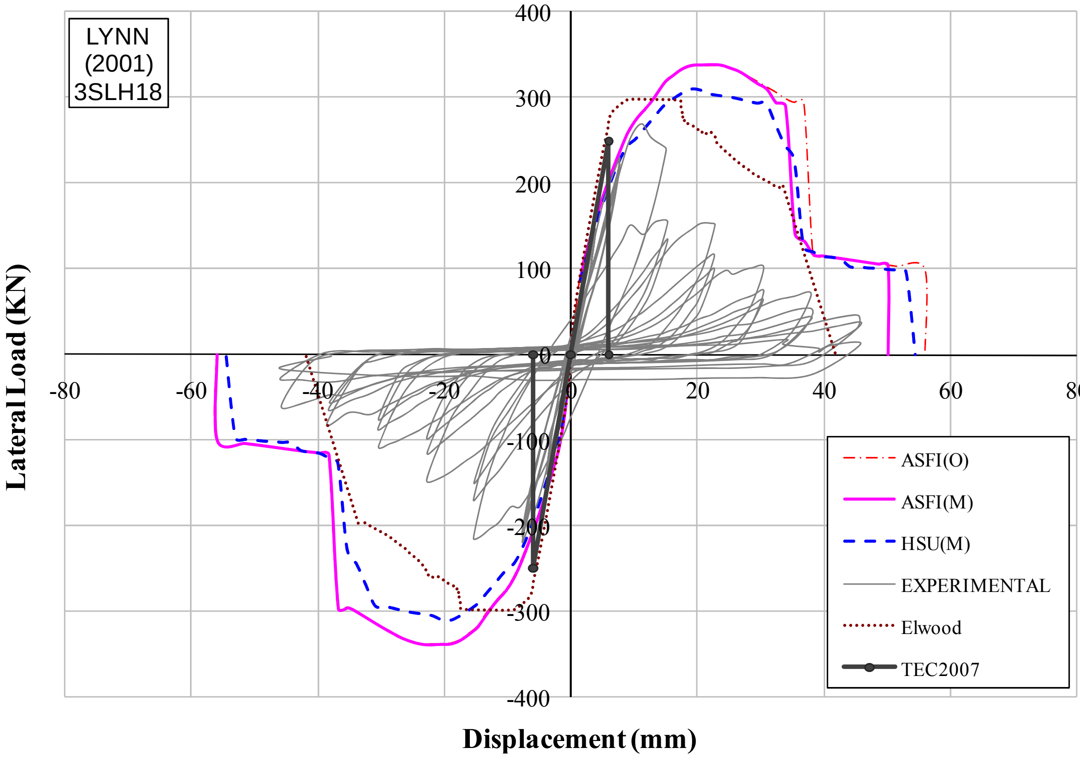

Figure 2.9 (Cont'd) Lateral Load Displacement Curves of Shear Failure Specimens Estimated by Use of Different Models and TEC2007 Nonlinear Procedure together with the Experimental One.

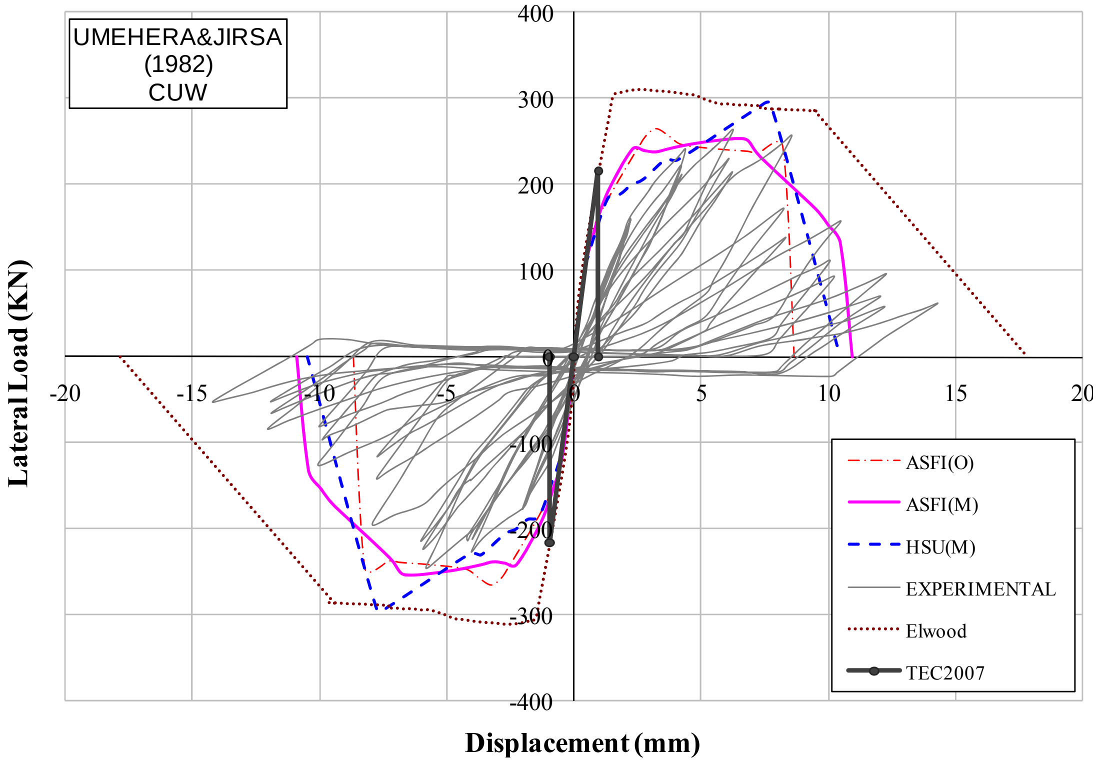

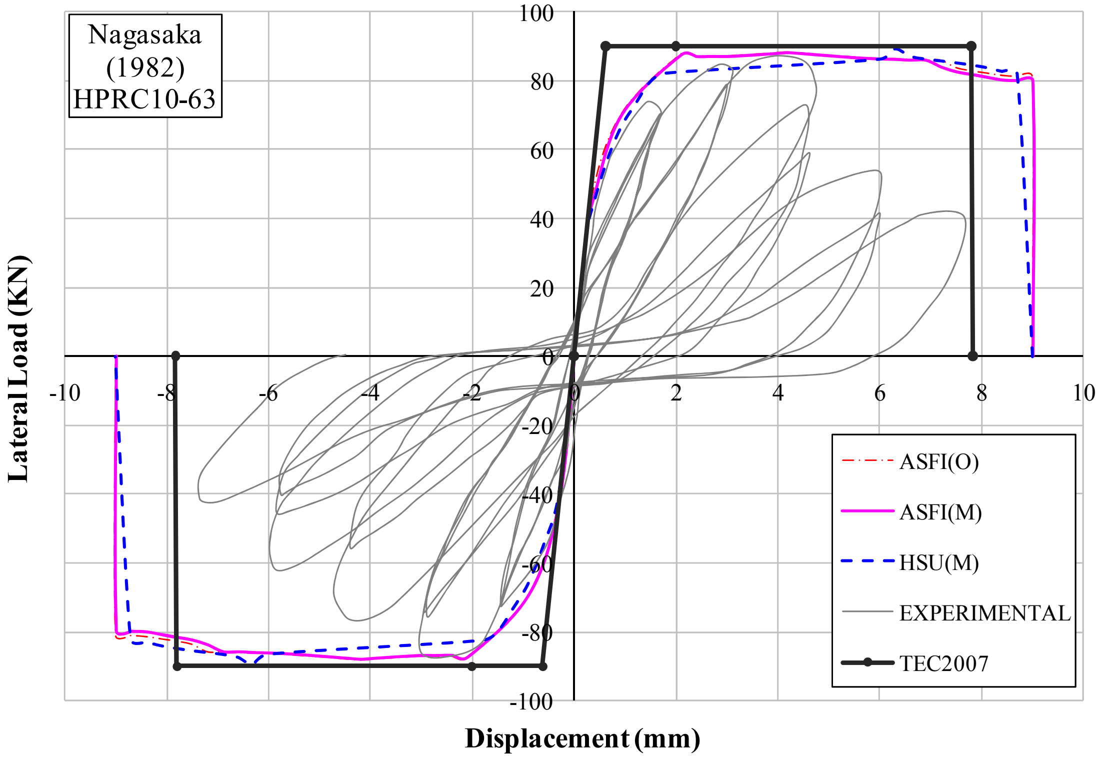

Figure 2.9 (Cont'd) Lateral Load Displacement Curves of Shear Failure Specimens Estimated by Use of Different Models and TEC2007 Nonlinear Procedure together with the Experimental One.

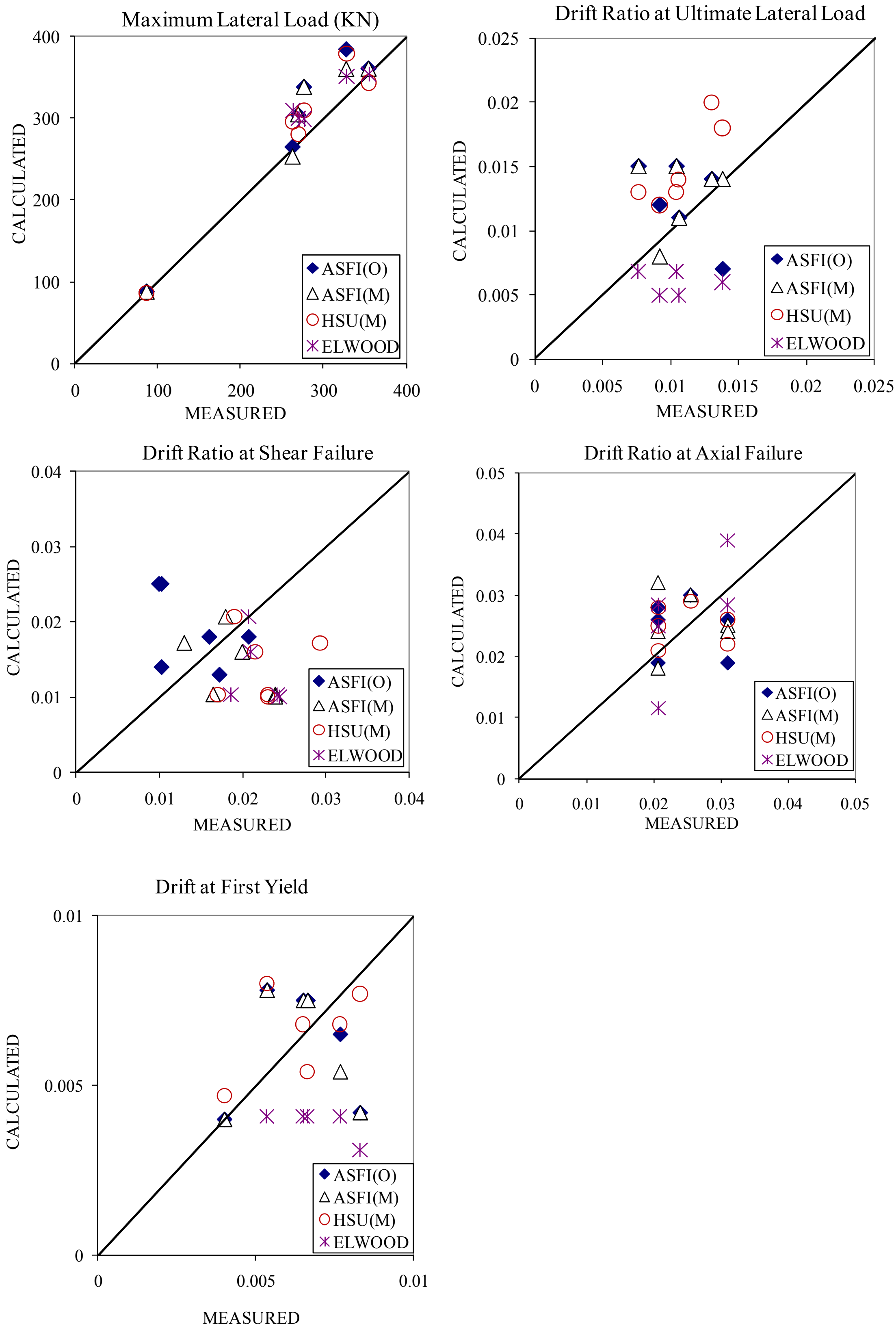

Figure 2.10 Comparison of Calculated and Measured Properties for Columns Experienced Shear Failure

When the results in Figure 2.10 are investigated, for performance of models used for the analysis of specimens that experienced shear failure, following conclusions can be drawn:

- Lateral load capacity is better estimated by HSU(M) and ASFI(M) both having mean value 1.07 and standard deviations 0.08 and 0.09 respectively. However, ASFI(O) (μ=1.09, σ=0.09) and ELWOOD (μ=1.09, σ=0.07) also predicted the lateral load capacity satisfactorily.
- Drift ratio at ultimate lateral load can be predicted hardly with a high accuracy because it depends on many factors such as rate of displacement increments and confinement properties. Drift ratio at ultimate lateral load is predicted with a moderate degree of accuracy by ASFI(M) (μ=1.24, σ=0.41) and ASFI(O) (μ=1.22, σ=0.49) models. HSU(M) (μ=1.41, σ=0.18) overestimated drift at ultimate lateral load and ELWOOD (μ=0.60, σ=0.18) predicted this column performance index conservatively. ELWOOD predictions of drift ratios before the shear failure is expected to be conservative because bar slip and shear deformations are neglected and only flexural deformations are included in calculation.
- None of the models is able to consider opening of the hoops and slip of the lateral reinforcements and the stiffness degradation due to opening and closing of the cracks resulting from cyclic nature of the loading. Therefore, drift ratio at shear failure could not be predicted accurately for any of the specimens. Drift ratio at shear failure is better estimated by ASFI(O) (μ=1.51, σ=0.77) and ASFI (M) (μ=1.53, σ=0.71) models. Scatter is high in prediction of this column performance index. This can be caused by complicated behavior of shear failure.
- Drift ratio at axial failure is predicted with a relatively high accuracy when compared to shear failure. ASFI(O) (μ=1.03, σ=0.28) and HSU(M) (μ=1.04, σ=0.24) models. However, ASFI(M) (μ=1.06, σ=0.30) and ELWOOD (μ=1.06, σ=0.33) models also predicted that performance point satisfactorily. It is observed that after shear failure occurred most of the columns able to carry the axial load until the loss of the lateral load carrying capacity.
- Drift ratio at first yield is predicted well by ASFI(O) (μ=1.02, σ=0.32) and ASFI(M) (μ=0.99, σ=0.34) models. That property is important to calculate the ductility of the section. All of the columns experienced yielding before failed in shear failure mode.

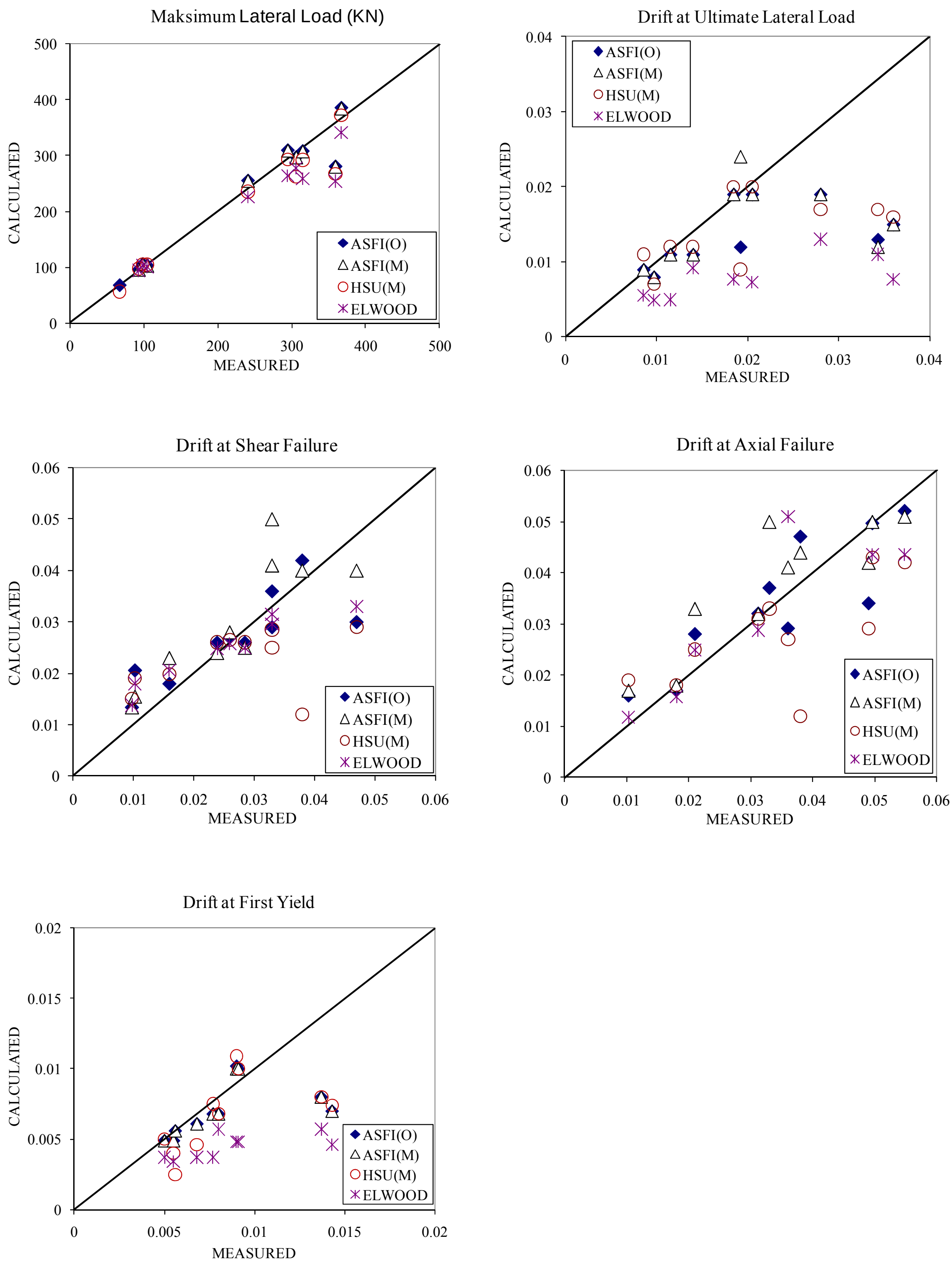

Figure 2.11 Comparison of Calculated and Measured Properties for Columns Experienced Flexure-Shear Failure

When the results in Figure 2.11 are investigated, for the performance of models used for the analysis of specimens experienced flexure shear failure, following conclusions can be drawn:

- Lateral load capacity of the sections is well predicted by ASFI(O) (μ=0.99, σ=0.08) and ASFI(M) (μ=0.99, σ=0.08) models with similar accuracies. HSU(M) (μ=0.95, σ=0.10) and ELWOOD(μ=92, σ=0.10) models also predicted satisfactorily being conservative than ASFI(M) and ASFI(O) models. Since flexure-shear failed specimens first reached moment capacity and then shear failure occurred at increased ductility demands, ELWOOD predictions are also good because it is based on flexural behavior of the section.
- Drift ratio at ultimate lateral load predicted at an early stage than the real case. That result is different from the result obtained for shear-failed specimens where predictions are late when compared to real case. The reason may be overestimation in stiffness values after the first cracking occurred. Because, after the first cracking occurs stiffness decreases and spalling of cover concrete causes stiffness degradation. Drift ratio at ultimate load is better predicted by ASFI(M) (μ=0.83, σ=0.28) model. ELWOOD (μ=0.45, σ=0.14) predictions are poor as in case of shear-failed specimens.
- Drift ratio at shear failure is predicted satisfactorily when compared to shear-failed specimens. ASFI(M) (μ=1.17, σ=0.29) has lower scatter but higher mean value. HSU(M) (μ=1.01, σ=0.49) has a better mean value but scatter is higher. ASFI(O) (μ=1.11, σ=0.40) and ELWOOD (μ=1.05, σ=0.33) also performed well to estimate that performance point. Drift ratio at shear failure is higher for most of the specimens when compared to shear-failed specimens.
- Drift ratio at axial failure is better predicted by ASFI(O) (μ=1.07, σ=0.25) model. HSU(M) (μ=0.93, σ=0.40), ASFI(M) (μ=1.19, σ=0.29), ELWOOD (μ=1.16, σ=0.36) models also predicted that performance point satisfactorily. Ductility of the flexure-shear critical specimens are higher when compared to shear failed specimens.
- Drift ratio at first yield is better predicted by ASFI(M) and ASFI(O) (μ=0.88, σ=0.20) models. Since two models mostly predicted the pre-peak response similarly, they both have similar mean and standard deviation values. HSU(M) (μ=0.81, σ=0.26) also predicted the response within acceptable limits. ELWOOD predictions are poor for drift at first yield. When predictions of all models are studied, it is seen that for most of the specimens drift ratio at yield point is predicted at early stage. This observation shows that stiffness is overestimated at the models.

Results of the statistical analysis are presented in Table 2.3 and Table 2.4.

Table 2.3 Statistical Analysis Performed on Estimated Properties of Column Specimens That Experienced Shear Failure

Specimen	Maximum Lateral Load				Drift at First Yield			
	$V_{ASFI(O)}/V_{TEST}$	$V_{ASFI(M)}/V_{TEST}$	$V_{HSU(M)}/V_{TEST}$	V_{ELWOOD}/V_{TEST}	ASFI(O)/TEST	ASFI(M)/TEST	HSU(M)/TEST	ELWOOD/TEST
3CLH18	1.22	1.22	1.12	1.08	1.15	1.15	1.05	0.63
3CMH18	1.17	1.10	1.16	1.07	0.85	0.70	0.89	0.53
3CMD12	1.02	1.01	0.97	1.00	1.13	1.13	0.81	0.62
3SLH18	1.13	1.13	1.04	1.11	1.46	1.46	1.50	0.77
CUW	1.01	0.96	1.12	1.18	0.51	0.51	0.93	0.37
HPRC10-63	1.01	1.01	0.99	NA	1.00	1.00	1.18	NA
μ(Mean)=	1.09	1.07	1.07	1.09	1.02	0.99	1.06	0.58
σ(St.Dev)=	0.09	0.09	0.08	0.07	0.32	0.34	0.25	0.14
COV:	0.09	0.09	0.07	0.06	0.32	0.34	0.24	0.25

Drift at Ultimate Lateral Load				Drift at Shear Failure			
ASFI(O)/TEST	ASFI(M)/TEST	HSU(M)/TEST	ELWOOD/TEST	ASFI(O)/TEST	ASFI(M)/TEST	HSU(M)/TEST	ELWOOD/TEST
1.44	1.44	1.25	0.65	2.43	2.33	2.23	2.35
1.31	0.87	1.31	0.55	1.36	1.60	1.65	1.81
1.04	1.04	1.32	0.47	1.13	1.25	1.34	1.31
1.97	1.97	1.71	0.89	2.50	2.40	2.30	2.44
0.51	1.01	1.30	0.43	0.87	0.87	0.92	1.00
1.08	1.08	1.54	NA	0.76	0.76	1.70	NA
1.22	1.24	1.41	0.60	1.51	1.53	1.69	1.78
0.49	0.41	0.18	0.18	0.77	0.71	0.53	0.63
0.40	0.33	0.13	0.31	0.51	0.46	0.31	0.35

Specimen	Drift at Axial Failure			
	ASFI(O)/TEST	ASFI(M)/TEST	HSU(M)/TEST	ELWOOD/TEST
3CLH18	1.26	1.16	1.21	1.38
3CMH18	0.92	0.87	1.01	0.56
3CMD12	1.35	1.55	1.35	1.20
3SLH18	0.84	0.81	0.84	0.92
CUW	0.61	0.77	0.71	1.26
HPRC10-63	1.18	1.18	1.14	NA
μ(Mean)=	1.03	1.06	1.04	1.06
σ(St.Dev)=	0.28	0.30	0.24	0.33
COV:	0.28	0.28	0.23	0.31

Table 2.4 Statistical Analysis Performed on Estimated Properties of Column Specimens That Experienced Flexure-Shear Failure

	Maximum Lateral Load				Drift at First Yield			
Specimen	$\frac{V_{ASFI(O)}}{V_{TEST}}$	$\frac{V_{ASFI(M)}}{V_{TEST}}$	$\frac{V_{HSU(M)}}{V_{TEST}}$	$\frac{V_{ELWOOD}}{V_{TEST}}$	$\frac{ASFI(O)}{TEST}$	$\frac{ASFI(M)}{TEST}$	$\frac{HSU(M)}{TEST}$	$\frac{ELWOOD}{TEST}$
2CLH18	1.06	1.06	0.98	0.94	0.98	0.98	1.00	0.74
2CMH18	0.97	0.97	0.86	0.91	0.89	0.89	0.73	0.62
3SMD12	1.05	1.05	1.01	0.93	0.88	0.88	0.97	0.48
NO:1	0.98	0.98	0.93	0.82	1.13	1.11	1.21	0.53
NO:2	0.78	0.78	0.75	0.71	0.90	0.90	0.68	0.54
NO:4	1.05	1.05	0.99	0.90	1.10	1.10	1.10	0.53
25.033	1.02	1.02	1.05	1.01	0.49	0.49	0.52	0.32
40.033a	1.06	1.06	1.07	1.05	0.85	0.85	0.85	0.71
40.048	0.98	0.98	1.00	0.97	0.58	0.58	0.58	0.42
223.09	1.00	0.99	0.84	NA	1.00	1.00	0.45	NA
μ(Mean)=	0.99	0.99	0.95	0.92	0.88	0.88	0.81	0.54
σ(St.Dev)=	0.08	0.08	0.10	0.10	0.20	0.20	0.26	0.13
COV:	0.08	0.08	0.11	0.11	0.23	0.23	0.32	0.25

	Drift at Ultimate Lateral Load				Drift at Shear Failure			
Specimen	$\frac{ASFI(O)}{TEST}$	$\frac{ASFI(M)}{TEST}$	$\frac{HSU(M)}{TEST}$	$\frac{ELWOOD}{TEST}$	$\frac{ASFI(O)}{TEST}$	$\frac{ASFI(M)}{TEST}$	$\frac{HSU(M)}{TEST}$	$\frac{ELWOOD}{TEST}$
2CLH18	0.79	0.79	0.86	0.66	1.04	1.08	1.02	1.02
2CMH18	0.82	0.82	0.72	0.51	2.00	1.50	1.84	1.79
3SMD12	0.96	0.96	1.04	0.43	1.16	1.48	1.28	1.26
NO:1	1.03	1.03	1.08	0.42	1.02	0.94	1.02	0.93
NO:2	1.05	1.05	1.29	0.64	1.52	1.52	1.70	1.27
NO:4	0.93	0.93	0.98	0.36	0.91	0.87	0.91	0.86
25.033	0.38	0.35	0.50	0.32	1.00	1.39	0.79	0.86
40.033a	0.42	0.42	0.44	0.21	0.80	1.13	0.69	0.84
40.048	0.68	0.68	0.61	0.46	0.54	0.72	0.52	0.62
223.09	0.63	1.25	0.47	NA	1.11	1.05	0.32	NA
μ(Mean)=	0.77	0.83	0.80	0.45	1.11	1.17	1.01	1.05
σ(St.Dev)=	0.24	0.28	0.29	0.14	0.40	0.29	0.49	0.35
COV:	0.31	0.34	0.37	0.32	0.36	0.25	0.48	0.33

	Drift at Axial Failure			
Specimen	$\frac{ASFI(O)}{TEST}$	$\frac{ASFI(M)}{TEST}$	$\frac{HSU(M)}{TEST}$	$\frac{ELWOOD}{TEST}$
2CLH18	1.03	1.03	0.99	0.92
2CMH18	1.55	1.65	1.84	1.15
3SMD12	1.33	1.57	1.19	1.18
NO:1	1.00	1.01	0.87	0.88
NO:2	0.94	1.00	1.00	0.88
NO:4	0.95	0.93	0.77	0.79
25.033	1.12	1.52	1.00	1.94
40.033a	0.81	1.14	0.75	1.42
40.048	0.69	0.86	0.59	1.24
223.09	1.24	1.16	0.32	NA
μ(Mean)=	1.07	1.19	0.93	1.16
σ(St.Dev)=	0.25	0.29	0.40	0.36
COV:	0.24	0.24	0.43	0.31

According to the statistical analysis and observations on graphical representations, following conclusions can be drawn:

- When shear-failed specimens are considered, it is seen that all models predicted shear strengths that agree well with the tests. When drift estimations are examined, it is seen that overall behavior is predicted well; however, standard deviations shows slightly more scatter. Lack of considering a mechanically sound bond model may cause this scatter. This drawback can lead to low accuracy in prediction of drift at shear failure. Another point is that due to cyclic nature of the lateral loads, after the cover concrete crushed, restraints of the ninety-degree lateral reinforcement hooks are lost. Therefore, opening of the hooks can occur so that reinforcement cannot fully yield and small strength and displacement ductility are obtained which is also not considered in models. As a result, accuracy in estimation of lateral strength, drift at ultimate lateral load, and drift at shear failure is not quite well but models predict the failure mode accurately. None of the models predicted all performance points with the same level of accuracy. However, predictions of ASFI(M) and ASFI(O) models are better than those of others. When the predictions of ASFI(M) and ASFI(O) are compared, it is seen that the difference is small. ELWOOD model predicted the drift at shear failure and drift at axial failure with accuracy close to those of ASFI(M) and ASFI(O). When TEC2007 procedure is examined, it is seen that procedure yields conservative results and predicts elastic perfectly brittle type of behavior for shear-failed specimens. Results showed that, a shear critical member could sustain gravity loads up to higher displacement levels even if it fails under shear.

- When statistical analyses of the Flexure-Shear failure specimens are examined, it is seen that lateral load capacity, drift at first yield and drift at shear failure agree well with the test results. Standard deviations are small when compared to estimations of shear-failed specimens. For flexure-shear failure specimens, standard deviations are acceptable for strength and deformation estimations. It is observed that none of the models predicts all performance points with the same level of accuracy. While one of the models predicts the drift at axial failure better, the other predicts drift at shear failure better. However, ASFI(M) and ASFI(O) models predicted the failure mode accurately for all models. ELWOOD predictions for drift at shear failure and drift at axial failure have accuracy comparable well with those of ASFI models. ASFI(M) and ASFI(O) models yielded similar results. Difference between their predictions is negligible. When TEC2007 procedure performance is studied, it is seen that predictions are overly conservative for all specimens. TEC2007 predicts the failure mode as “ductile” for shear critical members experience flexure-shear failure that has relatively high shear strength when compared to shear force to develop flexural strength. However, when shear strength and shear force to develop moment capacity are close and ratio of them is close to unity, TEC2007 predicts the response as “Brittle” being on conservative side. This prediction does not reflect the reality even if the results are conservative. It is observed that code predicts some of the flexure-shear failure cases as “Ductile” failure. TEC2007 predicted the response of a shear critical column (HPRC10-63) as a “ductile” column. Closely spaced transverse reinforcement resulted in higher drifts in performance levels. Because, its modeling process constructed on the mechanical background and it has better mean and less scatter of column performance indices as shown in Table 2.4, ASFI(M) model will be utilized throughout the study in order to estimate the performance of columns.

CHAPTER 3

PARAMETRIC STUDIES AND PROPOSED DRIFT LIMITS

3.1. General

Parametric studies are performed in order to develop simple equations for performance points such as drift ratio at shear failure and drift ratio at axial failure. In addition, relationships of drift ratio at shear failure and drift ratio at axial failure with different variables such as transverse reinforcement ratio, axial load ratio, shear span to depth ratio and flexural and shear strength of the section are examined. Developed simple equations are then used to estimate lateral load-displacement curves of the specimens described in Chapter 2 of the study.

3.2. Column Specimens

Column database properties presented in Chapter 2 does not fully comply with the properties of columns used in Turkish construction practice. Especially, concrete compressive strength, aspect ratio of column section size can show significant variation. To overcome this deficiency of the column database additional columns were analyzed by utilizing the ASFI(M) model, which was found to be the most accurate among the five examined models. Three widely used column sections are chosen for analysis. Those sections are 400 mm x 400 mm square column, 200 mm x 800 mm and 300mm x 500 mm rectangular columns. Reinforcement steel grade is taken as S420 with yield stress of 420 Mpa and S220 with yield stress of 220 Mpa for longitudinal and transverse reinforcement steel, respectively. Concrete compressive strength is taken as 10 Mpa. In order to cover most of the columns used in older construction practice in Turkey, five axial load ratios 0, 0.1, 0.2, 0.3, and 0.4 are examined.

Transverse reinforcement ratio, ρ_v is selected to range from 0.00126 to 0.0053. Longitudinal reinforcement ratio, ρ_l is selected as 0.01 and it is same for all specimens. Column lengths are chosen as 1000 mm, 1500 mm, 2000 mm, and 3000 mm. Shear span to effective depth ratio, *a/d* is varied between 0.65 and 3.27. Columns are considered to be under double curvature bending and shear span is taken as half of the column length. (i.e., inflection points are at mid points along the column length.) Selected specimens are named according to the labeling described in Figure 3.1. Column properties are presented in Table 3.1. Column sections and reinforcement configuration are shown in Figure 3.2. In addition to selected column specimens, a number of the shear critical columns that were used by Elwood [9] and some of the columns studied in chapter 2 are also used for verification purposes and in the development of new equations. Database of shear critical columns reported by Elwood [9] and taken as reference to this study is presented in Table 3.2. Database of shear critical columns that experienced axial failure from Peer Column Database [4] is also used to make comparison between estimations of developed equations and of equations proposed by Elwood [9]. Database of the columns that experienced axial failure is presented in Table 3.3.

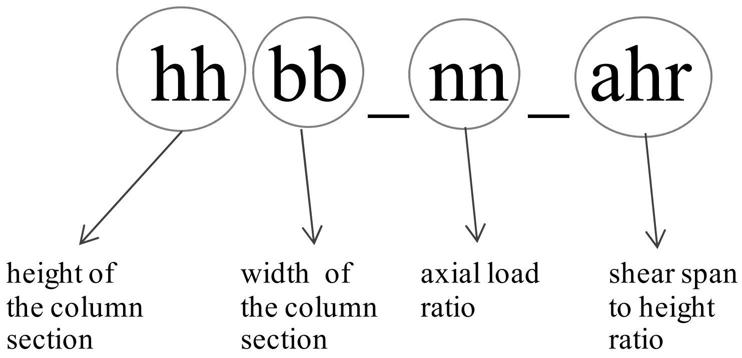

Figure 3.1 Notation for the Parametric Study Column Specimens

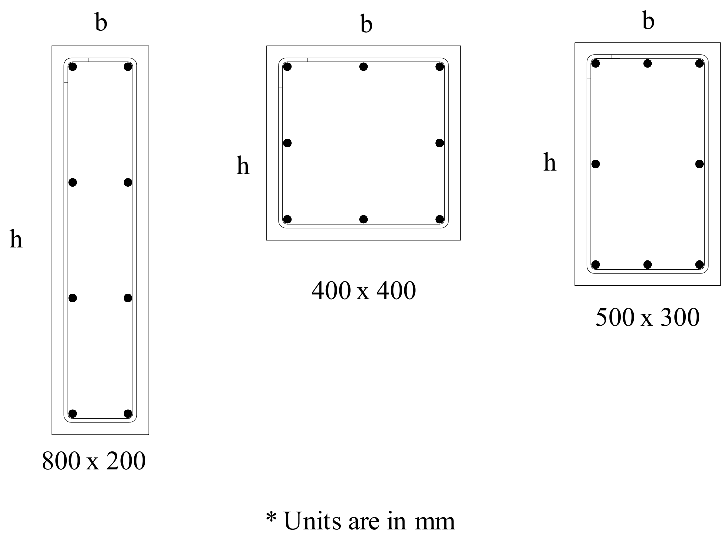

Figure 3.2 Geometry and Reinforcement Details of Parametric Study Columns

Table 3.1 Properties of the Shear Critical Columns Analyzed in Parametric Study

Specimen	b (mm)	h (mm)	cc (mm)	d (mm)	a (mm)	a/d	s (mm)	ρ_l	ρ_v	f_{yl} (Mpa)	f_{yv} (Mpa)	f_c' (Mpa)	P (KN)	$\frac{N}{A_g f_c'}$	M_n (KN.m)	V_n (KN)	V_y (KN)	$\frac{V_n}{V_y}$	V_{flex} (KN)	$\frac{V_n}{V_{flex}}$	Failure Type
8020_00_0.625	200	800	25	759	500	0.63	200	0.01	0.00251	420	220	10	0	0.0	217.1	171.3	310.0	0.55	434.2	0.39	S
8020_01_0.625	200	800	25	759	500	0.63	200	0.01	0.00251	420	220	10	160	0.1	243.6	177.4	390.0	0.45	487.2	0.36	S
8020_02_0.625	200	800	25	759	500	0.63	200	0.01	0.00251	420	220	10	320	0.2	264.2	183.5	456.0	0.40	528.4	0.35	S
8020_03_0.625	200	800	25	759	500	0.63	200	0.01	0.00251	420	220	10	480	0.3	269.3	189.6	512.0	0.37	538.6	0.35	S
8020_04_0.625	200	800	25	759	500	0.63	200	0.01	0.00251	420	220	10	640	0.4	272.2	195.8	556.0	0.35	544.4	0.36	S
8020_00_0.94	200	800	25	759	750	0.94	200	0.01	0.00251	420	220	10	0	0.0	217.1	171.3	206.7	0.83	289.5	0.59	S
8020_01_0.94	200	800	25	759	750	0.94	200	0.01	0.00251	420	220	10	160	0.1	243.6	177.4	260.0	0.68	324.8	0.55	S
8020_02_0.94	200	800	25	759	750	0.94	200	0.01	0.00251	420	220	10	320	0.2	264.2	183.5	304.0	0.60	352.3	0.52	S
8020_03_0.94	200	800	25	759	750	0.94	200	0.01	0.00251	420	220	10	480	0.3	269.3	189.6	341.3	0.56	359.1	0.53	S
8020_04_0.94	200	800	25	759	750	0.94	200	0.01	0.00251	420	220	10	640	0.4	272.2	195.8	370.7	0.53	362.9	0.54	S
8020_00_1.25	200	800	25	757	1000	1.25	150	0.01	0.00527	420	220	10	0	0.0	272.2	262.6	155.0	1.69	272.2	0.96	F-S
8020_01_1.25	200	800	25	757	1000	1.25	150	0.01	0.00527	420	220	10	160	0.1	272.2	268.7	194.0	1.38	272.2	0.99	F-S
8020_02_1.25	200	800	25	757	1000	1.25	150	0.01	0.00527	420	220	10	320	0.2	272.2	274.8	228.0	1.21	272.2	1.01	F-S
8020_03_1.25	200	800	25	757	1000	1.25	150	0.01	0.00527	420	220	10	480	0.3	272.2	280.9	259.0	1.08	272.2	1.03	F-S
8020_04_1.25	200	800	25	757	1000	1.25	150	0.01	0.00527	420	220	10	640	0.4	272.2	287.0	283.0	1.01	272.2	1.05	F-S
8020_00_1.875	200	800	25	757	1500	1.88	200	0.01	0.00395	420	220	10	0	0.0	272.2	218.7	103.3	2.12	181.5	1.20	F-S
8020_01_1.875	200	800	25	759	1500	1.88	200	0.01	0.00251	420	220	10	160	0.1	272.2	177.4	128.7	1.38	181.5	0.98	F-S
8020_02_1.875	200	800	25	759	1500	1.88	200	0.01	0.00251	420	220	10	320	0.2	272.2	183.5	152.0	1.21	181.5	1.01	F-S
8020_03_1.875	200	800	25	759	1500	1.88	200	0.01	0.00251	420	220	10	480	0.3	272.2	189.6	172.0	1.10	181.5	1.04	F-S
8020_04_1.875	200	800	25	759	1500	1.88	200	0.01	0.00251	420	220	10	640	0.4	272.2	195.8	184.7	1.06	181.5	1.08	F-S

Notation: b: width of the section, h: height of the section, cc: concrete cover to transverse reinforcement , d: effective depth of the section, a: shear span (half of the column length), a/d: shear span to effective depth ratio, s: spacing of transverse reinforcement, ρ_l: longitudinal reinforcement ratio, ρ_v: transverse reinforcement ratio, f_{yl}: yield stress of longitudinal reinforcement, f_{yv}: yield stress of transverse reinforcement, f_c': concrete compressive stress, P: applied axial load, $N/A_g f_c$': axial load ratio, M_n: moment capacity of the section, V_n=shear strength of the section, V_y: lateral load causing first yielding in longitudinal reinforcement, V_{flex}: lateral load causes column to reach its moment capacity M_n, F-S: Flexure-shear failure, S: shear failure

Table 3.1 (cont'd) Properties of the Shear Critical Columns Analyzed in Parametric Study

Specimen	b (mm)	h (mm)	cc (mm)	d (mm)	a (mm)	a/d	s (mm)	ρ_l	ρ_v	f_{yl} (Mpa)	f_{yv} (Mpa)	f_c' (Mpa)	P (KN)	$\frac{N}{A_g f_c'}$	M_n (KN.m)	V_n (KN)	V_y (KN)	$\frac{V_n}{V_y}$	V_{flex} (KN)	$\frac{V_n}{V_{flex}}$	Failure Type
5030_0.0_1	300	500	25	459	500	1.00	200	0.01	0.00168	420	220	10	0	0.0	141.3	130.0	228.0	0.57	282.6	0.46	S
5030_0.1_1	300	500	25	459	500	1.00	200	0.01	0.00168	420	220	10	150	0.1	165.7	135.6	274.0	0.49	331.4	0.41	S
5030_0.2_1	300	500	25	459	500	1.00	200	0.01	0.00168	420	220	10	300	0.2	173.8	141.1	316.0	0.45	347.6	0.41	S
5030_0.3_1	300	500	25	459	500	1.00	200	0.01	0.00168	420	220	10	450	0.3	180.8	146.7	352.0	0.42	361.6	0.41	S
5030_0.4_1	300	500	25	459	500	1.00	200	0.01	0.00168	420	220	10	600	0.4	185.0	152.2	378.0	0.40	370.0	0.41	S
5030_0.0_1.5	300	500	25	459	750	1.50	200	0.01	0.00168	420	220	10	0	0.0	141.3	130.0	152.0	0.86	188.4	0.69	S
5030_0.1_1.5	300	500	25	459	750	1.50	200	0.01	0.00168	420	220	10	150	0.1	165.7	135.6	184.0	0.74	220.9	0.61	S
5030_0.2_1.5	300	500	25	459	750	1.50	200	0.01	0.00168	420	220	10	300	0.2	173.8	141.1	206.7	0.68	231.7	0.61	S
5030_0.3_1.5	300	500	25	459	750	1.50	200	0.01	0.00168	420	220	10	450	0.3	180.8	146.7	236.0	0.62	241.1	0.61	S
5030_0.4_1.5	300	500	25	459	750	1.50	200	0.01	0.00168	420	220	10	600	0.4	185.0	152.2	253.3	0.60	246.7	0.62	S
5030_0.0_2	300	500	25	457	1000	2.00	200	0.01	0.00262	420	220	10	0	0.0	141.3	157.8	113.5	1.39	141.3	1.12	F-S
5030_0.1_2	300	500	25	457	1000	2.00	200	0.01	0.00262	420	220	10	150	0.1	165.7	163.4	136.5	1.20	165.7	0.99	F-S
5030_0.2_2	300	500	25	457	1000	2.00	200	0.01	0.00262	420	220	10	300	0.2	173.8	168.9	158.0	1.07	173.8	0.97	F-S
5030_0.3_2	300	500	25	457	1000	2.00	200	0.01	0.00262	420	220	10	450	0.3	180.8	174.4	168.0	1.04	180.8	0.96	F-S
5030_0.4_2	300	500	25	457	1000	2.00	200	0.01	0.00262	420	220	10	600	0.4	185.0	192.0	189.0	1.02	185.0	1.04	F-S
5030_0.0_3	300	500	25	459	1500	3.00	200	0.01	0.00168	420	220	10	0	0.0	141.3	130.0	76.0	1.71	94.2	1.38	F-S
5030_0.1_3	300	500	25	459	1500	3.00	200	0.01	0.00168	420	220	10	150	0.1	165.7	135.6	91.3	1.48	110.5	1.23	F-S
5030_0.2_3	300	500	25	459	1500	3.00	200	0.01	0.00168	420	220	10	300	0.2	173.8	141.1	105.3	1.34	115.9	1.22	F-S
5030_0.3_3	300	500	25	459	1500	3.00	200	0.01	0.00168	420	220	10	450	0.3	180.8	146.7	118.0	1.24	120.5	1.22	F-S
5030_0.4_3	300	500	25	459	1500	3.00	200	0.01	0.00168	420	220	10	600	0.4	185.0	152.2	126.7	1.20	123.3	1.23	F-S

Notation: b: width of the section, h: height of the section, cc: concrete cover to transverse reinforcement , d: effective depth of the section, a: shear span (half of the column length), a/d: shear span to effective depth ratio, s: spacing of transverse reinforcement, ρ_l: longitudinal reinforcement ratio, ρ_v: transverse reinforcement ratio, f_{yl}: yield stress of longitudinal reinforcement, f_{yv}: yield stress of transverse reinforcement, f_c': concrete compressive stress, P: applied axial load, $N/A_g f_c$': axial load ratio, M_n: moment capacity of the section, V_n=shear strength of the section, V_y: lateral load causing first yielding in longitudinal reinforcement, $V_{analysis}$: peak lateral load recorded at ASFI(M) analysis, V_{flex}: lateral load causes column to reach its moment capacity M_n, F-S: Flexure-shear failure, S: shear failure.

Table 3.1 (cont'd) Properties of the Shear Critical Columns Analyzed in Parametric Study

Specimen	b (mm)	h (mm)	cc (mm)	d (mm)	a (mm)	a/d	s (mm)	ρ_l	ρ_v	f_{yl} (Mpa)	f_{yv} (Mpa)	f_c' (Mpa)	P (KN)	$\frac{N}{A_g f_c'}$	M_n (KN.m)	V_n (KN)	V_y (KN)	$\frac{V_n}{V_y}$	V_{flex} (KN)	$\frac{V_n}{V_{flex}}$	Failure Type
4040_0.0_1.25	400	400	25	359	500	1.25	200	0.01	0.00126	420	220	10	0	0.0	108.8	122.3	179.3	0.68	217.6	0.56	S
4040_0.1_1.25	400	400	25	359	500	1.25	200	0.01	0.00126	420	220	10	160	0.1	129.2	128.1	216.0	0.59	258.4	0.50	S
4040_0.2_1.25	400	400	25	359	500	1.25	200	0.01	0.00126	420	220	10	320	0.2	138.2	133.9	250.0	0.54	276.4	0.48	S
4040_0.3_1.25	400	400	25	359	500	1.25	200	0.01	0.00126	420	220	10	480	0.3	144.4	139.7	276.0	0.51	288.8	0.48	S
4040_0.4_1.25	400	400	25	359	500	1.25	200	0.01	0.00126	420	220	10	640	0.4	146.9	145.5	304.0	0.48	293.8	0.50	S
4040_0.0_1.875	400	400	25	359	750	1.88	200	0.01	0.00126	420	220	10	0	0.0	108.8	122.3	120.0	1.02	145.1	0.84	S
4040_0.1_1.875	400	400	25	359	750	1.88	200	0.01	0.00126	420	220	10	160	0.1	129.2	128.1	142.7	0.90	172.3	0.74	S
4040_0.2_1.875	400	400	25	359	750	1.88	200	0.01	0.00126	420	220	10	320	0.2	138.2	133.9	166.7	0.80	184.3	0.73	S
4040_0.3_1.875	400	400	25	359	750	1.88	200	0.01	0.00126	420	220	10	480	0.3	144.4	139.7	184.0	0.76	192.5	0.73	S
4040_0.4_1.875	400	400	25	357	750	1.88	150	0.01	0.00263	420	220	10	640	0.4	146.9	187.9	200.0	0.94	195.9	0.96	F-S
4040_0.0_2.5	400	400	25	359	1000	2.50	200	0.01	0.00126	420	220	10	0	0.0	108.8	122.3	89.6	1.36	108.8	1.12	F-S
4040_0.1_2.5	400	400	25	359	1000	2.50	200	0.01	0.00126	420	220	10	160	0.1	129.2	128.1	108.0	1.19	129.2	0.99	F-S
4040_0.2_2.5	400	400	25	359	1000	2.50	200	0.01	0.00126	420	220	10	320	0.2	138.2	133.9	125.0	1.07	138.2	0.97	F-S
4040_0.3_2.5	400	400	25	359	1000	2.50	200	0.01	0.00126	420	220	10	480	0.3	144.4	139.7	138.0	1.01	144.4	0.97	F-S
4040_0.4_2.5	400	400	25	359	1000	2.50	200	0.01	0.00126	420	220	10	640	0.4	146.9	153.0	152.0	1.01	146.9	1.04	F-S

Notation: b: width of the section, h: height of the section, cc: concrete cover to transverse reinforcement , d: effective depth of the section, a: shear span (half of the column length), a/d: shear span to effective depth ratio, s: spacing of transverse reinforcement, ρ_l: longitudinal reinforcement ratio, ρ_v: transverse reinforcement ratio, f_{yl}: yield stress of longitudinal reinforcement, f_{yv}: yield stress of transverse reinforcement, f_c': concrete compressive stress, P: applied axial load, $N/A_g f_c$': axial load ratio, M_n: moment capacity of the section, V_n=shear strength of the section, V_y: lateral load causing first yielding in longitudinal reinforcement, V_{flex}: lateral load causes column to reach its moment capacity M_n, F-S: Flexure-shear failure, S: shear failure.

Table 3.2 Properties of Shear Critical Columns Taken from Database of Elwood [9]

Researcher	Specimen	b (mm)	h (mm)	d (mm)	a (mm)	a/d	s (mm)	ρ_l	ρ_v	f_{yl} (Mpa)	f_{yv} (Mpa)	f_c' (Mpa)	P (KN)	$\frac{N}{A_g f_c'}$	M_n (KN.m)	V_n (KN)	V_{test} (KN)	$\frac{V}{V_{test}}$	V_{flex} (KN)	$\frac{V_n}{V_{flex}}$	Failure Type
LYNN (2001)	3CLH18	457.2	457.2	381.0	1473.2	3.87	457	0.03	0.001	331	400	25.6	503	0.09	442	257.0	271.3	0.95	300.0	0.86	S
	3SLH18	457.2	457.2	381.0	1473.2	3.87	457	0.03	0.001	331	400	25.6	503	0.09	442	257.0	266.9	0.96	300.0	0.86	S
	2CLH18	457.2	457.2	381.0	1473.2	3.87	457	0.02	0.001	331	400	33.1	503	0.07	332	282.7	240.2	0.94	225.4	1.25	F-S
	2CMH18	457.2	457.2	381.0	1473.2	3.87	457	0.02	0.001	331	400	25.7	1512	0.28	408	311.9	315.8	0.88	276.9	1.13	F-S
	3CMH18	457.2	457.2	381.0	1473.2	3.87	457	0.03	0.001	331	400	27.6	1512	0.26	515	320.8	338.1	0.95	349.6	0.92	S
	3CMD12	457.2	457.2	381.0	1473.2	3.87	305	0.03	0.002	331	400	27.6	1512	0.26	515	369.5	355.9	0.98	349.6	1.06	F-S
	3SMD12	457.2	457.2	381.0	1473.2	3.87	305	0.03	0.002	331	400	25.7	1512	0.28	490	360.6	378.1	0.88	332.8	1.08	F-S
SEZEN (2002)	2CLD12	457.2	457.2	393.7	1473.2	3.74	305	0.025	0.002	441	469	21.1	667	0.15	382	327.6	314.9	0.82	259.3	1.26	F-S
	2CHD12	457.2	457.2	393.7	1473.2	3.74	305	0.025	0.002	441	469	21.1	2669	0.61	369	428.4	359.0	0.70	250.5	1.71	F
	2CLD12M	457.2	457.2	393.7	1473.2	3.74	305	0.025	0.002	441	469	21.8	667	0.15	386	330.5	294.5	0.89	262.0	1.26	F-S
ESAKI (1996)	H-2-1/5	200	200	175.0	398.8	2.28	50	0.025	0.005	359	365	23.0	161	0.17	35	105.6	103.2	0.86	88.4	1.19	F-S
	HT-2-1/5	200	200	175.0	398.8	2.28	75	0.025	0.005	359	365	20.2	141	0.18	33	102.2	101.9	0.82	83.8	1.22	F-S
PARK et al. (1991)	U-7	401.3	401.3	375.9	1000.8	2.66	119	0.024	0.005	446	382	29.0	463	0.1	283	448.5	327.8	0.86	282.6	1.59	F
	U-8	401.3	401.3	375.9	1000.8	2.66	119	0.024	0.005	446	382	33.5	1072	0.2	347	532.6	392.8	0.88	346.5	1.54	F
OZCEBE et. al. (1989)	U1	350.5	350.5	304.8	1000.8	3.28	150	0.033	0.003	430	470	43.6	0	0	240	279.1	274.9	0.87	239.5	1.16	F-S
	U2	350.5	350.5	304.8	1000.8	3.28	150	0.033	0.003	453	470	30.2	601	0.16	296	294.1	270.0	1.09	295.4	1.00	F-S
	U3	350.5	350.5	304.8	1000.8	3.28	76	0.033	0.006	430	470	34.8	601	0.14	287	455.4	268.2	1.07	287.2	1.59	F
IKEDA (1968)	43	200	200	173.0	500.4	2.89	99	0.02	0.003	434	558	19.6	80	0.1	32	85.8	73.8	0.86	63.3	1.36	F-S
	44	200	200	173.0	500.4	2.89	99	0.02	0.003	434	558	19.6	80	0.1	32	85.8	76.5	0.83	63.3	1.36	F-S
	45	200	200	173.0	500.4	2.89	99	0.02	0.003	434	558	19.6	156	0.2	36	89.5	82.3	0.88	72.6	1.23	F-S
	46	200	200	173.0	500.4	2.89	99	0.02	0.003	434	558	19.6	156	0.2	36	89.5	80.5	0.90	72.6	1.23	F-S
	62	200	200	173.0	500.4	2.89	99	0.02	0.003	345	476	19.6	80	0.1	30	77.8	57.8	1.04	60.2	1.29	F-S
	63	200	200	173.0	500.4	2.89	99	0.02	0.003	345	476	19.6	156	0.2	35	81.5	68.5	1.02	69.5	1.17	F-S
	64	200	200	173.0	500.4	2.89	99	0.02	0.003	345	476	19.6	156	0.2	35	81.5	68.5	1.02	69.5	1.17	F-S

Notation: b: width of the section, h: height of the section, d: effective depth of the section, a: shear span (half of the column length), a/d: shear span to effective depth ratio, s: spacing of transverse reinforcement, ρ_l: longitudinal reinforcement ratio, ρ_v: transverse reinforcement ratio, f_{yl}: yield stress of longitudinal reinforcement, f_{yv}: yield stress of transverse reinforcement, f_c': concrete compressive stress, P: applied axial load, $N/A_g f_c'$: axial load ratio, M_n: moment capacity of the section, V_n=shear strength of the section, V_{test}: peak lateral load recorded at test, V_{flex}: lateral load causes column to reach its moment capacity M_n. F-S: Flexure-shear failure, S: shear failure

Table 3.2 (cont'd) Properties of Shear critical Columns Taken from Database of Elwood [9]

Researcher	Specimen	b (mm)	h (mm)	d (mm)	a (mm)	a/d	s (mm)	ρ_l	ρ_v	f_{yl} (Mpa)	f_{yv} (Mpa)	f_c' (Mpa)	P (KN)	$\frac{N}{A_g f_c'}$	M_n (KN.m)	V_n (KN)	V_{test} (KN)	$\frac{V}{V_{test}}$	V_{flex} (KN)	$\frac{V_n}{V_{flex}}$	Failure Type
UMEMURO ENDO (1970)	205	200	200	180.1	599.4	3.33	99	0.02	0.003	462	324	17.6	156	0.22	42	67.6	71.2	0.95	69.5	0.97	F-S
	207	200	200	180.1	401.3	2.23	99	0.02	0.003	462	324	17.6	156	0.22	42	67.6	105.9	0.64	103.8	0.65	S
	214	200	200	180.1	599.4	3.33	201	0.02	0.001	462	324	17.6	391	0.56	39	62.6	82.7	0.76	65.8	0.95	F-S
	231	200	200	180.1	401.3	2.23	99	0.01	0.001	324	524	14.8	156	0.26	21	56.6	50.7	1.05	53.1	1.07	F-S
	232	200	200	180.1	401.3	2.23	99	0.01	0.001	324	524	13.1	156	0.3	21	54.7	58.3	0.88	51.3	1.07	F-S
	233	200	200	180.1	401.3	2.23	99	0.01	0.001	372	524	13.9	156	0.28	25	55.6	68.9	0.81	62.9	0.88	S
	234	200	200	180.1	401.3	2.23	99	0.01	0.001	372	524	13.1	156	0.3	25	54.7	67.2	0.81	62.1	0.88	S
KOKUSHO (1964)	372	200	200	169.9	500.4	2.94	99	0.01	0.003	524	352	19.9	156	0.2	31	72.1	74.3	0.82	61.2	1.18	F-S
	373	200	200	169.9	500.4	2.94	99	0.02	0.003	524	352	20.4	156	0.19	41	72.6	88.1	0.82	81.4	0.89	S
KOKUSHO et. al. (1965)	452	200	200	169.9	500.4	2.94	99	0.03	0.003	359	607	21.9	391	0.45	47	112.7	110.3	0.84	93.0	1.21	F-S
	454	200	200	169.9	500.4	2.94	99	0.04	0.003	359	607	21.9	391	0.45	57	112.7	110.3	1.02	113.0	1.00	F-S
WIGHT and SOZEN (1973)	40.033a	152.4	304.8	266.7	876.3	3.29	127	0.024	0.003	496	345	34.7	189	0.12	88	102.2	99.2	1.01	100.1	1.02	F-S
	40.033	152.4	304.8	266.7	876.3	3.29	127	0.024	0.003	496	345	33.6	178	0.11	82	100.6	101.4	0.92	93.4	1.08	F-S
	25.033	152.4	304.8	266.7	876.3	3.29	127	0.024	0.003	496	345	33.6	111	0.07	80	96.3	104.5	0.87	90.8	1.06	F-S
	0.033	152.4	304.8	266.7	876.3	3.29	127	0.024	0.003	496	345	32.0	0	0	65	88.1	98.3	0.75	73.8	1.19	F-S
	40.048	152.4	304.8	266.7	876.3	3.29	89	0.024	0.005	496	345	26.1	178	0.15	85	115.1	94.3	1.02	96.5	1.19	F-S
	0.048	152.4	304.8	266.7	876.3	3.29	89	0.024	0.005	496	345	25.9	0	0	63	104.9	105.0	0.69	72.1	1.45	F
YALCIN (1997)	BR-S1	551.2	551.2	482.6	1485.9	3.08	300	0.02	0.001	445	425	44.8	2086	0.15	964	592.9	578.3	1.03	648.5	0.91	S

Notation: b: width of the section, h: height of the section, d: effective depth of the section, a: shear span (half of the column length), a/d: shear span to effective depth ratio, s: spacing of transverse reinforcement, ρ_l: longitudinal reinforcement ratio, ρ_v: transverse reinforcement ratio, f_{yl}: yield stress of longitudinal reinforcement, f_{yv}: yield stress of transverse reinforcement, f_c': concrete compressive stress, P: applied axial load, $N/A_g f_c$': axial load ratio, M_n: moment capacity of the section, V_n=shear strength of the section, V_{test}: peak lateral load recorded at test, V_{flex}: lateral load causes column to reach its moment capacity M_n. F-S: Flexure-shear failure, S: shear failure

Table 3.3 Properties of Shear critical Columns Taken from Database of Elwood [9] for Which Axial failure is Reported

Researcher	Specimen	b (mm)	h (mm)	d (mm)	a (mm)	a/d	s (mm)	ρ_l	ρ_v	f_{yl} (Mpa)	f_{yv} (Mpa)	f_c' (Mpa)	P (KN)	$\frac{N}{A_g f_c'}$	M_n (KN.m)	V_n (KN)	V_{test} (KN)	$\frac{V}{V_{test}}$	V_{flex} (KN)	$\frac{V_n}{V_{flex}}$	d_c (mm)	Failure Type
LYNN (2001)	3CLH18	457	457	393	1473.2	3.75	457	0.03	0.001	331	400	26	503	0.09	442	257.0	271.3	0.95	300.0	0.86	371	S
	2CLH18	457	457	397	1473.2	3.71	457	0.02	0.001	331	400	33	503	0.07	332	282.7	240.2	0.94	225.4	1.25	371	F-S
	3SLH18	457	457	393	1473.2	3.75	457	0.03	0.001	331	400	26	503	0.09	442	257.0	266.9	0.96	300.0	0.86	371	S
	2SLH18	457	457	397	1473.2	3.71	457	0.02	0.001	331	400	33	503	0.07	319	282.7	231.3	0.94	216.3	1.31	371	F-S
	2CMH18	457	457	397	1473.2	3.71	457	0.02	0.001	331	400	26	1512	0.28	408	311.9	315.8	0.88	276.9	1.13	371	F-S
	3CMH18	457	457	393	1473.2	3.75	457	0.03	0.001	331	400	28	1512	0.26	515	320.8	338.1	0.95	349.6	0.92	371	S
	3CMD12	457	457	393	1473.2	3.75	305	0.03	0.002	331	400	28	1512	0.26	515	369.5	355.9	0.98	349.6	1.06	371	F-S
	3SMD12	457	457	393	1473.2	3.75	305	0.03	0.002	331	400	26	1512	0.28	490	360.6	378.1	0.88	332.8	1.08	371	F-S
SEZEN (2002)	2CLD12	457	457	392	1473.2	3.76	305	0.025	0.002	441	469	21	667	0.15	382	327.6	314.9	0.82	259.3	1.26	365	F-S
	2CHD12	457	457	392	1473.2	3.76	305	0.025	0.002	441	469	21	2667	0.61	369	428.4	359.0	0.70	250.5	1.71	365	F
	2CVD12	457	457	392	1473.2	3.76	305	0.025	0.002	441	469	21	2224	0.34	415	404.7	300.7	0.94	281.5	1.44	365	F
	2CLD12M	457	457	392	1473.2	3.76	305	0.025	0.002	441	469	22	667	0.15	386	330.5	294.5	0.89	262.0	1.26	365	F-S

Notation: b: width of the section, h: height of the section, d: effective depth of the section, a: shear span (half of the column length), a/d: shear span to effective depth ratio, s: spacing of transverse reinforcement, ρ_l: longitudinal reinforcement ratio, ρ_v: transverse reinforcement ratio, f_{yl}: yield stress of longitudinal reinforcement, f_{yv}: yield stress of transverse reinforcement, f_c': concrete compressive stress, P: applied axial load, $N/A_g f_c$': axial load ratio, M_n: moment capacity of the section, V_n=shear strength of the section, V_{test}: peak lateral load recorded at test, V_{flex}: lateral load causes column to reach its moment capacity capacity M_n.d_c: depth of the core concrete, F-S: Flexure-shear failure, S: shear failure

3.3. Classification of Failure Types of Members

In order to estimate the lateral load-displacement behavior and ductility of a column, failure type should be identified. Failure type of the sections used in parametric study and database is classified based on the study performed by Sezen and Setzler [32]. Failure types of the columns are determined according to the following criteria:

Shear Failure; $\frac{V_n}{V_{flex}} < 0.95$

Flexure-Shear Failure; $0.95 \leq \frac{V_n}{V_{flex}} \leq 1.4$

Flexure Failure; $1.4 < \frac{V_n}{V_{flex}}$

where, V_n is the shear strength of the section calculated according to reinforced concrete design codes (Provisions of TS500 [31] are employed in this study with nominal material strength for concrete and steel) and V_{flex} is the the lateral load to cause formation of plastic hinges at the critical locations of the column.. Moment capacity of the section is calculated from sectional analysis, and V_{flex} is obtained by dividing the moment capacity of the column section to the shear span of the column.

As it is explained in Chapter 2 of the study, none of the models, which are utilized to estimate the load-deformation of columns failing in shear mode, produced reasonable accuracy for the drift ratio at shear failure. Furthermore, variations of estimations are high. Therefore, it would not be realistic to develop drift capacity equation for drift at shear failure for those members. Conversely, results for drift at shear failure for shear critical columns can be used only for providing lower bound estimations. Considering this, only flexure-shear specimens classified according to the procedure given above are used in development of improved drift capacity equations for drift at shear failure and axial failure. Those members have the ability to reach flexural yielding of longitudinal reinforcement before shear failure occurred. Columns, which did not experience flexural yielding before shear failure occurred, are not considered in study of Elwood [9] as well. Number of parametric and database columns utilized in development of equations are summarized in Table 3.4.

Failure type of the members, shear strength, V_n, flexural shear strength, V_{flex}, drift ratio at first yielding of the longitudinal reinforcement, DR_y, drift ratio at shear failure , DR_s, drift ratio at axial failure, DR_a are presented in Table 3.5 for parametric study and in Table 3.6 for database columns. Determination of the performance points are realized by following the procedure described in Section 2.2.1.

Table 3.4 Number of Columns Used in Analyses

Used for analysis of	Parametric Study		Database		
	Shear	Flexure Shear	Shear	Flexure Shear	Flexure
Drift Ratio at Shear Failure	29	26	8	29	5
Drift Ratio at Axial Failure	23	19	3	7	2

Table 3.5 Capacities and Calculated Drift Ratios of Parametric Study Columns

Specimen	V_n (KN)	V_y (KN)	$\frac{V_n}{V_y}$	V_{flex} (KN)	$\frac{V_n}{V_{flex}}$	Failure Type	DR_y	DR_s	DR_a
8020_00_0.625	171.3	310.0	0.55	434.2	0.39	S	0.0030	0.0116	NA
8020_01_0.625	177.4	390.0	0.45	487.2	0.36	S	0.0020	0.0170	0.0280
8020_02_0.625	183.5	456.0	0.40	528.4	0.35	S	0.0032	0.0160	0.0240
8020_03_0.625	189.6	512.0	0.37	538.6	0.35	S	0.0012	0.0120	0.0240
8020_04_0.625	195.8	556.0	0.35	544.4	0.36	S	0.0012	0.0050	0.0230
8020_00_0.94	171.3	206.7	0.83	289.5	0.59	S	0.0037	0.0190	NA
8020_01_0.94	177.4	260.0	0.68	324.8	0.55	S	0.0033	0.0220	0.0370
8020_02_0.94	183.5	304.0	0.60	352.3	0.52	S	0.0013	0.0200	0.0350
8020_03_0.94	189.6	341.3	0.56	359.1	0.53	S	0.0011	0.0120	0.0330
8020_04_0.94	195.8	370.7	0.53	362.9	0.54	S	0.0020	0.0070	0.0320
8020_00_1.25	262.6	155.0	1.69	272.2	0.96	F-S	0.0040	0.0620	NA
8020_01_1.25	268.7	194.0	1.38	272.2	0.99	F-S	0.0040	0.0690	NA
8020_02_1.25	274.8	228.0	1.21	272.2	1.01	F-S	0.0038	0.0420	0.0660
8020_03_1.25	280.9	259.0	1.08	272.2	1.03	F-S	0.0037	0.0364	0.0640
8020_04_1.25	287.0	283.0	1.01	272.2	1.05	F-S	0.0035	0.0352	0.0570
8020_00_1.875	218.7	103.3	2.12	181.5	1.20	F-S	0.0043	0.0560	NA
8020_01_1.875	177.4	128.7	1.38	181.5	0.98	F-S	0.0040	0.0430	0.0630
8020_02_1.875	183.5	152.0	1.21	181.5	1.01	F-S	0.0030	0.0320	0.0600
8020_03_1.875	189.6	172.0	1.10	181.5	1.04	F-S	0.0040	0.0323	0.0520
8020_04_1.875	195.8	184.7	1.06	181.5	1.08	F-S	0.0035	0.0250	0.0310
5030_0.0_1	130.0	228.0	0.57	282.6	0.46	S	0.0044	0.0160	NA
5030_0.1_1	135.6	274.0	0.49	331.4	0.41	S	0.0036	0.0190	0.0300
5030_0.2_1	141.1	316.0	0.45	347.6	0.41	S	0.0020	0.0170	0.0280
5030_0.3_1	146.7	352.0	0.42	361.6	0.41	S	0.0010	0.0030	0.0280
5030_0.4_1	152.2	378.0	0.40	370.0	0.41	S	0.0010	0.0030	0.0270
5030_0.0_1.5	130.0	152.0	0.86	188.4	0.69	S	0.0049	0.0300	NA
5030_0.1_1.5	135.6	184.0	0.74	220.9	0.61	S	0.0020	0.0250	0.0440
5030_0.2_1.5	141.1	206.7	0.68	231.7	0.61	S	0.0016	0.0160	0.0380
5030_0.3_1.5	146.7	236.0	0.62	241.1	0.61	S	0.0019	0.0050	0.0390
5030_0.4_1.5	152.2	253.3	0.60	246.7	0.62	S	0.0043	0.0060	0.0170

Notation: V_n: Shear strength of the section calculated using nominal material strength (TS500), V_{flex}: lateral load causes column to reach its moment capacity M_n.d_c: depth of the core concrete, F-S: Flexure-shear failure, S: shear failure, Dry; drift ratio at first yielding of the longitudinal reinforcement, Drs: drift ratio at shear failure, DRa: drift ratio at axial failure, NA: no axial failure is observed.

Table 3.5 (cont'd) Capacities and Calculated Drift Ratios of Parametric Study Columns

Specimen	V_n (KN)	V_y (KN)	$\frac{V_n}{V_y}$	V_{flex} (KN)	$\frac{V_n}{V_{flex}}$	Failure Type	DR_y	DR_s	DR_a
5030_0.0_2	157.8	113.5	1.39	141.3	1.12	F-S	0.0055	0.0615	NA
5030_0.1_2	163.4	136.5	1.20	165.7	0.99	F-S	0.0065	0.0395	NA
5030_0.2_2	168.9	158.0	1.07	173.8	0.97	F-S	0.0050	0.0390	0.0780
5030_0.3_2	174.4	168.0	1.04	180.8	0.96	F-S	0.0048	0.0345	0.0510
5030_0.4_2	192.0	189.0	1.02	185.0	1.04	F-S	0.0047	0.0275	0.0380
5030_0.0_3	130.0	76.0	1.71	94.2	1.38	F-S	0.0060	0.0630	NA
5030_0.1_3	135.6	91.3	1.48	110.5	1.23	F-S	0.0070	0.0403	0.0620
5030_0.2_3	141.1	105.3	1.34	115.9	1.22	F-S	0.0060	0.0340	0.0580
5030_0.3_3	146.7	118.0	1.24	120.5	1.22	F-S	0.0060	0.0280	0.0480
5030_0.4_3	152.2	126.7	1.20	123.3	1.23	F-S	0.0060	0.0230	0.0390
4040_0.0_1.25	122.3	179.3	0.68	217.6	0.56	S	0.0050	0.0245	NA
4040_0.1_1.25	128.1	216.0	0.59	258.4	0.50	S	0.0016	0.0240	0.0330
4040_0.2_1.25	133.9	250.0	0.54	276.4	0.48	S	0.0020	0.0040	0.0430
4040_0.3_1.25	139.7	276.0	0.51	288.8	0.48	S	0.0022	0.0040	0.0330
4040_0.4_1.25	145.5	304.0	0.48	293.8	0.50	S	0.0030	0.0050	0.0250
4040_0.0_1.875	122.3	120.0	1.02	145.1	0.84	S	0.0060	0.0350	NA
4040_0.1_1.875	128.1	142.7	0.90	172.3	0.74	S	0.0070	0.0400	0.0400
4040_0.2_1.875	133.9	166.7	0.80	184.3	0.73	S	0.0056	0.0070	0.0250
4040_0.3_1.875	139.7	184.0	0.76	192.5	0.73	S	0.0052	0.0090	0.0230
4040_0.4_1.875	187.9	200.0	0.94	195.9	0.96	F-S	0.0050	0.0355	0.0440
4040_0.0_2.5	122.3	89.6	1.36	108.8	1.12	F-S	0.0065	0.0410	NA
4040_0.1_2.5	128.1	108.0	1.19	129.2	0.99	F-S	0.0070	0.0420	0.0660
4040_0.2_2.5	133.9	125.0	1.07	138.2	0.97	F-S	0.0060	0.0360	0.0600
4040_0.3_2.5	139.7	138.0	1.01	144.4	0.97	F-S	0.0060	0.0290	0.0480
4040_0.4_2.5	153.0	152.0	1.01	146.9	1.04	F-S	0.0060	0.0245	0.0390

Notation: V_n: Shear strength of the section calculated using nominal material strength (TS500), V_{flex}: lateral load causes column to reach its moment capacity M_n.d_c: depth of the core concrete, F-S: Flexure-shear failure, S: shear failure, DR_y; drift ratio at first yielding of the longitudinal reinforcement, DR_s: drift ratio at shear failure, DR_a: drift ratio at axial failure, NA: no axial failure is observed.

Table 3.6 Capacities and Calculated Drift Ratios of Columns Given in the Database by Elwood [9]

Researcher	Specimen	$\frac{V}{V_{test}}$	V_{flex} (KN)	$\frac{V_n}{V_{flex}}$	Failure Type	DR_y	DR_s
LYNN (2001)	3CLH18	0.95	300.0	0.86	S	0.0067	0.0103
	3SLH18	0.96	300.0	0.86	S	0.0053	0.0099
	2CLH18	0.94	225.4	1.25	F-S	0.0062	0.0259
	2CMH18	0.88	276.9	1.13	F-S	0.0053	0.0103
	3CMH18	0.95	349.6	0.92	S	0.0053	0.0103
	3CMD12	0.98	349.6	1.06	F-S	0.0064	0.0155
	3SMD12	0.88	332.8	1.08	F-S	0.0074	0.0155
SEZEN (2002)	2CLD12	0.82	259.3	1.26	F-S	0.0090	0.0256
	2CHD12	0.70	250.5	1.71	F	0.0049	0.0088
	2CLD12M	0.89	262.0	1.26	F-S	0.0096	0.0287
ESAKI (1996)	H-2-1/5	0.86	88.4	1.19	F-S	0.0051	0.0252
	HT-2-1/5	0.82	83.8	1.22	F-S	0.0061	0.0261
PARK et al. (1991)	U-7	0.86	282.6	1.59	F	0.0089	0.0355
	U-8	0.88	346.5	1.54	F	0.0084	0.0211
OZCEBE et. al. (1989)	U1	0.87	239.5	1.16	F-S	0.0170	0.0530
	U2	1.09	295.4	1.00	F-S	0.0150	0.0429
	U3	1.07	287.2	1.59	F	0.0160	0.0449
IKEDA (1968)	43	0.86	63.3	1.36	F-S	0.0066	0.0264
	44	0.83	63.3	1.36	F-S	0.0066	0.0162
	45	0.88	72.6	1.23	F-S	0.0096	0.0162
	46	0.90	72.6	1.23	F-S	0.0096	0.0122
	62	1.04	60.2	1.29	F-S	0.0061	0.0371
	63	1.02	69.5	1.17	F-S	0.0061	0.0279
	64	1.02	69.5	1.17	F-S	0.0071	0.0335
UMEMURO ENDO (1970)	205	0.95	69.5	0.97	F-S	0.0081	0.0208
	207	0.64	103.8	0.65	S	0.0101	0.0158
	214	0.76	65.8	0.95	F-S	0.0102	0.0174
	231	1.05	53.1	1.07	F-S	0.0025	0.0203
	232	0.88	51.3	1.07	F-S	0.0032	0.0203
	233	0.81	62.9	0.88	S	0.0038	0.0171
	234	0.81	62.1	0.88	S	0.0038	0.0203
KOKUSHO (1964)	372	0.82	61.2	1.18	F-S	0.0051	0.0213
	373	0.82	81.4	0.89	S	0.0071	0.0198
KOKUSHO et. al. (1965)	452	0.84	93.0	1.21	F-S	0.0061	0.0152
	454	1.02	113.0	1.00	F-S	0.0046	0.0102
WIGHT and SOZEN (1973)	40.033a	1.01	100.1	1.02	F-S	0.0087	0.0362
	40.033	0.92	93.4	1.08	F-S	0.0139	0.0501
	25.033	0.87	90.8	1.06	F-S	0.0136	0.0359
	0.033	0.75	73.8	1.19	F-S	0.0087	0.0319
	40.048	1.02	96.5	1.19	F-S	0.0165	0.0554
	0.048	0.69	72.1	1.45	F	0.0154	0.0377
YALCIN (1997)	BR-S1	1.03	648.5	0.91	S	0.0055	0.0156

Notation: V_n: Shear strength of the section calculated using nominal material strength (TS500), V_{flex}: lateral load causes column to reach its moment capacity M_n.d_c: depth of the core concrete, F-S: Flexure-shear failure and S: shear failure (based on the classification given in Section 3.3), DR_y; drift ratio at first yielding of the longitudinal reinforcement, DR_s: drift ratio at shear failure.

Table 3.6 (cont'd) Capacities and Measured Drift Ratios of Columns Given in Database by Elwood [9] (Axial failure Reported Specimens)

Researcher	Specimen	V_n (KN)	V_{test} (KN)	$\frac{V}{V_{test}}$	V_{flex} (KN)	$\frac{V_n}{V_{flex}}$	Failure Type	DR_y	DR_s	DR_a
LYNN (2001)	3CLH18	257.0	271.3	0.95	300.0	0.86	S	0.0065	0.0103	0.0207
	2CLH18	282.7	240.2	0.94	225.4	1.25	F-S	0.0051	0.0259	0.0310
	3SLH18	257.0	266.9	0.96	300.0	0.86	S	0.0053	0.0103	0.0310
	2SLH18	282.7	231.3	0.94	216.3	1.31	F-S	0.0044	0.0207	0.0362
	2CMH18	311.9	315.8	0.88	276.9	1.13	F-S	0.0056	0.0103	0.0103
	3CMH18	320.8	338.1	0.95	349.6	0.92	S	0.0077	0.0103	0.0207
	3CMD12	369.5	355.9	0.98	349.6	1.06	F-S	0.0066	0.0155	0.0207
	3SMD12	360.6	378.1	0.88	332.8	1.08	F-S	0.0077	0.0155	0.0207
SEZEN (2002)	2CLD12	327.6	314.9	0.82	259.3	1.26	F-S	0.0089	0.0259	0.0500
	2CHD12	428.4	359.0	0.70	250.5	1.71	F	0.0068	0.0086	0.0190
	2CVD12	404.7	300.7	0.94	281.5	1.44	F	0.0071	0.0190	0.0293
	2CLD12M	330.5	294.5	0.89	262.0	1.26	F-S	0.0091	0.0284	0.0509

Notation: V_n: Shear strength of the section calculated using nominal material strength (TS500), V_{flex}: lateral load causes column to reach its moment capacity M_n. d_c: depth of the core concrete, F-S: Flexure-shear failure and S: shear failure (based on the classification given in Section 3.3), DR_y; drift ratio at first yielding of the longitudinal reinforcement, DR_s: drift ratio at shear failure.

3.4. Development of Drift Capacity Equations

In order to perform statistical analysis, variation of the drift capacity with possible important variables is investigated. It should be noted that database columns and parametric columns are shown with different labels in the plots.

3.4.1. Drift Ratio at Shear Failure for Columns Failing in Flexure-Shear Mode

There are 26 parametric columns and 29 database columns whose expected failure mode were determined as flexure-shear according to the criteria of failure type classification given in Section 3.3. Their properties are presented in Table 3.1 for parametric columns and in Table 3.2 for database columns. Properties are summarized below.

- Shear span to depth ratio: $1.32 \leq \frac{a}{d} \leq 3.9$
- Axial load ratio: $0 \leq n \leq 0.56$
- Concrete compressive strength: $10 \leq f_c^{'} \leq 43.6$ Mpa
- Longitudinal reinforcement nominal yield stress: $324 \leq f_{yl} \leq 524$ Mpa
- Longitudinal reinforcement ratio: $0.01 \leq \rho_l \leq 0.04$
- Transverse reinforcement ratio: $0.001 \leq \rho_v \leq 0.0053$
- Transverse reinforcement nominal yield stress : $220 \leq f_{yv} \leq 607$ Mpa
- Maximum shear stress: $0.24 \leq \frac{v}{\sqrt{f_c^{'}}} \leq 0.70$ (Mpa units)

For the flexure-shear failure specimens lateral load causing the flexural hinging in column end is taken as maximum lateral load. For the database columns, it is taken as maximum lateral load recorded at the test.

Variables are chosen similar to those selected by Elwood [9]. For the purpose of statistical analysis, 26 parametric flexure shear critical column sections from Table 3.5 and 29 shear critical column sections from the database presented in Table 3.6 were utilized. Drift at ratio at shear failure of parametric columns were obtained from analysis performed by ASFI(M) method and that of database columns were taken from those given in the database of Elwood [9]. Variation of drift at shear failure with different variables is given in Figure 3.3.

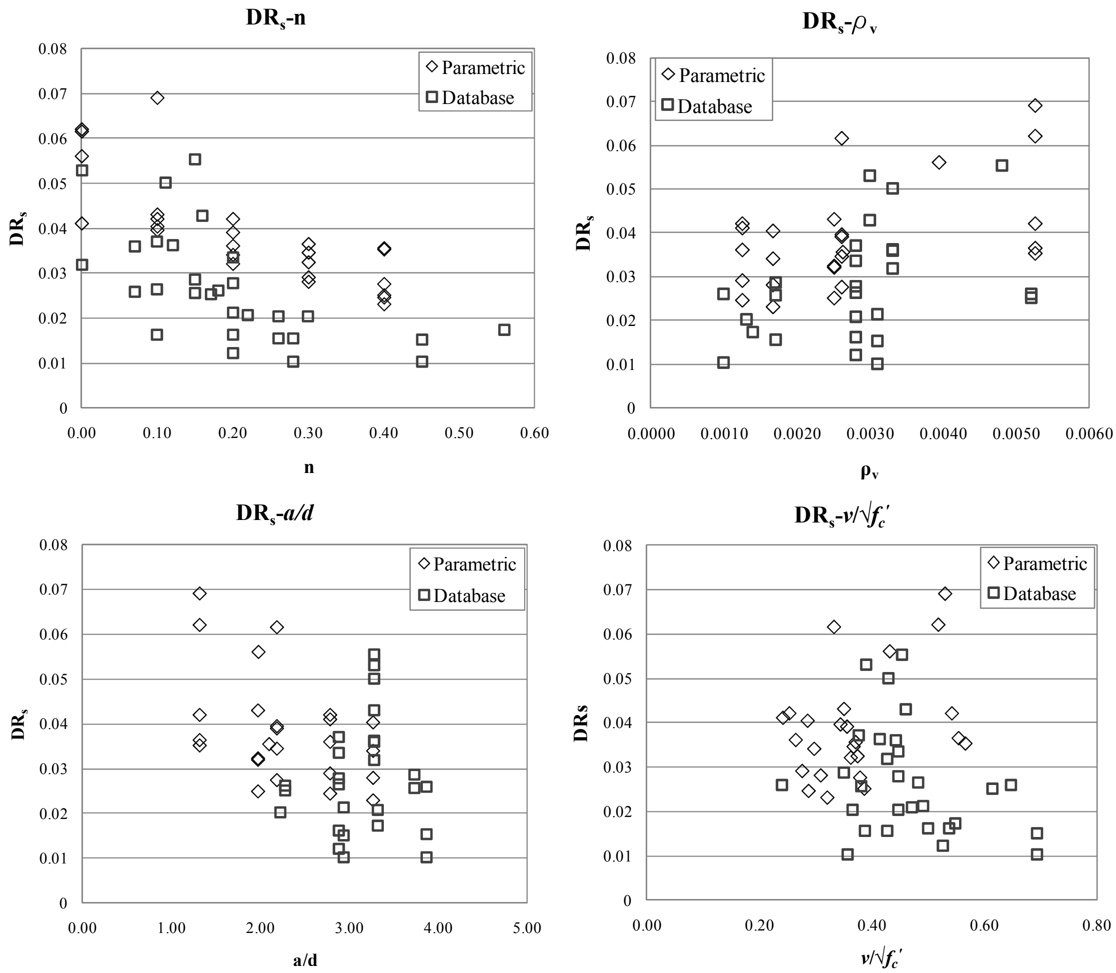

Figure 3.3 Effect of Variables on Drift at Shear Failure for Flexure-Shear Critical Columns

Upon examination of the Figure 3.3, following conclusions can be drawn;

- As the axial load ratio increases, drift ratio at shear failure decreases.
- Drift ratio at shear failure increases as the transverse reinforcement ratio increases.
- There is no indication of a clear relationship between the shear span to effective depth ratio and the drift ratio at shear failure. This variable was not included in development of drift capacity equation.
- Drift ratio at shear failure, in general, decreases as the $\frac{v}{\sqrt{f_c'}}$ ratio increases.

Nonlinear regression analysis was performed and Eq. (3.1) was obtained from the analysis giving best fit to the data.

$$DR_s = 0.05 + 10\rho_v - 0.023\left[\frac{P}{A_g f_c^{'}}\right]^{0.8} - 0.097\frac{v}{\sqrt{f_c^{'}}} \geq 0.01 \quad \textbf{(3.1)}$$

Eq. (3.1) was utilized to estimate the drift at shear failure and statistical analysis performed on ratio of measured to calculated drift ratios are summarized separately for all columns and database columns in Table 3.7.

Table 3.7 Statistical Analysis Results of Estimated Drift Ratios at Shear Failure for Flexure-Shear Critical Columns

		Equation	
		Proposed (Eq. (3.1))	Elwood (Eq. (2.1))
All Specimens (55 Columns)	Mean	1.05	1.24
	Standard Deviation	0.26	0.35
	Coefficient of Variation	0.24	0.28
Database (29 Columns)	Mean	1.01	1.07
	Standard Deviation	0.32	0.37
	Coefficient of Variation	0.32	0.35

As it is summarized in Table 3.7, proposed Eq. (3.1) produced estimations that are more reliable (mean of 1.05 and coefficient of variation 0.24 for all column specimens, and with a mean value of 1.01 and coefficient of variation 0.32 for database column specimens). On the other hand, Elwood [9] Eq. (2.1) obtained a mean value of 1.24 and coefficient of variation 0.28 for all columns specimens and a mean value of 1.07 and coefficient of variation 0.35 for the database columns. Results shows that, proposed Eq. (3.1) gives better estimates of drift at shear failure for specimens whose failure mode is expected as flexure-shear. The reason of getting a better accuracy for the flexure-shear failure expected specimens could be the accuracy of ASFI (M) method on estimating behavior of such columns. Calculated and measured values are plotted for proposed Eq. (3.1) and Eq. (2.1) proposed by Elwood [9] and shown in Figure 3.4.

.

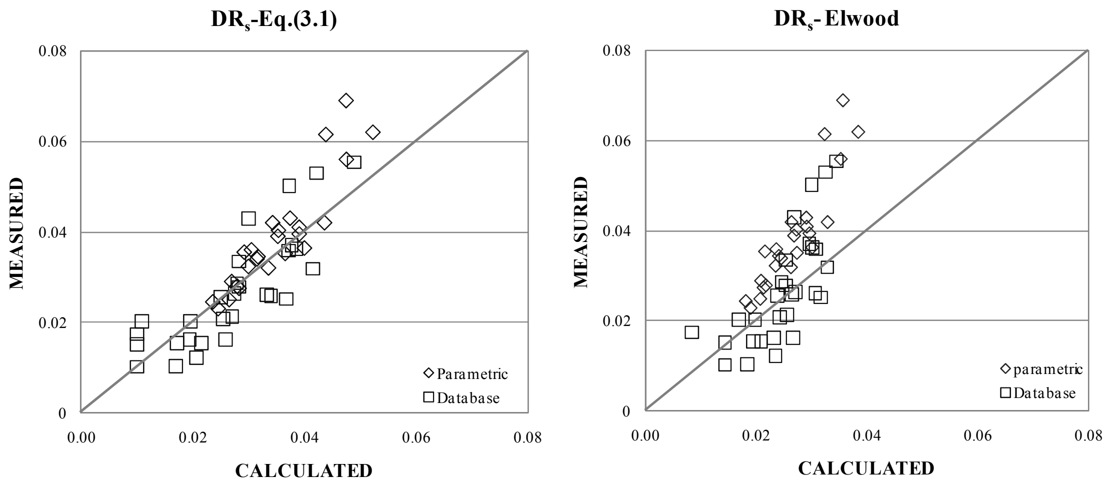

Figure 3.4 Comparison of Measured and Calculated Drift Ratios for Eq. (3.1) and Equation Proposed by Elwood [9] for Flexure-Shear Failure Expected Columns

Figure 3.4 shows that variation of the estimations is smaller when compared to estimations of equation proposed by Elwood [9].

3.4.2. Drift Ratio at Axial Failure for Columns Failing in Flexure-Shear Mode

As explained in Chapter 2.1.4, equation to estimate drift ratio at axial failure proposed by Elwood [9] is developed based on the shear-friction concept. In this study, it is attempted to develop an equation from statistical analysis of parametric and database flexure-shear critical columns.

To develop an equation specific for flexure-shear failure specimens in order to estimate drift ratio at axial failure, 19 parametric study columns and 7 of the database columns whose failure mode is estimated as flexure-shear are included in statistical analysis. Properties of those columns are presented in Table 3.1 for parametric study columns and in Table 3.2 for database columns.

Properties of those 26 columns are summarized below;

- Shear span to depth ratio: $1.25 \leq \frac{a}{d} \leq 3.76$
- Concrete compressive strength: $10 \leq f_c{}' \leq 33$ Mpa
- Longitudinal reinforcement nominal yield stress: $331 \leq f_{yl} \leq 420$ Mpa
- Longitudinal reinforcement ratio: $0.01 \leq \rho_l \leq 0.03$
- Transverse reinforcement ratio: $0.001 \leq \rho_v \leq 0.0053$
- Transverse reinforcement nominal yield stress : $220 \leq f_{yv} \leq 469$ Mpa

Same variables used in development of Eq. (2.2) are employed in statistical analysis. Range of variables is as follows;

Axial load ratio, n; $0.07 \leq n \leq 0.4$

Transverse reinforcement ratio, ρ_v; $0.001 \leq \rho_v \leq 0.0053$

Ratio of axial load to shear strength provided by lateral reinforcement, $\frac{P}{V_s}$; $1.88 \leq \frac{P}{V_s} \leq 33$

Effect of parameters on drift ratio at axial failure for flexure-shear failure specimens are presented in Figure 3.5.

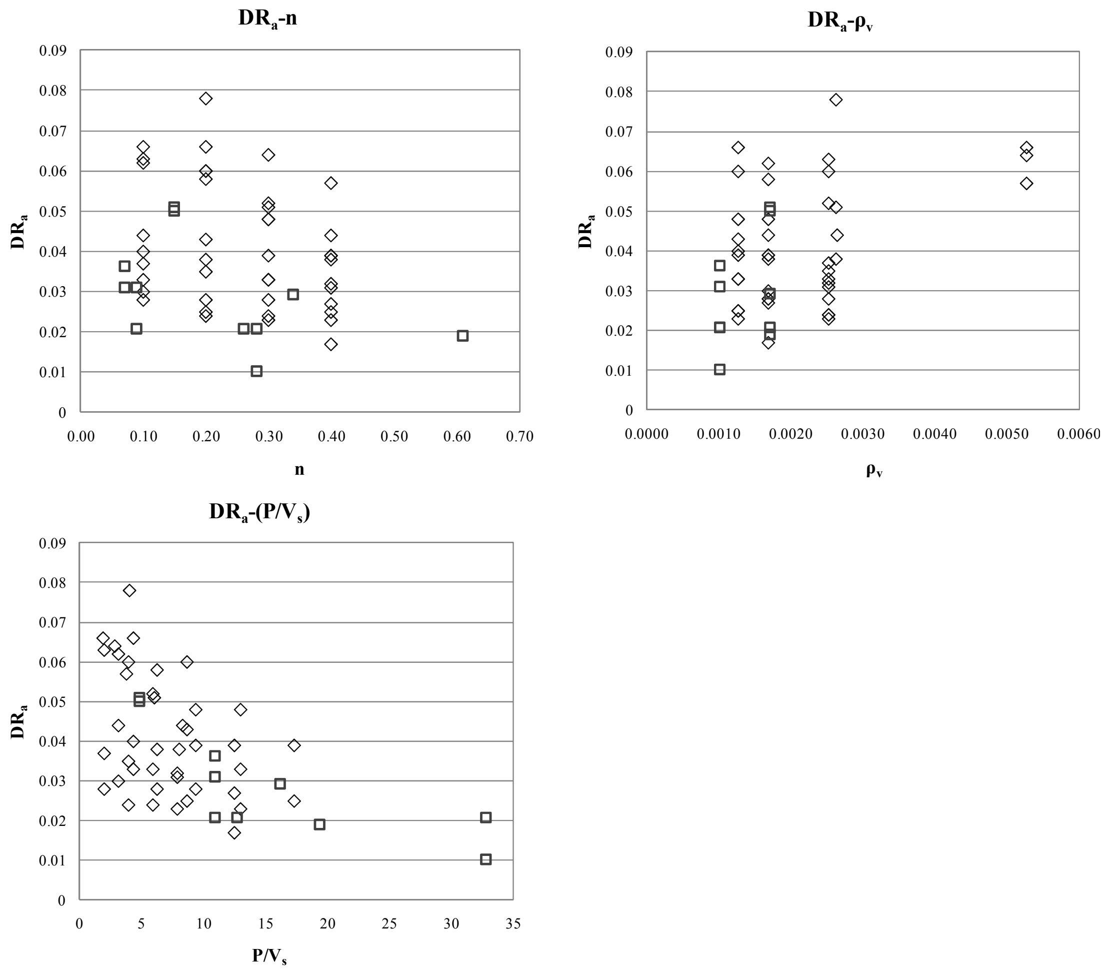

Figure 3.5 Effect of Key Parameters on the Drift Ratio at Axial failure for Flexure-Shear Failure Specimens

Figure 3.5 reveals that as the axial load ratio increases drift ratio at axial failure decreases. As ratio of the shear strength provided by the transverse reinforcement steel to applied axial load increases, drift ratio at axial failure increases. Finally, as transverse reinforcement ratio increases, drift capacity at axial failure increases proportionally.

Considering variables nonlinear regression analysis was performed and Eq. (3.2) is obtained as a best fit to the data.

$$DR_a = \frac{0.2}{2.7 + 0.04P^2 \left(V_s\right)^{-0.8}} \tag{3.2}$$

In Eq. (3.2), P is applied axial load in KN, V_s is the shear strength provided by transverse reinforcement in N and DR_a is the drift ratio at axial failure for flexure-shear critical column.

Statistical analysis results based on ratio of measured to calculated values are presented in Table 3.8 including comparison with those of Eq. (2.2) proposed by Elwood [9].

Table 3.8 Summary of Statistical Analysis performed on Drift at Axial Failure Data Estimated by Proposed Equation and Equation Developed by Elwood [9] for Flexure-Shear Failure Specimens

		Equation	
		Proposed (Eq. (3.2))	Elwood (Eq. (2.2))
All Specimens (26 Columns)	Mean	0.99	1.13
	Standard Deviation	0.13	0.29
	Coefficient of Variation	0.13	0.26
Database (7 Columns)	Mean	0.97	0.92
	Standard Deviation	0.15	0.16
	Coefficient of Variation	0.15	0.17

Table 3.8 reveals that proposed equation has better accuracy when both mean values and coefficient of variation values are compared. Drift ratio at axial failure is better estimated for database and all specimens in comparison to that estimated with Eq. (2.2) proposed by Elwood [9]. Therefore, it is suggested to use proposed Eq. (3.2) in order to estimate the drift ratio at axial failure for flexure-shear critical columns. Measured and calculated values are plotted and presented in Figure 3.6.

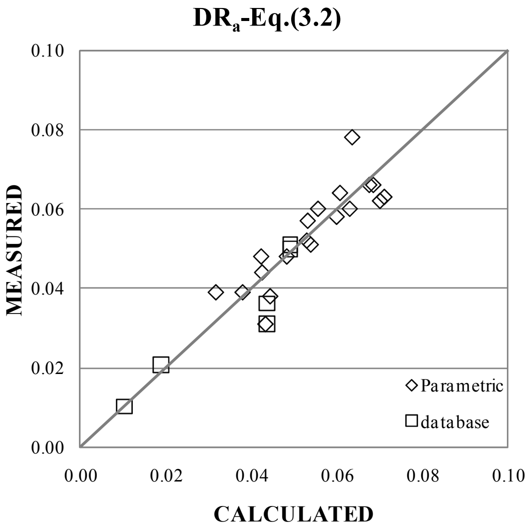

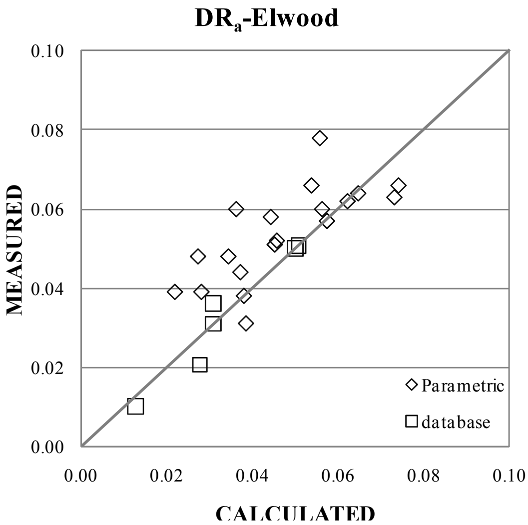

Figure 3.6 Comparison of Measured and Calculated Drift Ratios at Axial failure for Eq. (3.2) and Equation Proposed by Elwood [9] for Flexure-Shear Critical Columns

3.4.3. Simplified Drift Limits

Considering the database of the columns used in the derivation of drift capacity equations, simplified safe drift limits were obtained based on a lower bound limit with a probability of safety such that 85 % of the data is on the safe side for flexure-shear columns and 95% of the data is on the safe side for shear critical columns. Considering V_n/V_{flex} ratio, a lower bound equation is developed for drift ratio at shear failure, DR_s, and for drift ratio at axial failure, DR_a, for the specimens that experienced yielding before shear capacity is reached. In the development of the lower bound equations, shear critical and flexure-shear critical members are considered. In order to determine drift limits and to fit an equation, data is plotted against V_n/V_{flex} ratio. Plots are presented in Figure 3.7. Boundary lines for the failure modes are identified on plots.

Drift ratio at first yielding of reinforcement is determined by utilizing the Eq. (3.3). Simplified drift ratio equations were obtained separately for columns failing in shear and flexure shear mode.

For the drift ratio at first yielding of longitudinal reinforcement;

$$DR_y = \frac{M_p L}{3EI_e} \tag{3.3}$$

In Eq. (3.3), M_p is the plastic moment capacity of the section, EI_e is the effective flexural rigidity of the column section calculated according to the TEC2007 [1] procedure, L is the length of the column measured from end to inflection point or shear span.

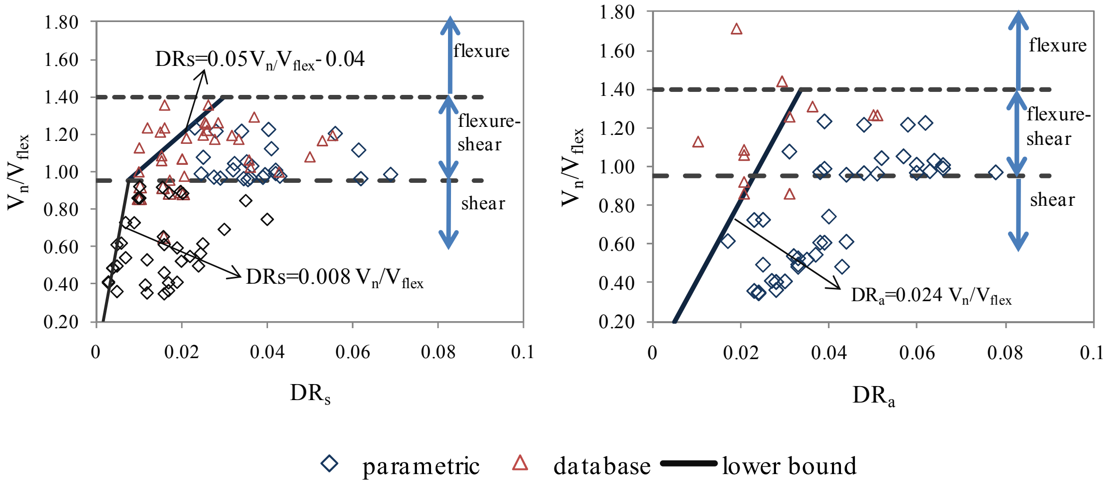

Figure 3.7 Simplified Drift Limits for Drift Ratio at Shear Failure, DR_s, and Drift Ratio at Axial Failure DR_a

For derivation of simplified safe drift ratio equations at shear failure, properties of the data included in analyses are;

For columns failing in shear mode ($V_n/V_{flex}<0.95$),

- Shear span to depth ratio: $0.65 \leq \frac{a}{d} \leq 3.9$
- Axial load ratio: $0 \leq n \leq 0.4$
- Transverse reinforcement ratio: $0.001 \leq \rho_v \leq 0.0031$
- Maximum shear stress: $0.24 \leq \frac{v}{\sqrt{f_c{}'}} \leq 0.70$ (Mpa units)

For columns failing in flexure-shear mode ($0.95<V_n/V_{flex}<1.4$),

- Shear span to depth ratio: $1.32 \leq \frac{a}{d} \leq 3.9$
- Axial load ratio: $0 \leq n \leq 0.56$
- Transverse reinforcement ratio: $0.001 \leq \rho_v \leq 0.0053$
- Maximum shear stress: $0.24 \leq \frac{v}{\sqrt{f_c{}'}} \leq 0.70$ (Mpa units)

For derivation of simplified safe drift ratio equations at axial failure, properties of the data included in analyses are;

For columns failing in shear mode ($V_n/V_{flex}<0.95$),

- Shear span to depth ratio:$0.65 \leq \frac{a}{d} \leq 3.75$
- Axial load ratio: $0.09 \leq n \leq 0.4$
- Transverse reinforcement ratio: $0.001 \leq \rho_v \leq 0.0025$

For columns failing in flexure-shear mode ($0.95<V_n/V_{flex}<1.4$),

- Shear span to depth ratio: $1.25 \leq \frac{a}{d} \leq 3.75$
- Axial load ratio: $0.07 \leq n \leq 0.4$
- Transverse reinforcement ratio: $0.001 \leq \rho_v \leq 0.0053$

Simplified drift ratio equations are obtained as follows;

$$DR_s = 0.008\frac{V_n}{V_{flex}} \qquad \text{for} \qquad 0.2 \leq \frac{V_n}{V_{flex}} \leq 0.95 \qquad \textbf{(3.5)}$$

$$DR_s = 0.05\frac{V_n}{V_{flex}} - 0.04 \qquad \text{for} \qquad 0.95 \leq \frac{V_n}{V_{flex}} \leq 1.4 \qquad \textbf{(3.6)}$$

For the drift ratio at axial failure;

$$DR_a = 0.024\frac{V_n}{V_{flex}} \qquad \text{for} \qquad 0.2 \leq \frac{V_n}{V_{flex}} \leq 1.4 \qquad \textbf{(3.7)}$$

In Eq.(3.5) thorough Eq. (3.7), V_n is the shear strength of the column section calculated according to the TS500 [31], V_{flex} is the flexural shear strength which is obtained from dividing the moment capacity, calculated with equivalent rectangular stress block assumption or by section analysis, of the column end section with the shear span, a. In calculation of V_n and V_{flex}, nominal material strengths are used.

Simplified drift limit equation are proposed in order to estimate an idealized lateral load-displacement response for a shear critical column, especially a shear critical column for which yielding of longitudinal reinforcement occurs before shear capacity is reached. In this way, some inelastic deformations are expected. Lateral strength of the column is determined by comparing shear strength, V_n with flexural shear strength, V_{flex} and selecting the smaller one as the lateral load capacity. Once the lateral load-displacement curve is obtained, ductility of the section can be estimated. Figure 3.8 shows a generic representation of the lateral load-drift ratio response.

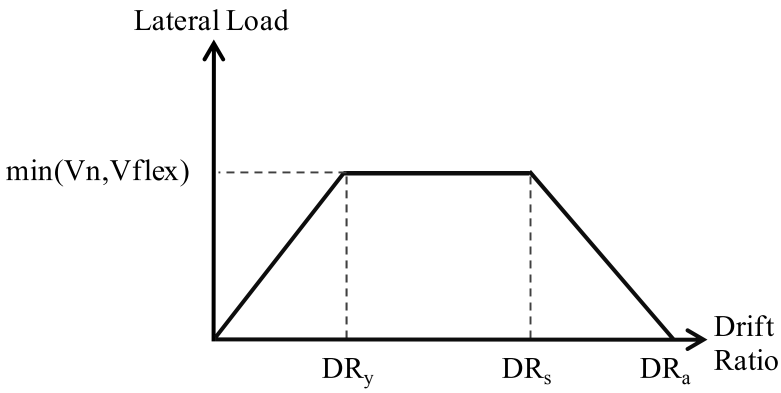

Figure 3.8 Lateral Load-Drift Ratio Graphical Representation of a Shear Critical Column

The response of shear critical members presented in Chapter 2, are compared with the estimations of the simplified drift ratio models. They are also assessed according to the FEMA356 [23] and ASCE/SEI41 [22] update supplement. Lateral load capacities, and drift ratios for different performance points are determined and presented in Table 3.9. Failure modes of columns estimated by linear and nonlinear procedures according to the TEC2007 [1], and by nonlinear procedures according to FEMA356 [23], EC8 [25], and ASCE/SEI41 [22], and failure modes reported in Peer Column Database [4] are presented. V_n and V_{flex} were calculated according to the procedures explained in TEC2007 [1]. In Table 3.9, M_n is the moment capacity of the section; V_n is the shear strength of the section. Failure (1) is the failure type reported in database. Failure TEC (L1) is the failure type determined according to the linear procedure given in TEC2007 [1] where moment capacity is taken as 1.4 times design moment capacity of the section. Failure TEC (L2) is the failure mode determined according to the procedure explained in TEC2007 [1] where moment capacity is determined by moment-curvature analysis. Failure F356 is the failure mode determined according to the nonlinear procedure given in FEMA356 [23], failure EC8 is the failure mode determined according to the procedures given in Eurocode 8 [25], and finally, failure ASCE_UP is the failure type determined according to the nonlinear procedure defined in ASCE/SEI41 [22] update document.

Table 3.9 Properties of Column Specimens Modeled with Simplified Drift Limits and Estimated Failure Modes by Different Approaches

Specimen	a (mm)	M_n (KN.m)	V_n (KN)	M_d (KN.m)	V_d (KN)	V_{test} (KN)	V_{flex} (KN)	$\frac{V_n}{V_{flex}}$	DR_y	DR_s	DR_a	Failure (1)	Failure TEC(L1)	Failure TEC(L2)	Failure F356	Failure ASCE_UP	Failure EC8
Lynn (2001)																	
2CLH18	1473.2	332.0	272.8	292.0	225.5	240.8	225.4	1.21	0.004	0.021	0.029	F-S	B	D	S	II	D
2CMH18	1473.2	408.0	302.0	320.0	249.3	306.0	276.9	1.09	0.003	0.015	0.026	F-S	B	D	F	II	D
3SMD12	1473.2	501.0	371.6	398.0	309.9	367.0	340.1	1.09	0.004	0.015	0.026	F-S	B	D	S	II	D
3CLH18	1473.2	442.0	248.9	377.0	205.9	277.0	300.0	0.83	0.005	0.007	0.020	S	B	B	S	III	B
3CMH18	1473.2	515.0	309.7	411.0	255.5	328.0	349.6	0.89	0.004	0.007	0.021	S	B	B	S	III	B
3CMD12	1473.2	515.0	381.6	411.0	318.1	355.0	349.6	1.09	0.004	0.015	0.026	S	B	D	S	II	D
3SLH18	1473.2	442.0	248.9	377.0	205.9	270.0	300.0	0.83	0.005	0.007	0.020	S	B	B	S	III	B
Nagasaka (1982)																	
HPRC10-63	300	26.0	119.9	23.0	102.3	86.9	86.7	1.38	0.001	0.029	0.033	S	D	D	F	II	D
Sezen and Moehle (2002)																	
NO:1	1473.2	382.0	308.4	322.0	259.1	314.8	259.3	1.19	0.004	0.019	0.029	F-S	D	D	F	II	D
NO:2	1473.2	369.0	402.8	232.0	336.1	359.0	250.5	1.61	0.007	0.030	0.039	F-S	D	D	F	II	D
NO:4	1473.2	386.0	311.3	325.0	261.4	294.6	262.0	1.19	0.004	0.019	0.029	F-S	D	D	F	II	D
Umehera and Jirsa (1982)																	
CUW	455	127.0	216.4	112.0	182.0	263.2	279.1	0.78	0.003	0.006	0.019	S	B	B	S	III	B
Wight and Sozen (1973)																	
25.033	876	79.6	95.2	69.9	80.1	93.3	90.9	1.05	0.006	0.012	0.025	F-S	B	B	F	II	B
40.033a(East)	876	87.7	95.2	77.6	85.0	98.8	100.1	0.95	0.006	0.010	0.024	F-S	B	B	S	II	B
40.048(East)	877	84.6	101.1	74.9	95.1	104.6	96.5	1.05	0.005	0.018	0.028	F-S	B	D	S	II	D

Notation: a: Shear span, V_{test}: Peak lateral load recorded in test data, DR_y: Drift ratio at yielding of longitudinal reinforcement, DR_s: Drift ratio at shear failure, DR_a: Drift ratio at axial failure. B: failure type classified as "Brittle", D: Failure type classified as "Ductile", F : flexure controlled column, S: shear controlled column (FEMA356). II: flexure-shear critical column, III: shear critical column.

If Table 3.9 is studied for the estimations of TEC2007 [1] procedures, it can be observed that failure types predicted by procedures (L1) and (L2) are not compatible. Procedure (L1) produces conservative results, since it is based on approximate solutions. All procedures predicted the failure type of the specimen HPRC10-63 incorrectly as “ductile” which was reported to have failed in shear. This may be resulted from the small shear span to depth ratio of 1.7. Failure mode of another shear-failed specimen, 3CMD12, is also predicted as “ductile” failure by L2 procedure contrary to test result, which is “brittle”. This overestimation may have resulted from large spacing of lateral reinforcement or opening of hoops causing rapid degradation of shear strength. When specimens 25.033, 40.033 and 40.048 are considered, it is seen that all procedures predicts the response conservatively for V_n/V_{flex} ratio close to unity even if those specimens failed in flexure-shear mode.

When failure type estimations of FEMA356 [23] nonlinear procedure and ASCE/SEI41 [22] nonlinear procedures are compared, it is seen that they are completely different. FEMA356 [23] predicted the failure mode of the most of the flexure-shear critical columns as “brittle” or “shear controlled” and inelastic deformation is not permitted for those specimens being much more on the conservative side. However, by including an additional failure type that is type II for flexure-shear critical members, ASCE/SEI41 [22] update supplement provisions yielded more accurate failure modes for the specimens. When compared to TEC2007 [1] nonlinear procedure, the difference is that ASCE/SEI41 [22] supplement nonlinear procedures included a new failure mode for flexure-shear critical elements and therefore, failure types of specimens 25.033, 40.033 and 40.048 were predicted as type II and inelastic deformations were permitted for those specimens. On the other hand TEC2007 [1] predicted the failure type conservatively. Eurocode8 (EC8) [25] procedure yielded failure types similar to TEC (L2) procedure. When the failure type classification for EC8 [25] was performed comparing the shear strength calculated according to the formulation based on ductility demand (Equation A.12 given in section A.3.3.1 of the EC8 [25]) it has been discovered that all members are classified as “brittle”. This classification is observed to be overly conservative. Therefore, shear strength of columns obtained from the equations proposed in reinforced concrete design part of Eurocode 2 [33] was employed while deciding on the failure mode. Calculated shear strengths were compared to lateral load causing hinging at column ends and failure type was determined for each column specimen. When compared with the failure types given in database, ASCE/SEI41 [22] update provisions predicted the all failure mode correctly except from the specimen HPRC10-63 whose failure mode was predicted wrongly by all procedures.

Specimens for which properties given in Table 3.9, load-displacement curves given in database, estimated according to the NL procedures given in seismic assessment codes and predicted by proposed simplified drift limits are plotted together on same graph to make comparison. Plots are presented in Figure 3.9 for specimens whose failure mode is reported as flexure-shear and in Figure 3.10 for specimens whose failure mode is reported as shear. In Figure 3.9 and Figure 3.10, legend "SDL" stands for the estimations obtained by simplified drift limit equations. Drift ratio at shear failure, drift ratio at axial failure are calculated with simplified drift limit equations and plotted. Therefore, SDL plots drift ratios at yield, at shear failure and at axial failure points.

It should be noted that monotonic backbone curves plotted according to the guidelines of seismic codes are based on performance levels. This representation is explicitly presented in Figure 2.6 for TEC 2007 procedure and it is obtained in similar manner for other codes. True estimation of backbone curves for ASCE 41 update supplement and FEMA 356 should be determined from the prescribed modeling parameters.

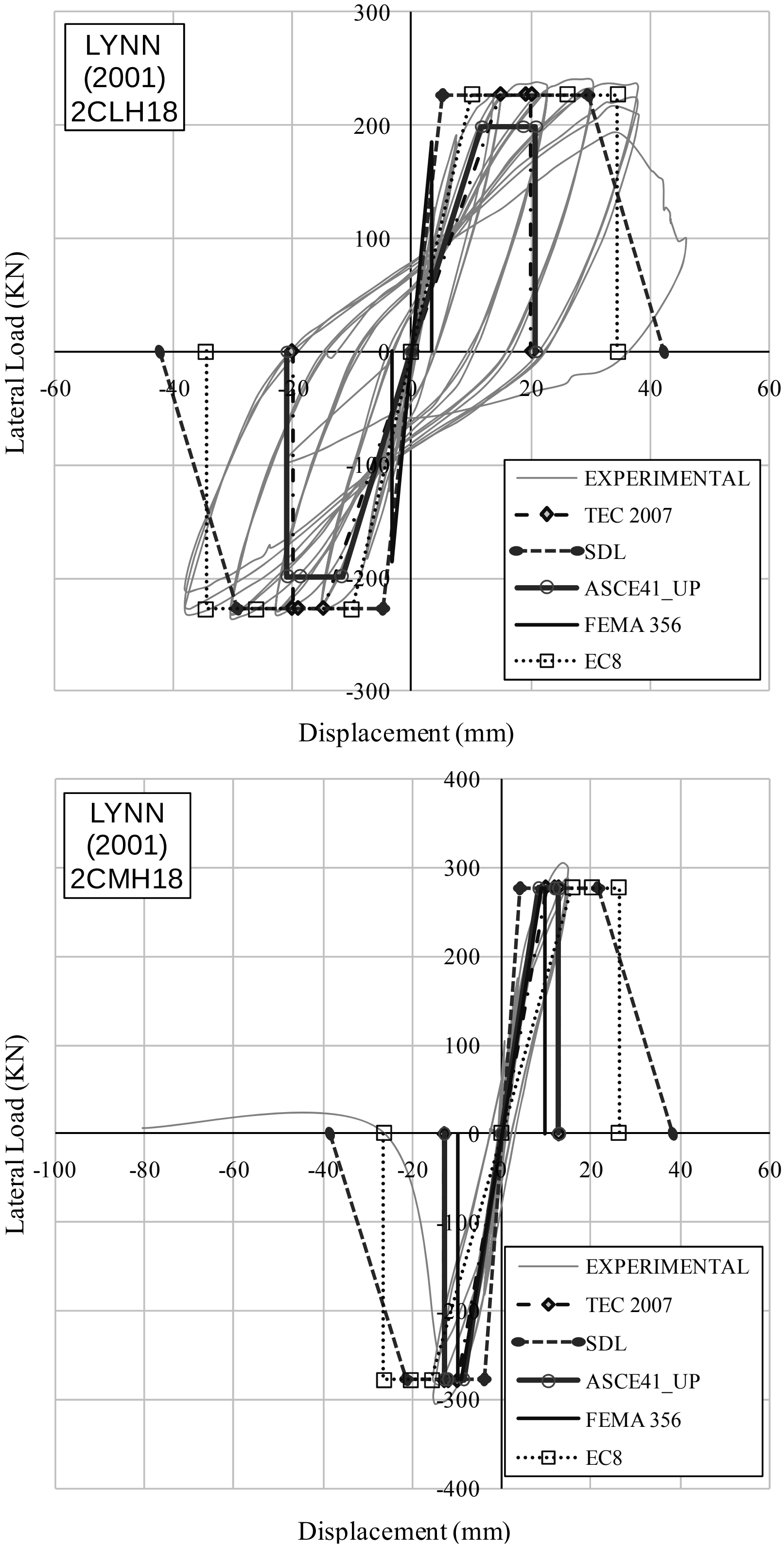

Figure 3.9 Lateral Load-Displacement Curves of Flexure-Shear Failure Specimens

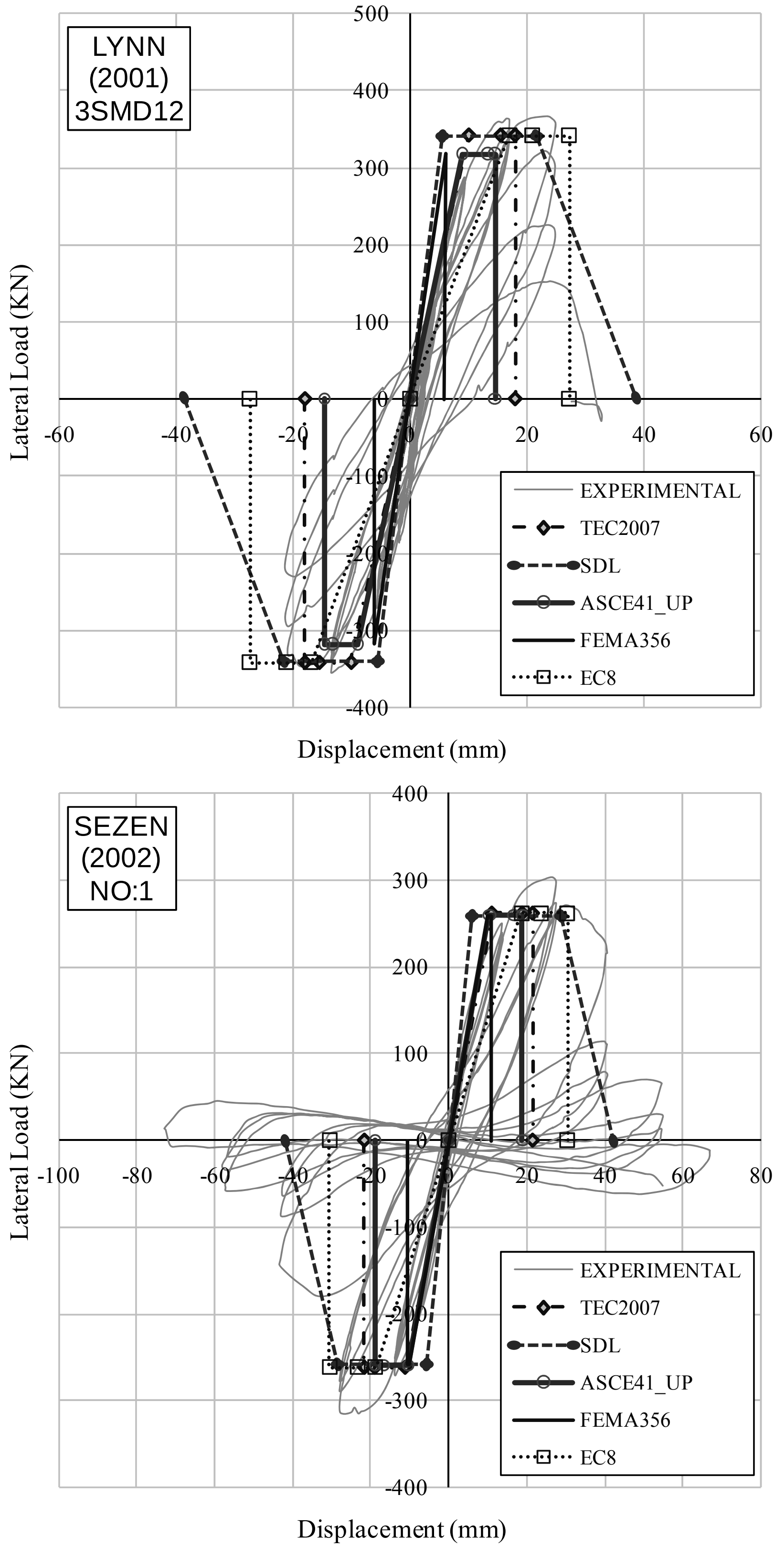

Figure 3.9 (Cont'd) Lateral Load-Displacement Curves of Flexure-Shear Failure Specimens

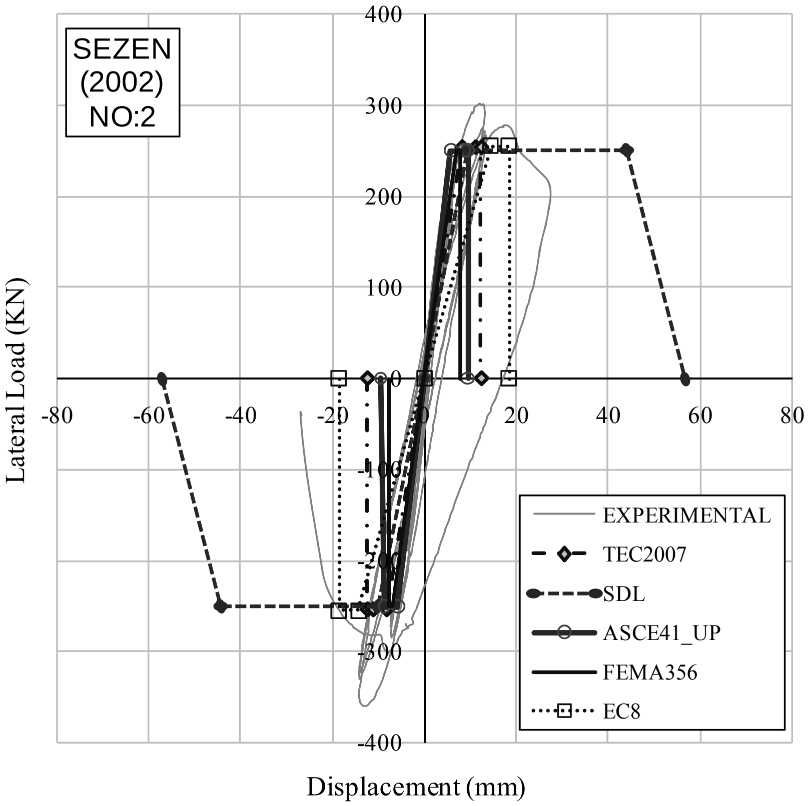

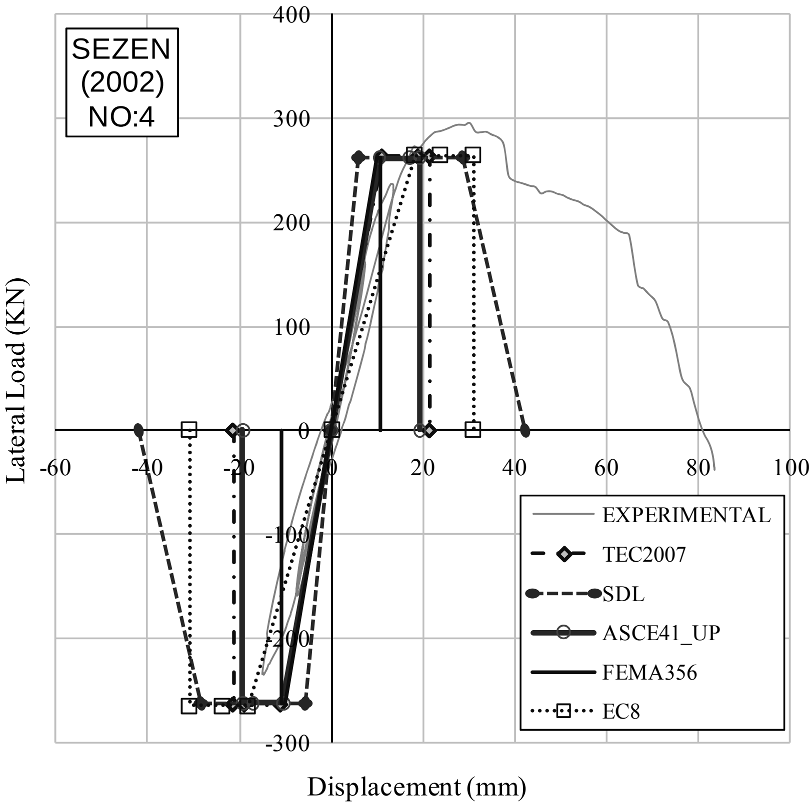

Figure 3.9 (Cont'd) Lateral Load-Displacement Curves of Flexure-Shear Failure Specimens

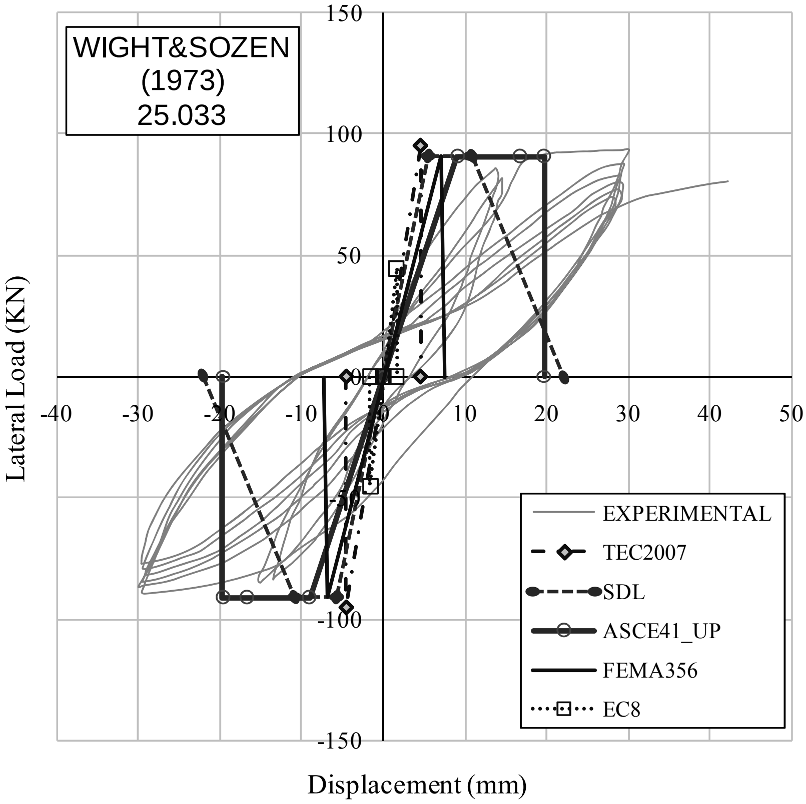

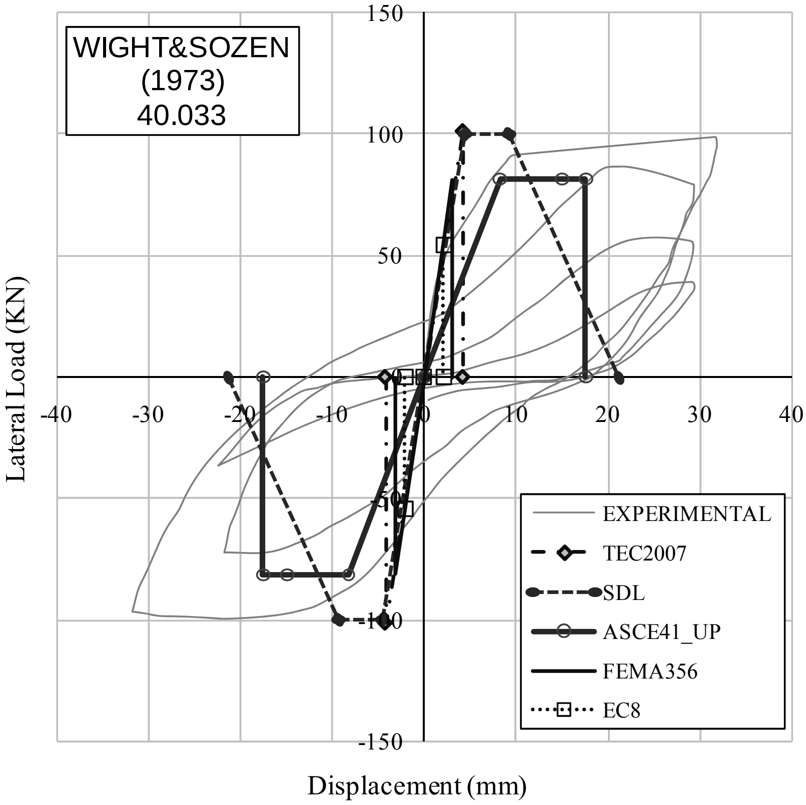

Figure 3.9 (Cont'd) Lateral Load-Displacement Curves of Flexure-Shear Failure Specimens

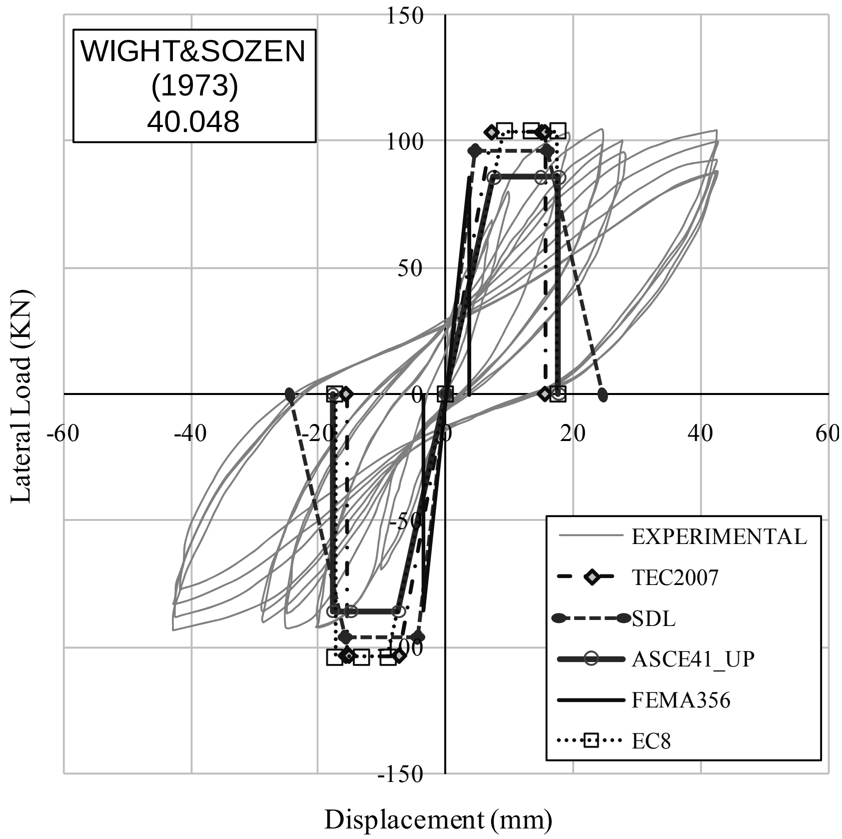

Figure 3.9 (Cont'd) Lateral Load-Displacement Curves of Flexure-Shear Failure Specimens

Figure 3.9 shows that performances of most of the flexure-shear critical columns are underestimated by the TEC2007 [1]. When columns reached collapse prevention damage limit according to the TEC2007 [1], they did not reach even shear failure point considering lower bound drift ratio limit given in Section 3.4.3. Considering, specimens 25.033, 40.033, and 40.048 that experienced inelastic deformations and had displacement ductility of approximately 4 in cyclic tests, it is inferred that TEC2007 [1] underestimates the response of flexure-shear columns having V_n/V_{flex} ratio around unity. None of the columns that are at the collapse prevention damage limit state according to the TEC2007 [1] in Figure 3.9 reached the shear failure drift ratio estimated by simplified drift ratio limits. That conclusion also shows that TEC2007 [1] underestimates the response of flexure-shear critical columns and may results in unnecessary retrofitting solutions. FEMA356 [23] nonlinear procedures estimated the failure mode more conservatively than TEC2007 [1] did. Even if the failure mode is estimated correctly, performance levels are predicted conservatively when compared to ASCE/SEI41 update and TEC 2007 [1]. Same deformation capacities are accepted for IO and LS performance level, therefore conservative results were obtained even for semi-ductile members. When the estimations of the EC8 [25] are examined, it is seen that performance level limits are overestimated for most of the columns which are classified as "ductile columns". According to the procedures of EC8 [25], for brittle columns, lateral load capacities were lowered considering that the ductility demand causes decrease in lateral load capacity of a column. Proposed simplified drift capacity equations yielded results that agree with test results. Load-deformation response of some of the columns was overestimated. However, it is noted that equations were developed for a safety level of 15%.

Table 3.9 summarizes the estimations of failure types of columns for different code procedures. Considering the columns of which failure mode is estimated as ductile, statistical analysis is performed on estimations. For this purpose, performance level or acceptance criteria are determined from the test results based on procedure given in FEMA356 [23]. Performance levels of primary members by procedure given in FEMA356 [23] are as follows;

- Immediate Occupancy (IO): 0.67 times the deformation limit for life safety.
- Life Safety (LS): 0.75 times the deformation at shear failure.
- Collapse Prevention (CP): Deformation at shear failure but not greater than the 0.75 times the deformation at loss of lateral load capacity.

Drift limits for immediate occupancy (IO), life safety (LS) and collapse prevention (CP) performance levels are determined for all code provisions and proposed simplified drift limits. Ratio of measured drifts to calculated drifts are obtained. Statistical analyses are performed to determine the safety of the procedures. Results of the analysis are presented in Table 3.10. Calculated drift limits and lateral load capacities are presented in Table 3.11.

Table 3.10 Statistical Analysis Results for Ductile Specimens

		Performance Level			Capacity
Procedure	Stat.	IO	LS	CP	V
TEC2007	μ	1.50	1.32	1.47	1.12
	σ	0.79	0.55	0.51	0.13
	cov	0.53	0.42	0.35	0.12
FEMA356	μ	1.70	2.23	2.48	1.15
	σ	0.64	1.00	1.19	0.16
	cov	0.38	0.45	0.48	0.14
ASCE/SEI 41 UPDATE	μ	1.74	1.48	1.54	1.16
	σ	0.63	0.42	0.41	0.12
	cov	0.36	0.29	0.26	0.10
EC8	μ	1.13	1.15	1.07	1.10
	σ	0.73	0.64	0.48	0.13
	cov	0.65	0.56	0.45	0.14
Simplified Equations	μ	1.57	1.57	1.50	1.11
	σ	1.07	1.07	0.81	0.11
	cov	0.68	0.68	0.54	0.10

Table 3.11 Failure Types, Drift Limits for Performance Levels, and Lateral Load Capacity of Columns Obtained by Different Procedures

		Failure Types-Drift Ratio Limits for Performance Levels-Lateral Load Capacity of Columns																												
		TEST					ASCE UPDATE					FEMA 356					EUROCODE 8-Part3					TEC2007					SIMP. DRFT. EQTNS			
Speciemen	L_{in}	FT	IO	LS	CP	V	FT	IO	LS	CP	V	FT	IO	LS	CP	V	FT	IO	LS	CP	V	FT	IO	LS	CP	V	IO	LS	CP	V
Lynn (2001)																														
2CLH18	1473	F-S	0.0131	0.0195	0.0234	241	II	0.0080	0.0127	0.0142	199	S	-	-	0.002	186	D	0.0068	0.0178	0.0235	227	D	0.0101	0.0129	0.0136	227	0.0101	0.0151	0.0151	227
2CMH18	1473	F-S	0.0052	0.0077	0.0077	306	II	0.0057	0.0081	0.0087	277	F	0.006	0.006	0.007	277	D	0.0107	0.0138	0.0179	278	D	0.0068	0.0081	0.0088	277	0.0073	0.0109	0.0109	277
3SMD12	1473	F-S	0.0078	0.0116	0.0155	367	II	0.0061	0.0090	0.0099	318	S	-	-	0.004	318	D	0.0115	0.0143	0.0186	341	D	0.0069	0.0106	0.0123	340	0.0074	0.0110	0.0110	340
3CLH18	1473	S	-	-	0.0103	277	III	-	-	0.0048	222	S	-	-	0.003	222	B	-	-	0.0026	178	B	-	-	0.0041	249	0.0033	0.0050	0.0050	249
3CMH18	1473	S	-	-	0.0103	328	III	-	-	0.0033	286	S	-	-	0.004	286	B	-	-	0.0036	278	B	-	-	0.0031	310	0.0036	0.0053	0.0053	310
3CMD12	1473	S	0.0080	0.0120	0.0155	355	II	0.0062	0.0093	0.0103	328	S	-	-	0.004	328	D	0.0105	0.0147	0.0192	353	D	0.0067	0.0086	0.0097	350	0.0073	0.0109	0.0109	350
3SLH18	1473	S	-	-	0.0100	270	III	-	-	0.0048	222	S	-	-	0.003	222	B	-	-	0.0026	178	B	-	-	0.0041	249	0.0033	0.0050	0.0050	249
Nagasaka (1982)																														
HPRC10-63	300	S	0.0086	0.0129	0.0172	87	II	0.0042	0.0118	0.0148	87	F	0.004	0.010	0.012	87	D	0.0084	0.0118	0.0150	90	D	0.0067	0.0260	0.0261	87	0.0147	0.0219	0.0219	87
Sezen and Moehle (2002)																														
NO:1	1473	F-S	0.0129	0.0192	0.0256	315	II	0.0070	0.0113	0.0128	259	F	0.007	0.007	0.007	259	D	0.0127	0.0160	0.0207	262	D	0.0075	0.0128	0.0147	259	0.0098	0.0146	0.0146	259
NO:2	1473	F-S	0.0044	0.0066	0.0088	359	II	0.0039	0.0059	0.0064	250	F	0.005	0.005	0.005	250	D	0.0098	0.0098	0.0126	255	D	0.0055	0.0075	0.0083	250	0.0151	0.0225	0.0225	250
NO:4	1473	F-S	0.0144	0.0215	0.0287	295	II	0.0071	0.0116	0.0131	262	F	0.007	0.007	0.007	262	D	0.0123	0.0161	0.0209	264	D	0.0075	0.0128	0.0145	262	0.0097	0.0145	0.0145	262
Umehera and Jirsa (1982)																														
CUW	455	S	0.0104	0.0155	0.0207	263	III	-	-	0.0024	216	S	-	-	0.002	216	B	-	-	0.0022	171	B	-	-	0.0021	216	0.0031	0.0047	0.0047	216
Wight and Sozen (1973)																														
25.033	876	F-S	0.0180	0.0269	0.0269	93	II	0.0103	0.0190	0.0225	91	F	0.008	0.008	0.008	91	B	-	-	0.0019	45	B	-	-	0.0170	91	0.0062	0.0093	0.0093	91
40.033a(East)	876	F-S	0.0182	0.0272	0.0272	99	II	0.0094	0.0171	0.0200	81	S	-	-	0.003	81	B	-	-	0.0024	54	B	-	-	0.0048	100	0.0053	0.0079	0.0079	100
40.048(East)	877	F-S	0.0278	0.0416	0.0416	105	II	0.0086	0.0169	0.0202	86	S	-	-	0.004	86	D	0.0103	0.0153	0.0199	104	D	0.0083	0.0173	0.0178	96	0.0091	0.0136	0.0136	96

Notation: L_{in}: Column length from column end to inflection point measured in mm's, FT: failure type, IO: Immediate occupancy, LS: Life safety, CP: Collapse prevention performance levels, V: Lateral load capacity (KN), unit. F-S: Flexure-shear failure, S: Shear failure, II: flexure-shear critical, III: Shear critical (ASCE update), D: ductile member, B: brittle member, F: flexure controlled, S: shear controlled (FEMA356), (Filled cells shows that estimated drift ratio is unsafe with respect to test results)

If Figure 3.9, Table 3.11 and results of statistical analysis performed on data are examined, following conclusions can be drawn;

- IO performance level is best estimated by TEC2007 [1] procedure however, estimations have a higher probability of failure when compared to estimations of ASCE/SEI41 [22] update supplement. Simplified equations also produced satisfactory estimations with a mean value that is close to that of TEC2007. FEMA356 [23] and ASCE/SEI41 [22] update supplement yielded close mean and standard deviation for that level. However, FEMA356 yielded a higher unsafe estimation. Accuracy of EC8 [25] is better when the average of the values is considered. However, it has higher percentage of unsafe estimations. Responses of some of the ductile members are overestimated.
- LS performance level is best estimated by TEC2007 [1] update procedure when the mean values are considered. TEC2007 [1] procedure yielded a small mean value when compared to that of the ASCE/SEI41 [22] procedure did. However, scatter of the estimations is high when compared to that of ASCE/SEI41 [22] update procedure. Percentage of unsafe estimations is also higher when compared to estimations of ASCE/SEI41 [22]. FEMA356 [23] yielded very conservative mean value and higher standard deviation for that performance level. EC8 [25] procedure yielded estimations similar to IO case. Accuracy is better when the mean values are compared. However, percentage of unsafe estimations is high.
- CP limit state is best estimated by TEC2007 [1] update procedure. Mean value is 1.47 and coefficient of variation is 0.35. ASCE/SEI41[22] update procedure has higher accuracy when compared to the other code procedures. Percentage of unsafe estimations are also low when compared to the TEC2007 [1] procedure. EC8 [25] procedure overestimated that performance level. When the mean values are considered it is best, however percentage of unsafe estimations is higher. Simplified drift limits produced estimations with acceptable accuracy.
- Another important conclusion is that failure mode is well estimated by ASCE/SEI41 [22] update procedure. TEC 2007[1] and FEMA356 [23] and EC8 [25] tend to be on over conservative side when estimating the failure mode. Being overconservative in estimating the failure mode may lead to incorrect and uneconomical retrofit solutions.
- To conclude ASCE/SEI41 [22] update procedure is better when both statistical results and percentage of unsafe estimations are considered.

Figure 3.10 summarizes the response of shear-failed specimens and estimations of code procedures together with simplified drift estimations. In general, all of the estimations of TEC2007 [1], FEMA356 [23] and ASCE/SEI41 [22] update and EC8 [25] procedures are on the safe side being conservative. However, simplified drift limit estimations show that procedures are also conservative for estimating the collapse limit state of the shear-failed specimens. None of the members reached axial failure limit or even shear failure limit at the drift ratio where code procedures predicted the collapse of member. There are elements such as 3CMD12 and HPRC10-63 for which failure mode is predicted incorrectly by nonlinear procedures of TEC2007 [1], FEMA356 [23], EC8 [25], and ASCE/SEI41 [22] update. Simplified drift limits well predicted the response of shear critical or brittle members.

Table 3.12 Statistical Analysis Results for Performance of Brittle Specimens

		Performance Level		
Procedure	Stat.	IO	LS	CP
TEC2007	μ	-	-	4.26
	max	-	-	9.88
	min	-	-	1.81
FEMA356	μ	-	-	6.16
	max	-	-	10.38
	min	-	-	2.81
ASCE/SEI 41 UPDATE	μ	-	-	3.43
	max	-	-	8.63
	min	-	-	2.10
EC8	μ	-	-	7.62
	max	-	-	14.31
	min	-	-	2.85
Simplified Equations	μ	-	-	1.96
	max	-	-	3.34
	min	-	-	1.45

Inelastic deformation is not allowed for the shear failure or brittle members in modeling. However, mean values obtained from statistical analysis performed on brittle members for all procedures (FEMA356, ASCE/SEI41 update, TEC2007, EC8 and simplified drift limits) showed that axial failure occurs at higher drifts obtained from elastic analysis. Therefore, it can be concluded that deformation capacity at axial failure of shear critical columns is underestimated by EC8 [25], TEC2007 [1] and FEMA356 [23] nonlinear procedures. Based on that fact, ASCE/SEI41 [22] update supplement proposed a limited plastic deformation capacity for shear critical members in modeling parameters.

Statistical analysis results for shear critical members are presented in Table 3.12. It is seen that mean values are high. Maximum and minimum values shows that procedures yielded over conservative results for shear critical columns. Simplified drift limits produced estimations being safe and having lower conservatism when compared to estimations of other procedures.

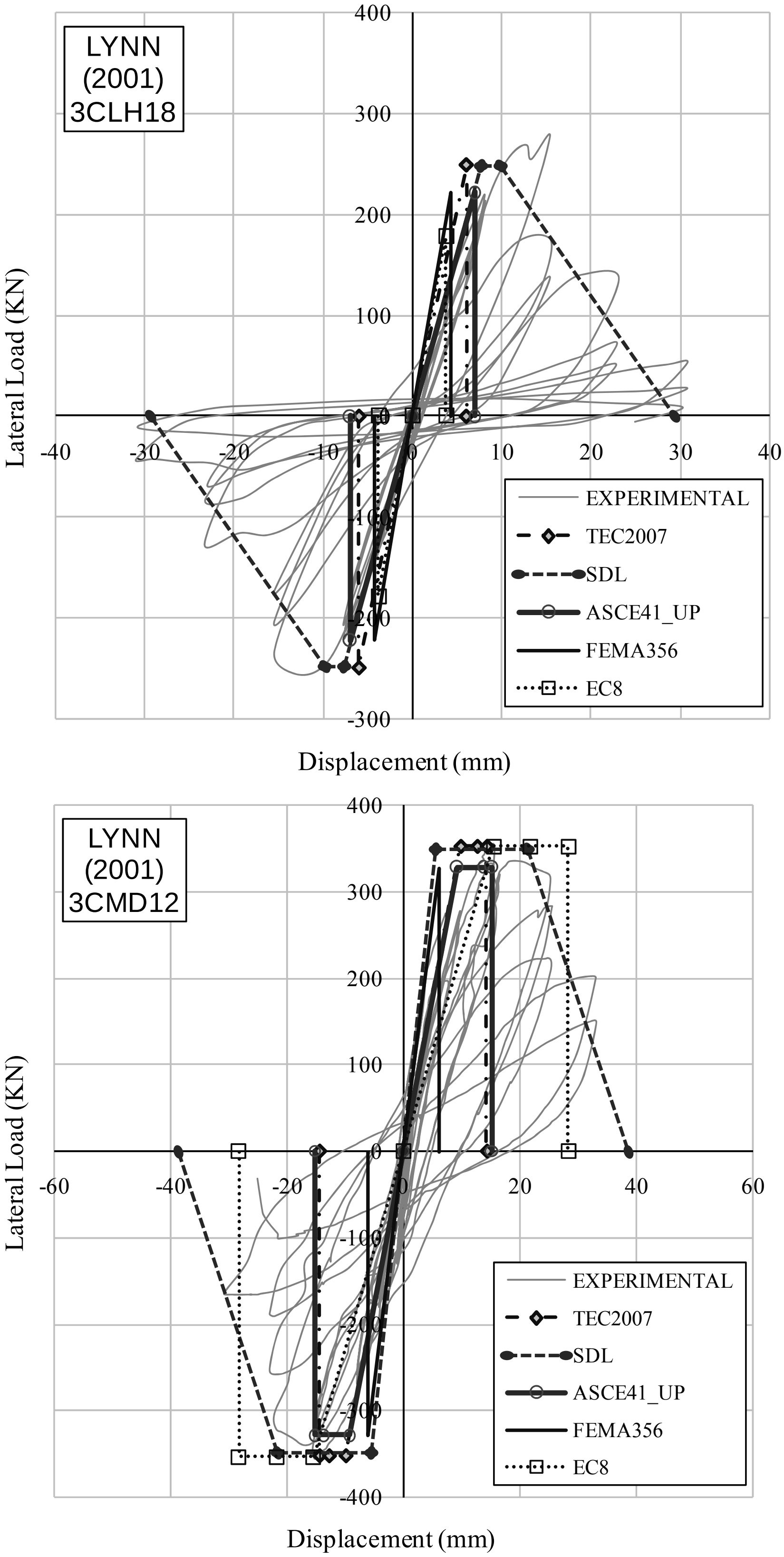

Figure 3.10 Lateral Load-Displacement Curves of Shear Failure Specimens

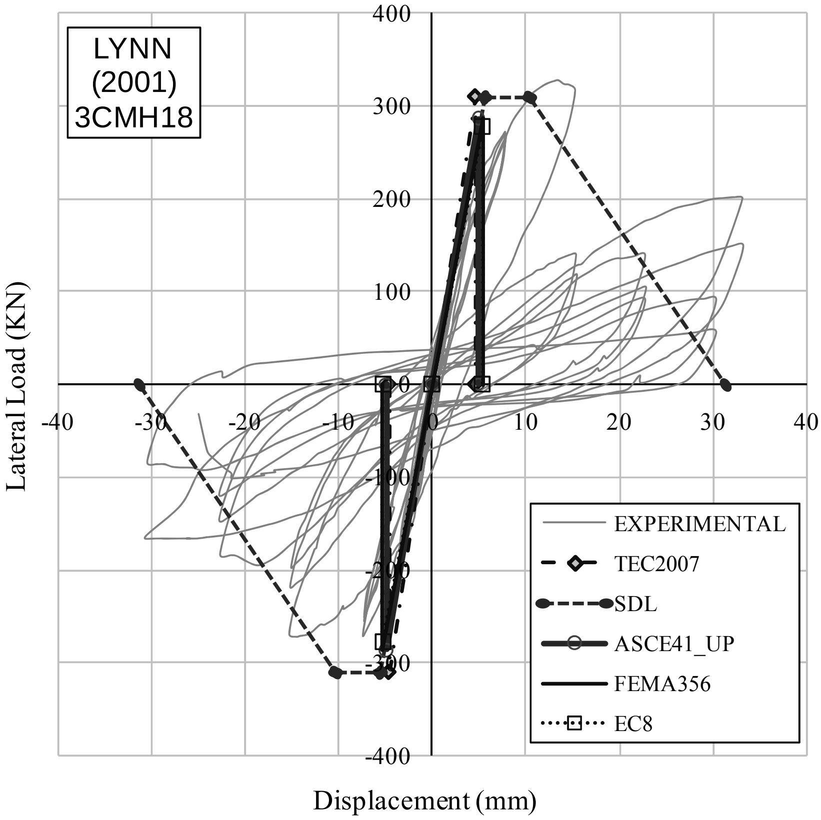

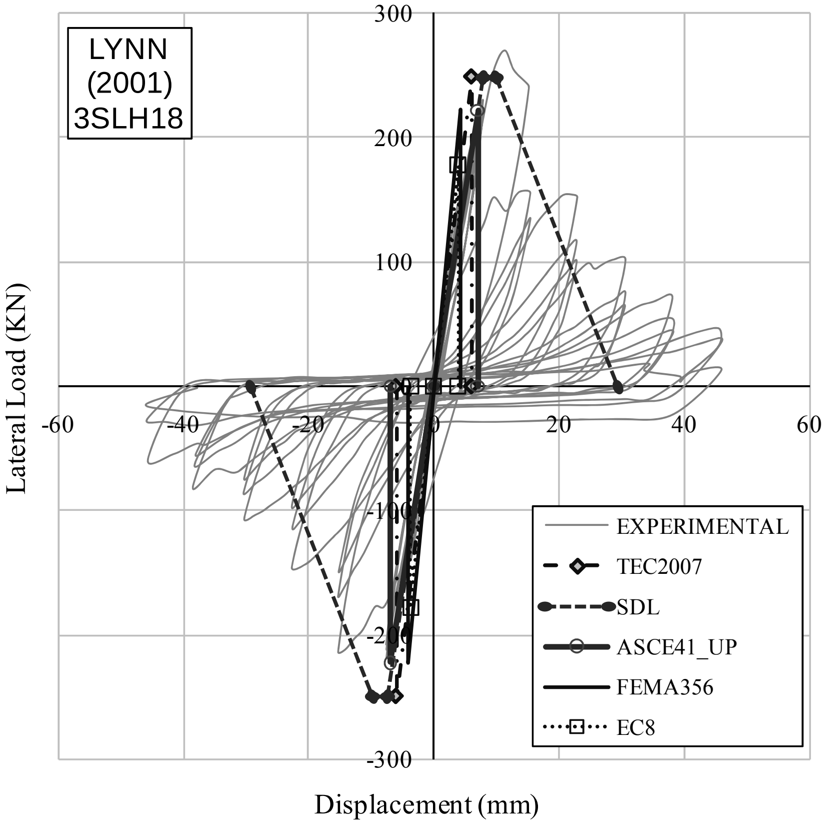

Figure 3.10 (Cont'd) Lateral Load-Displacement Curves of Shear Failure Specimens

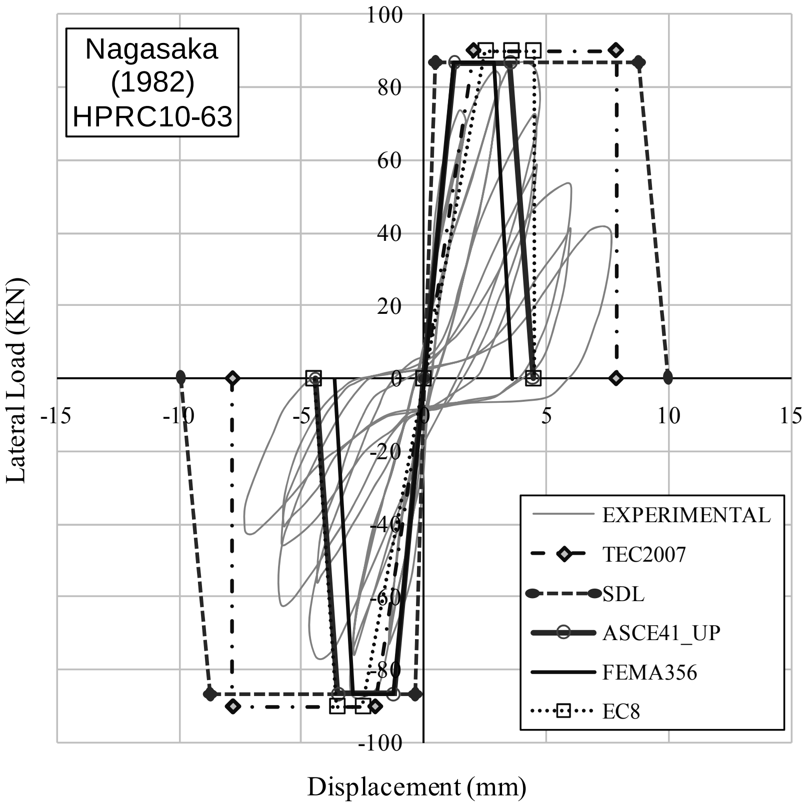

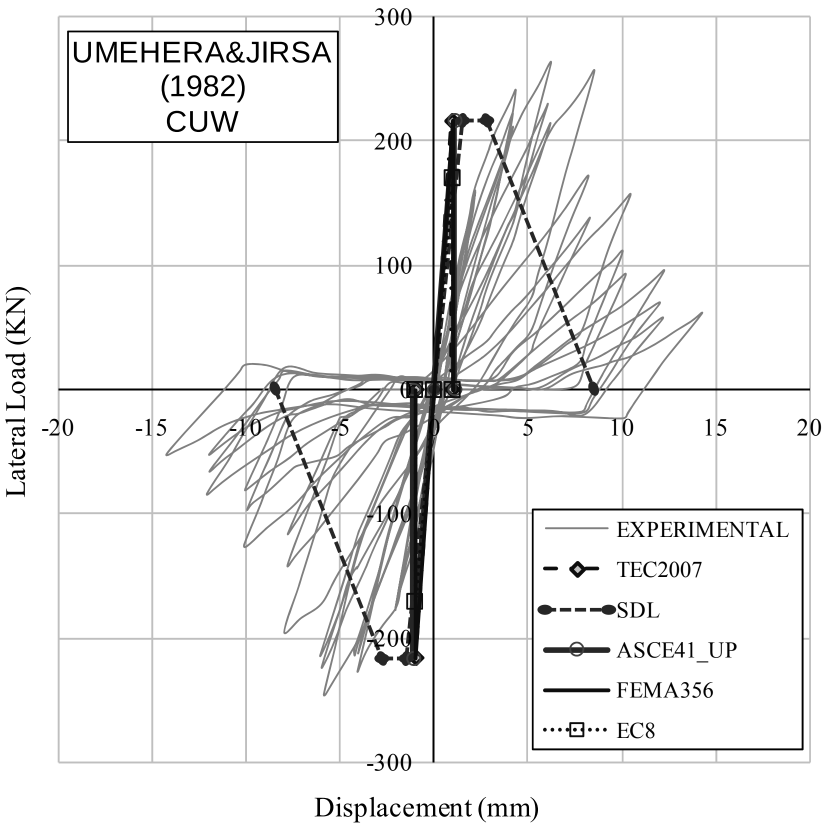

Figure 3.10 (Cont'd) Lateral Load-Displacement Curves of Shear Failure Specimens

CHAPTER 4

CONCLUSIONS AND RECOMMENDATIONS

4.1. General

This study presented analytical investigation of behavior of the reinforced concrete columns under the combined effects of the lateral loads and axial loads. The aim of the study was to investigate the reliability of the performance assessment criteria of reinforced concrete columns. Considering the columns of older reinforced concrete buildings, study mainly focused on behavior of shear-critical columns having possibility of failing in flexure-shear or shear failure modes.

The main content of the study can be divided into two parts. Firstly, studies were performed to obtain a reliable analytical model that predicts a backbone curve to estimate the load deformation behavior of the reinforced concrete columns under the combined effect of lateral and axial loads. Secondly, using the most reliable analytical model, studies were continued to develop simplified drift limit equations for estimation of important deformation levels such as drift shear failure and drift at loss of axial load carrying capacity. In addition, studies were conducted on development of capacity equations for drift ratio at shear failure and drift ratio at loss of axial load capacity based on statistical analyses including tested columns from database and parametric study columns analyzed with selected reliable model. Finally, acceptance criteria and performance levels of the different code provisions (TEC2007 [1], FEMA356 [23], ASCE/SEI41 [22] update supplement, EC8 [25]) are investigated to find out the level of conservatism and deficiencies of the nonlinear procedure specified in TEC2007 [1].

4.2. Conclusions

Conclusions drawn from the study are as follows;

- Axial-shear-flexure interaction is important for the determination of behavior of reinforced concrete columns.

- Obtained results showed that ASFI (M) model predicts the behavior of flexure-shear critical columns with an acceptable accuracy.
- Estimations of the all models showed significant scatter for the columns whose failure mode is shear. Low accuracy is associated with the complex nature of the shear failure.
- Transverse reinforcement ratio and the axial load ratio are the main parameters that mostly affect the drift at shear failure and drift at axial failure. Other parameters have small influence on the drift capacity.
- Bar slip and shear deformations may have important contributions to total drift of the reinforced concrete columns of older structures due to low transverse reinforcement ratio and greater spacing of transverse reinforcement.
- Drift capacity equations proposed by Elwood [9] can be utilized to determine the drift ratio at shear failure and at loss of axial load capacity for shear critical members if properties of the columns are similar to those of Elwood [9] database.
- For the flexure-shear critical members two new empirical drift capacity equations with improved accuracies are proposed to determine drift ratio at shear failure and drift ratio at loss of axial load carrying capacity. Properties of columns included in development of equations are expanded. In other words, columns that are widely used in older construction in Turkey are also analyzed and included in derivations of equations.
- Simplified drift ratio limits are proposed based on ratio of calculated shear strength to shear force to cause flexural hinging of the section. They can be utilized in order to obtain lower bound drift capacities with a safety level of 85 % (probability of failure of 15%) for flexure-shear critical columns and with a safety level of 95% for shear critical columns.
- It is seen that as the ratio of the calculated shear strength to flexural shear strength demand increases, ductility of the column increases and drift capacity at shear failure and at axial failure increases.
- Even if a column is shear critical, it can preserve its axial load capacity up to appreciable drift levels especially under the low axial load levels. Analyses revealed that a shear critical column having V_n/V_{flex} around unity preserves its lateral and axial load capacity over a drift ratio of 0.01. Strengthening of those members against shear failure may not be vital, if the drift ratio is kept under 0.01.
- Failure mode classification including all failure modes such as shear, flexure-shear and flexure, is important to determine the performance level of a column. All failure modes have some ductility and drift capacity characteristics up to collapse.

- Considering the results of analysis performed on database given in the study, it is concluded that determination of failure mode according to the procedures of TEC2007 [1] is misleading and over conservative for columns having shear strength close to shear force that causes hinging of the section and closely spaced transverse reinforcement. That inaccuracy may cause underestimation of behavior of such columns leading to uneconomical retrofit solutions.
- Performance limits stated in nonlinear procedure of TEC2007 [1] are based on strain limits of materials which yields little deformability between the life safety performance level and collapse prevention performance level. This is because strain limits are a function of transverse reinforcement ratio (ρ_v), which in turn is very small for deficient columns.
- A plastic deformation capacity permitted to shear critical columns especially with low axial load levels in modeling will lead to more realistic and economical retrofit solutions.

4.3. Recommendations

Following recommendations are suggested based on findings of the study;

- Failure mode classification can be revised in nonlinear and linear procedures of TEC2007 [1] so that failure mode and deformability of a column is captured correctly and performance is determined realistically.
- Acceptance criteria can be revised so that new provisions are included for flexure-shear critical columns.
- Determination of performance level can be based on an acceptance criterion that is founded on plastic deformation capacities not on strain limits of materials.
- Acceptance criteria of reinforced concrete columns in nonlinear procedures can be revised so that affects of axial load level, shear demand and transverse reinforcement ratio together with the confinement properties can be reflected.
- Limited plastic deformation capacity can be allowed to shear failure expected members with low axial loads, in modeling the load deformation of such members, to account for the ability of carrying axial load beyond loss of lateral load capacity.
- Some full scale or model tests can be performed to have more data on behavior of flexure-shear critical members with details encountered in Turkey particularly for those having V_n/V_{flex} values around unity.

REFERENCES

1.Turkish Earthquake Code (2007). Ministry of Public Works and Settlement, Government of Republic of Turkey.

2. Kong, F. K. (2003). Reinforced Concrete Deep Beams. London: Blackie.

3. JSCE Concrete Committee (2002). *Guidelines of Seismic Assessment of Reinforced Concrete Structures as a Part of Standard Specification*. Marusen Publishing Co. Ltd.

4. Eberdhard, M. (2003). Structural performance database. Pacific Earthquake Engineering Research Center, University of Washington.

5. Wight, J. K., and Sozen, M. A. (1975). Strength decay of RC columns under shear reversals. *Journal of Structural Division*, 101(5), 1053-1065.

6. Saatcioglu, M., and Ozcebe, G. (1989). Response of reinforced concrete columns to simulated seismic loading. *ACI Structural Journal*, 86(1), 3-12.

7. Lynn, A. C., Moehle, J. P., Mahin, S. A, and Holmes, W. T. (1996). Seismic evaluation of existing reinforced concrete building columns. *Earthquake Spectra*, 124(4), 715–739.

8. Sezen, H. (2002). Seismic behavior and modeling of the reinforced concrete building columns. Ph.D. dissertation, University of California at Berkeley, Berkeley, California.

9. Elwood, J.K (2003). Shake table tests and analytical studies on the gravity collapse of reinforced concrete frames. Ph.D. dissertation, University of California at Berkeley, Berkeley, California.

10. Pincheira, J.A., Dotiwalla, f. S., and D'Souza, J. T. (1999) Seismic analysis of older reinforced columns. *Earthquake Spectra*, 15(2), 245-272.

11. Vecchio, F. J., and Collins, M. P. (1986). The modified compression field theory for reinforced concrete elements subjected to shear. *ACI Journal Proceedings*, 83(2), 219-231.

12. Pujol, S, Ramirez, J. A., and Sozen, M. A. (1999). Drift capacity of reinforced concrete columns subjected to cyclic shear reversals. *ACI* , Special Publication 187, 1999, 255-274.

13. Takeda, T., Sozen, M. A., and Nielsen, N. N. (1970). Reinforced concrete response to simulated earthquakes. *ASCE Journal of Structural Engineering*, 96(12), 2557-2573.

14. Saatcioglu, M., Alsiwat, J. M., and Ozcebe, G. (1992). Hysteretic behavior of anchorage slip in R/C members. *Journal of Structural Engineering*, 118(9), 2439-2458.

15. Saatcioglu, M., and Ozcebe, G. (1989). Hysteretic shear model for reinforced concrete members. *Journal of Structural Engineering*, 115(1), 132-148.

16. Sezen, H., Chowdhury, T. (2009). Hysteretic model for RC columns including effect of shear and axial failure. *Journal of Structural Engineering*, 135 (2), 139-146.

17. Petrangeli, M., Pinto, P. E., and Ciampi, V. (1999). Fiber element for cyclic bending and shear of RC structures. I: Theory. *Journal of Engineering Mechanics*, 125(9), 994-1001.

18. Sarıtaş, A. (2006). Mixed formulation frame element for shear critical steel and reinforced concrete members. Ph.D. dissertation, University of California at Berkeley, Berkeley, California.

19. Lee, D. H., and Elnashai, A. S. (2001). Seismic analysis of rc bridge columns with flexure-shear interaction. *Journal of Structural Engineering*, 127(5), 546-553.

20. Mostafaei, H., and Kabeyesawa, T. (2007). Axial-shear-flexure interaction approach for reinforced concrete columns. *ACI Structural Journal*, 104(2), 218-226.

21. Mostafaei, H., and Vecchio, F.J. (2008). Uniaxial shear-flexure model for reinforced concrete elements. *Journal of Structural Engineering*, 134(9), 1538-1547.

22. ASCE/SEI41 (2007). *Seismic rehabilitation of existing buildings*. American Society of Civil Engineers, Reston, Virginia.

23. FEMA356 (2000). *Prestandard and commentary for the seismic rehabilitation of buildings*. American Society of Civil Engineers for the Federal Emergency Management Agency, Washington D.C.

24. EERI/PEER (2006). *New information on the seismic performance of existing concrete buildings*. Seminar notes, Earthquake Engineering Research Institute, Oakland, California.

25. Eurocode 8, Part-3 (2005). *Assessment and retrofitting of buildings*. European Committee for standardization.

26. Dhakal, R. P., and Maekawa, K. (2002). Path-dependent cyclic stress-strain relationship of reinforcing bars including buckling. *Engineering Structures*, 24, 1383-1396.

27. Dhakal, R. P., and Maekawa, K. (2002). Reinforcement stability and fracture of cover concrete in reinforced concrete members. *Journal of Structural Engineering*, 128(10), 1253-1262.

28. Wang, T., and Hsu, T. T. C. (2001). Nonlinear finite element analysis of concrete structures using new constitutive models. *Computers and Structures*, 79, 2781-2791

29. Hsu, T.T.C. (1988). Softening truss model theory for shear and torsion. *Structural Journal of ACI*, 85(6), 624-635.

30. Vecchio, F. J. (1989). Nonlinear finite element analysis of reinforced concrete membranes. *ACI structural Journal*, 26-35.

31. TS500 (2000). *Requirements for Design and Construction of Reinforced Concrete Structures*.Turkish Standards Institute.

32. Setzler E. J., and Sezen, H. (2008). Model for the Lateral behavior of Reinforced Concrete Columns Including Shear Deformations. *Earthquake Spectra*, 24(2), 493-511

33. Eurocode 2, Part-1 (2004). Design of Concrete Structures. European Committee for standardization

34. Park, R., Priestly , M. J. N., and Gill, W. D. (1982) Ductility of square confined concrete columns. *Journal of Structural Division, ASCE*, 108(4), 929-950.

35. Okamura, H., and Maekawa, K. (2001). *Nonlinear Analysis and Constitutive Models of Reinforced Concrete Columns*. Gihodo Shuppan Co., Ltd.,182 pp.

APPENDIX A

MODIFIED COMPRESSION FIELD THEORY (MCFT)

MCFT is developed to predict the load deformation response of the reinforced concrete elements subjected to in-plane shear and normal stresses. In MCFT model, cracked concrete is considered as a new material with its own stress-strain characteristics. Equilibrium, compatibility and stress-strain relationships are formulated in terms of average stresses and average strains. Local stress conditions are also considered in the model. Here, assumptions behind the theory and the constitutive models will be briefly mentioned only. Extensive information can be reached from the MCFT paper written by Vecchio. [11]

A.1. Definition of the Model

A membrane element with its in-plane stresses and strains is shown in Figure A.1. It represents a portion of the reinforced concrete structure. In this study, this membrane element represents the axial-shear element, which is defined from the inflection point to the end of the column.

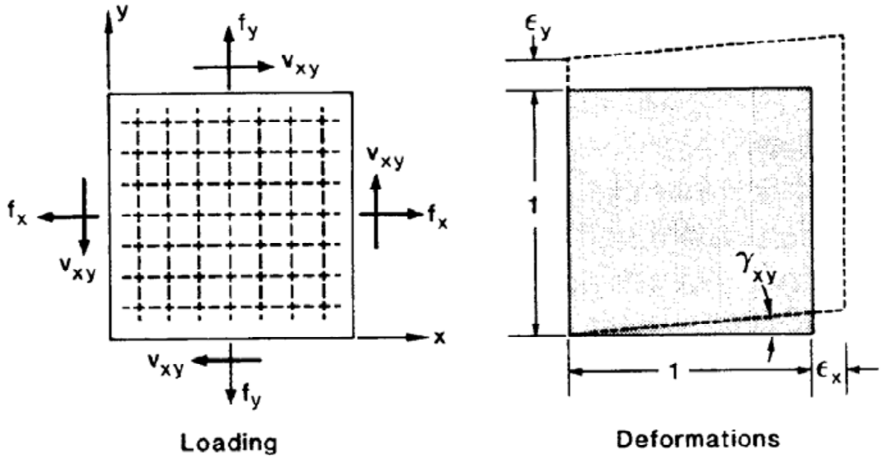

Figure A.1 Membrane Element [11]

Membrane element in Figure A.1 contains an orthogonal grid of reinforcement with the longitudinal (x) and transverse (y) axes are chosen to coincide with the reinforcement directions. Loads acting on the element's edge planes are assumed to consist of the uniform axial stresses f_x and f_y and the uniform shear stress v_{xy}. Element deforms in a way that the edges remain straight and parallel. The deformed shape is defined by the two normal strains ε_x and ε_y and the shear strain γ_{xy}. First step is to find relation between strains and stresses developed in element. In order to solve that step following assumptions are made:

- For each strain state there exists only one corresponding stress state.
- Stresses and strains can be considered in terms of average values when taken over areas large enough to include several cracks.
- The concrete and the reinforcing bars are perfectly bonded at the boundaries of element.
- The longitudinal and transverse reinforcement are distributed uniformly over the element.

Tensile stresses and strains are treated as positive quantities while compressive stresses and strains are taken as negative. Strains and stresses are converted to principal stresses and principal strains using principals of Mohr's circle.

A.1.1. Formulations of MCFT used in Axial-Shear Model

Principal compressive stress in concrete f_{c2} is affected by presence of principal tensile strains. Therefore, softening of compressive stress occurs due to co-existing principal tensile strains. A softening factor is applied to the calculated principal compressive stress. In the study to include positive effect of the confinement on concrete compressive strength Modified Kent and Park Model [34] is utilized to model the concrete in compression.

$$f_{c2} = \beta f_c^{'} \tag{A.1}$$

In Eq. (A.1), β is the compressive strength-softening factor calculated using Eq. (A.2).

$$\beta = \frac{1}{0.8 - 0.34\,\varepsilon_1 / \varepsilon_c^{'}} \leq 1.0 \tag{A.2}$$

In Eq. (A.2) $\varepsilon_c^{'}$ is a negative quantity taken as -0.002. Eq. (A.2) reveals that as the principal tensile strain in element increases softening factor increases therefore compressive strength decreases.

For concrete in tension, following relationships are utilized to relate the average principal stress to average principal strain.

Prior to cracking of concrete,

$$f_{c1} = E_c \varepsilon_1 \qquad \text{for} \qquad \varepsilon_1 \le \varepsilon_{cr} \tag{A.3}$$

Where E_c is the modulus of elasticity of the concrete, which is taken as $2\frac{f_c^{'}}{\varepsilon_c^{'}}$.

After cracking,

$$f_{c1} = \frac{f_{cr}}{1+\sqrt{500\varepsilon_1}} \qquad \text{for} \qquad \varepsilon_1 > \varepsilon_{cr} \tag{A.4}$$

Stress strain relationship of reinforcement steel is taken as linearly elastic perfectly plastic and stress in reinforcement is related to strains with the following equations.

$$f_{sx} = E_s \varepsilon_x \le f_{yx} \tag{A.5}$$

$$f_{yx} = E_s \varepsilon_y \le f_{yy} \tag{A.6}$$

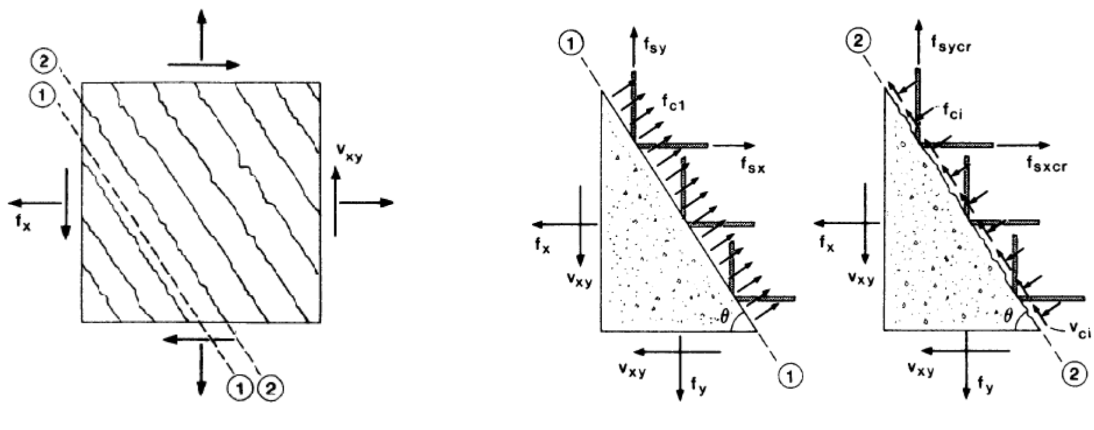

(a) (b) (c)

Figure A.2 Comparison of Local Stresses at a Crack with calculated Average Stresses a) Stresses Applied to cracked Element b) Calculated Average Stresses c) Local Stresses at a Crack [11]

In addition to above, equations used to estimate the shear stress that can be transferred across the crack by the aggregate interlock mechanism. Stresses on a cracked and uncracked section are displayed in Figure A.2.

Figure A.3 presents aggregate interlock mechanism. Crack check equations are presented below;

$$\rho_{sy}\left(f_{sycr}-f_{sy}\right)=f_{c1}+f_{ci}+v_{ci}/\tan\theta \tag{A.7}$$

$$\rho_{sx}\left(f_{sxcr}-f_{sx}\right)=f_{c1}+f_{ci}+v_{ci}/\tan\theta \tag{A.8}$$

Equilibrium of Eq. (A.7) and Eq. (A.8) can be satisfied only if no shear stress exists on the crack and no compressive stress on the crack so that Eq. (A.9) is obtained.

$$\rho_{sx}\left(f_{sxcr}-f_{sx}\right)=\rho_{sy}\left(f_{sycr}-f_{sy}\right)=f_{c1} \tag{A.9}$$

However, stress in the reinforcement at a crack cannot be greater than the yield strength of the reinforcement, that is

$$f_{sxcr}\le f_{yx} \tag{A.10}$$

$$f_{sycr}\le f_{yy} \tag{A.11}$$

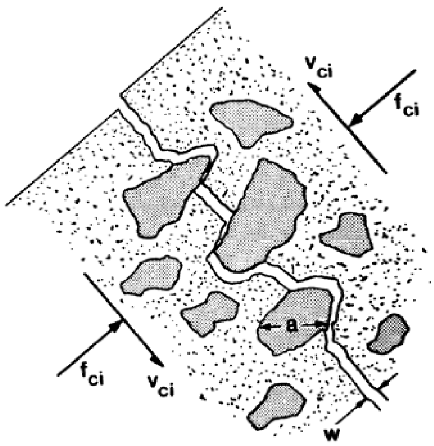

Figure A.3 Transmitting Shear Stress Across a Crack by Aggregate Interlock [11]

If the calculated average stress in either reinforcement is high, it may not be possible to satisfy Eq. (A.9) and equilibrium will require shear stress on crack. Limiting value of the shear stress v_{ci} on the crack is calculated using Eq. (A.12).

$$v_{ci\max}=\frac{0.18\sqrt{f_c'}}{0.3+\dfrac{24w}{a+16}} \quad \text{units(N.mm)} \tag{A.12}$$

In Eq. (A.12), a is the maximum aggregate size and w is the average crack width over the crack surface and calculated using Eq. (A.13).

$$w = \varepsilon_1 \cdot s_\theta \tag{A.13}$$

Crack spacing s_θ in Eq. (A.13) is calculated by using Eq. (A.14)

$$s_\theta = \frac{1}{\dfrac{\sin\theta}{s_{mx}} + \dfrac{\cos\theta}{s_{my}}} \tag{A.14}$$

In Eq. (A.14) s_{mx} and s_{my} are crack spacing in x direction and y direction respectively. Crack spacing is the indicators of the crack control characteristics of the x and y reinforcement respectively.

Crack check is performed to assure that principal tensile stress in concrete does not exceed the tension capacity of the crack in order to satisfy equilibrium equations.

APPENDIX B

THEORY OF THE AXIAL-SHEAR-FLEXURE INTERACTION METHODOLOGY

B.1.1. Compatibility Relationships

Regarding compatibility relationships, total drift ratio of a column between two sections is equal to the summation of shear strain γ_s, flexural drift ratio γ_f, and drift ratio γ_{pul} due to the pullout deformations resulting from anchorage slip. Furthermore, the total axial strain of a column is obtained by the summation of axial strains due to axial ε_{xa}, shear ε_{xs}, and flexural ε_{xf} mechanisms.

$$\gamma = \gamma_s + \gamma_f + \gamma_{pul} \, ; \varepsilon_x = \varepsilon_{xs} + \varepsilon_{xf} + \varepsilon_{xa} \tag{B.1}$$

The axial-flexure model yields axial strain caused by axial and flexure mechanisms, $\varepsilon_{xaf} + \varepsilon_{xf}$, which is the centroidal strain of the end section. On the other hand, axial strain $\varepsilon_{xas} + \varepsilon_{xs}$ due to axial and shear mechanism, is obtained from axial-shear model. To obtain the ε_x in Eq. (B.1), ε_{xf} is extracted from the section analyses and added to the axial deformation of the axial-shear model.

Axial strain due to flexure ε_{xf} is determined based on relative centroidal deformation between the two sections considering linear strain relationship by Eq. (B.2).

$$\varepsilon_{xf} = \int_0^{l_{12}} \left(\varepsilon_{01} - \varepsilon_{02}\right) \frac{x}{l_{12}} dx = 0.5\left(\varepsilon_{01} - \varepsilon_{02}\right) \tag{B.2}$$

Where $\varepsilon_{01}$and ε_{02} are centroidal strains of the two consecutive flexural sections and l_{12} is the distance between the two sections. In ASFI method two sections stand for end section and section at the inflection point of the column. Before yielding of reinforcement, Eq. (B.2) gives realistic estimations, because linear distribution assumption holds. After yielding of the tensile reinforcement, Eq. (B.2) gives an average axial strain in the plastic zone of the column considering a linear axial strain distribution in the plastic zone. This is the expected axial deformation to be considered in axial-shear model. Therefore, axial-shear model is evaluating the shear behavior of the plastic zone. As a result, Eq.(B.2) becomes;

$$\varepsilon_{xf} = 0.5\left(\varepsilon_0 - \varepsilon_{xa}\right) \tag{B.3}$$

Where ε_0 is the centroidal strain of the end section and, ε_{xa} equals to axial strain due to the axial mechanism. Compatibility of axial deformation is satisfied when axial strains of axial-shear, axial-flexure and applied axial load are the same.

$$\varepsilon_{xas} = \varepsilon_{xaf} = \varepsilon_{xa} \tag{B.4}$$

In order to calculate ε_{xa}, Eq. (B.5) is used considering a section at the inflection point where the bending moment is zero.

$$\varepsilon_{xa} = \frac{P}{\sum E_i A_i} \tag{B.5}$$

Where E_i equals the secant modulus of fiber i, steel or concrete, in the fiber model; A_i equals to cross section area of fiber i; and P equals the applied axial load. To satisfy the compatibility defined by Eq. (B.4) same constitutive models for steel and concrete shall be utilized in axial-shear, axial-flexure and in Eq. (B.5).

B.1.2. Equilibrium Relationships

Equilibrium conditions in ASFI method are satisfied in average stress-strain field. The shear stress τ_f and the axial stress σ_0 of the axial-flexure model are determined by converting moment and axial load into stresses. Shear stress of the axial-flexure is determined by Eq. (B.6)

$$\tau_f = \frac{1}{Bd_f}\frac{(M_1 M_2)}{l_{12}} \tag{B.6}$$

Where M_1 and M_2 are the moments at the sections 1 and 2 respectively. B equals the width of the section, and d_f equals the flexural depth of the section. Until the section cracks due to flexure d_f is taken equal to section depth H and after the cracking occurred, d_f is taken as effective depth d defined as distance from extreme concrete fiber to centre of tensile bar.

Shear stress of the axial-shear model is defined by Eq. (B.7)

$$\tau_s = \frac{V}{Bd_s} \tag{B.7}$$

Where V is the applied lateral load, B is the width of the section, and d_s is the shear depth of the section. In the model, d_s is taken equal to H until the tensile cracking occurs, after that it is taken equal to the effective depth d of the section. Equilibrium of shear stress is satisfied under the condition of having same shear stress in both axial-shear and axial-flexure models.

$$\tau_s = \tau_f \tag{B.8}$$

Axial stress for both models is determined from Eq. (B.9).

$$\sigma_0 = \frac{P}{\sum A_i} \text{ or } \sigma_0 = \frac{P}{BH} \tag{B.9}$$

Where P equals the applied axial load and A_i equals the cross-section area of the fiber i, H equals the depth of the section and B equals the width of the section. Normal stresses in directions perpendicular to column axis, or clamping stresses σ_y and σ_z are neglected because there is no lateral force in those directions along the column.

$$\sigma_y = \sigma_z = 0 \tag{B.10}$$

B.1.3. Constitutive Models

The secant stiffness method was applied to both concrete and reinforcement elements in ASFI approach as it was used in modified compression field theory by Vecchio [30]. Secant stiffness method was applied due to simplicity of the method used in practice and its applicability for the shear model. Modified Kent and Park model [34] was utilized to model stress-strain relationship of the confined and unconfined concrete. Linearly elastic-perfectly plastic stress-strain model is used for reinforcement steel. Tension stiffening effect, compression softening and tensile strength of concrete were taken into account to model. Constitutive laws that were employed to model concrete are displayed in Figure B.1. Same constitutive models were utilized for axial-shear and axial flexure models.

In Figure B.1, f_{cc} is compressive strength of confined concrete; f_c is the compressive strength of the unconfined concrete, ε_{cc} is the strain at the peak compressive stress of unconfined concrete, ε_{coc} is the strain at the peak compressive stress of confined concrete, ε_{cu} is the crushing strain of the unconfined concrete, ε_{20c} is the strain at the point where concrete stress drops to the 20 % of its peak stress, $f_t^{'}$ is the tensile strength of the concrete and $\varepsilon_t^{'}$ is the corresponding tensile strain, f_{c1} is the principal tensile stress in concrete and ε_1 is the corresponding tensile strain, and E_c is the elasticity modulus of concrete.

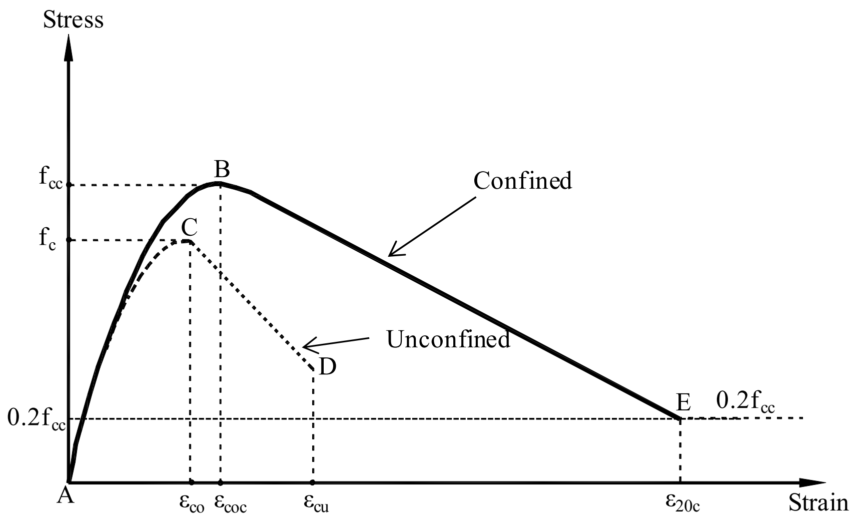

(a)

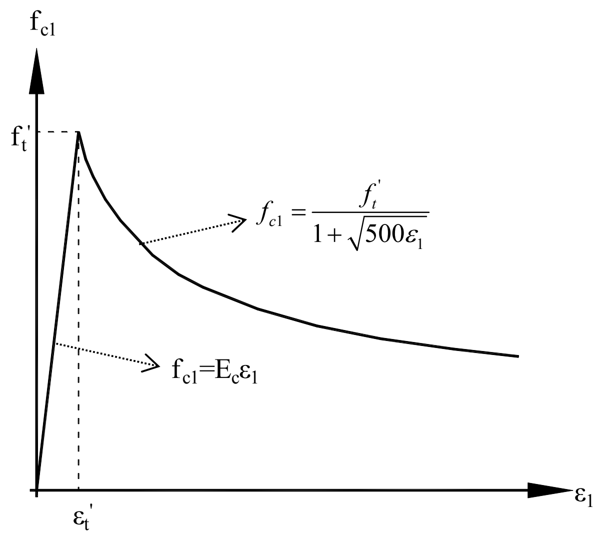

(b)

Figure B.1 Constitutive Models used to Model Concrete a) In Compression b) In tension

In Figure B.1.a concrete stresses are calculated as follows:

For confined concrete;

Between A-B:

$$\sigma_{cc} = Kf_c\left[\frac{2\varepsilon_c}{\varepsilon_{coc}} - \left(\frac{\varepsilon_c}{\varepsilon_{coc}}\right)^2\right] \tag{B.11}$$

$$\varepsilon_{coc} = K\varepsilon_{co} \quad ; \quad \varepsilon_{co} = 0.002 \tag{B.12}$$

$$K = 1.0 + \frac{\rho_s f_{ywk}}{f_c} \qquad \textbf{(B.13)}$$

Between B-E;

$$\sigma_{cc} = K f_c \left[1 - Z(\varepsilon_c - \varepsilon_{coc})\right] \qquad \textbf{(B.14)}$$

$$Z = \frac{0.5}{\frac{3 + 0.0285 f_c}{14.2 f_c - 1000} + 0.75 \rho_s \left(\frac{b_k}{s}\right)^{0.5} - \varepsilon_{coc}} \qquad (\mathrm{f_c}\ \text{in kg/cm}^2) \qquad \textbf{(B.15)}$$

For unconfined concrete;

Between A-C;

$$\sigma_c = f_c \left[\frac{2\varepsilon_c}{\varepsilon_{co}} - \left(\frac{\varepsilon_c}{\varepsilon_{co}}\right)^2\right] \qquad \textbf{(B.16)}$$

Between C-D;

$$\sigma_c = f_c \left[1 - Z(\varepsilon_c - \varepsilon_{co})\right] \qquad \textbf{(B.17)}$$

$$Z = \frac{0.5}{\frac{3 + 0.0285 f_c}{14.2 f_c - 1000} - \varepsilon_{co}} \qquad (\mathrm{f_c}\ \text{in kg/cm}^2) \qquad \textbf{(B.18)}$$

In equations from B.11 through B.18 abbreviations are,

σ_{cc}: compressive stress of confined concrete

σ_c: compressive stress of unconfined concrete

ε_c: compressive strain in concrete

K: confinement factor

ρ_s: volumetric ratio of transverse reinforcement

f_{ywk}: yield strength of the transverse reinforcement

s: spacing of the transverse reinforcement

B.1.4. Anchorage Slip Effect

Column tests showed that deformations due to the anchorage slip of reinforcing bars in foundation column interface, played important role in determination of total lateral displacement and should be considered in analysis. Anchorage slip deformations were stated as pull out deformation by ASFI approach. Due to the pull out effect, two deformation components occur. One is rotation of the section at the end and the other one is axial straining. Pullout model in ASFI approach was adopted from the model proposed by Okamura and Maekawa [35]. Lateral drift due to pullout of reinforcing bars was calculated by multiplication of the end rotation due to pullout with the column length. End rotation due to anchorage slip or pullout was determined by dividing the slip deformation of the tensile bar by distance from neutral axis to the tensile reinforcement. The pullout model and deformation components were shown in Figure B.2. In Figure B.2, S_y is the slip corresponding to yielding in tensile reinforcement; ε_{sy} is yield strain of longitudinal reinforcement, ε_{st} is the tensile strain in longitudinal reinforcement, ε_{sh} is the strain at the start of strain hardening in longitudinal steel, f_{ux} is the ultimate tensile strength of longitudinal steel, f_{yx} is the yield strength of the longitudinal reinforcement, ε_{pul} is the axial strain due to the slip in tensile reinforcement, e is the distance from neutral axis to centre of the section, γ_{pul} is the rotation of the section due to the pullout deformations.

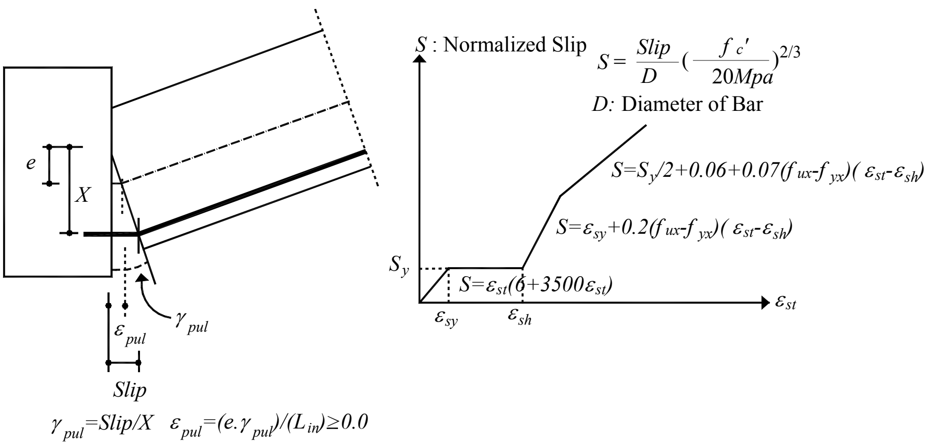

Figure B.2 Pullout model and Deformation Components [20]

B.1.5. Axial Deformation Interaction Procedure

Axial deformation due to flexure obtained from axial–flexure model by Eq. (B.2) or (B.3) is taken into account axial-shear model. This procedure is fulfilled based on flexibility relationship. Flexibility term for axial deformation of axial-flexure model is added to the flexibility term of axial deformation obtained in axial-shear model. Flexibility component for the axial deformation of the axial-flexure model is obtained by Eq. (B.19).

$$f_{xf} = \frac{\varepsilon_{xf}}{\sigma_0} \tag{B.19}$$

Where σ_0 is the applied axial stress obtained by Eq. (B.9). In case of beams in which axial load may be zero, a small value is assigned to the σ_0 in order not to cause numerical errors. The stress strain relationship in terms of flexibility terms is considered for axial shear model as;

$$\begin{pmatrix} f_{11} & f_{12} & f_{13} \\ f_{21} & f_{22} & f_{23} \\ f_{31} & f_{32} & f_{33} \end{pmatrix} \begin{pmatrix} \sigma_x \\ \sigma_y \\ \tau_s \end{pmatrix} = \begin{pmatrix} \varepsilon_x \\ \varepsilon_y \\ \gamma_s \end{pmatrix} \tag{B.20}$$

Where, f_{ij} $(i\ j = 1,2,3)$ equals the flexibility components of the axial-shear model; ε_x, ε_y, γ_s are average strains; and σ_x, σ_y, τ_s are average stresses. Axial strain flexibility term of axial-flexure model obtained from Eq. (B.19) is added to the axial deformation flexibility term of axial-shear model, which is f_{11} in Eq. (B.20). Here, x-axis is assumed to be the main axis of the column, so that, σ_x is the applied axial stress. Stress in y- direction is considered zero, $\sigma_y = 0$, because of having no applied load along the column. Hence;

$$\begin{pmatrix} f_{11} + f_{xf} & f_{12} & f_{13} \\ f_{21} & f_{22} & f_{23} \\ f_{31} & f_{32} & f_{33} \end{pmatrix} \begin{pmatrix} \sigma_0 \\ 0 \\ \tau_s \end{pmatrix} = \begin{pmatrix} \varepsilon_x = (\varepsilon_{xs} + \varepsilon_{xa}) + \varepsilon_{xf} \\ \varepsilon_y \\ \gamma_s \end{pmatrix} \tag{B.21}$$

Where $(\varepsilon_{xs} + \varepsilon_{xa})$ is the axial strain of the axial shear model, considering the compatibility, $\varepsilon_{xas} = \varepsilon_{xa}$.

Flexibility matrix in Eq. (B.21) is obtained by secant stiffness procedure as follows;

Let D_c be the stiffness matrix of the concrete element, D_s be the stiffness matrix of the steel elements. D_c is calculated as in Eq. (B.22).

$$D_c = \begin{pmatrix} E_{c1} & 0 & 0 \\ 0 & E_{c2} & 0 \\ 0 & 0 & G_c \end{pmatrix} \quad \textbf{(B.22)}$$

In Eq. (B.22), $E_{c1}=f_1/\varepsilon_1$, $E_{c2}=f_2/\varepsilon_2$ (f_1 and f_2 are principal tensile stress and principal compressive stresses, respectively and ε_1 and ε_2 are the principal tensile strain and principal compressive strain respectively.) and $G_c= E_{c1}E_{c2}/(E_{c1}+ E_{c2})$. D_s is calculated as in Eq. (B.23).

$$D_s = \begin{pmatrix} E_{sx} & 0 & 0 \\ 0 & E_{sy} & 0 \\ 0 & 0 & 0 \end{pmatrix} \quad \textbf{(B.23)}$$

Where $E_{sx}=\rho_x E_x$ and $E_{sy}=\rho_y E_y$. (ρ_x and ρ_y are reinforcement ratios in x and y directions respectively. E_x and E_y is secant stiffness of reinforcement in x and y directions respectively.). Since concrete stiffness matrix is calculated for principal directions, it is transformed to global x and y axes by transformation matrix T that is obtained by Eq. (B.24).

$$T = \begin{pmatrix} \cos(\varphi)^2 & \sin(\varphi)^2 & \cos(\varphi)\sin(\varphi) \\ \sin(\varphi)^2 & \cos(\varphi)^2 & \cos(\varphi)\sin(\varphi) \\ -2\cos(\varphi)\sin(\varphi) & 2\cos(\varphi)\sin(\varphi) & \cos(\varphi)^2 - \sin(\varphi)^2 \end{pmatrix} \text{ where } \varphi = \frac{\pi}{2} + \theta \quad \textbf{(B.24)}$$

Where, θ is the angle of principal axis measured from the x-axis in counter-clockwise direction.

Global stiffness matrix is obtained by Eq. (B.25).

$$K = [T]^T [D_c][T] + [D_s] \quad \textbf{(B.25)}$$

Global flexibility matrix in Eq. (B.20) is obtained by Eq. (B.26).

$$f = [K]^{-1} \quad \textbf{(B.26)}$$

B.1.6. Analysis Procedure of ASFI Method

ASFI method has two model components that are axial-flexure and axial-shear models. The structural input data related to material properties and geometry of a column is entered to the axial-flexure model. On the other hand, input data of the axial-shear model is formed by converted stresses and strains obtained from axial-flexure model components. The analytical process of the ASFI method is explained based on the displacement method for two-dimensional problems.

As mentioned before, axial-flexure model of ASFI method is based on section analysis. A fiber model was constructed for a two-dimensional reinforced concrete column section with two variables of section curvature Φ, and axial strain ε_0. In fiber model, column section was divided into two parts. First part is confined concrete core, and the other part is unconfined cover concrete. Each part divided into small fibers and corresponding strains, stresses, and secant stiffness values were computed. At the start point, an initial value was assigned to curvature. Strains and stresses were calculated by Eq. (B.27) and Eq. (B.28).

$$\varepsilon_i = \varepsilon_0 + \gamma_i \phi \tag{B.27}$$

$$\sigma_i = E_i \varepsilon_0 + E_i \gamma_i \phi \tag{B.28}$$

Where ε_i is the strain of the fiber i, y_i is the distance from the centre of the fiber i to centre of the cross section E_i is the secant elasticity modulus and σ_i is the stress in that fiber i. After that under the applied axial load, centroidal strain ε_0, and end moment m were obtained by solving 2x2 stiffness matrix given in Eq. (B.29).

$$\begin{pmatrix} M \\ P \end{pmatrix} = \begin{pmatrix} \sum E_i A_i y_i^2 & \sum E_i A_i y_i \\ \sum E_i A_i y_i & \sum E_i A_i \end{pmatrix} \begin{pmatrix} \phi \\ \varepsilon_0 \end{pmatrix} \tag{B.29}$$

Where A_i is the area of the fiber i, and y_i is the distance from the centroid. Then, axial deformation due to axial mechanism was determined by using Eq. (B.5). After that, axial deformation due to flexure ε_{xf} and shear stress τ_f were computed by employing Eq. (B.3) and Eq. (B.30) respectively, considering $M_1=m$, $M_2=0$, and $l_{12}=L_{in}$.

$$\tau_f = \frac{m}{B d_f l_{12}} \tag{B.30}$$

Where, L_{in} was the distance from the inflection point to the end section. Then, applied axial stress σ_0 and flexibility component of axial deformation was determined based on Eq. (B.9) and Eq. (B.19), respectively. Flexural stiffness and drift ratio can be obtained using curvature distribution along the column by Eq. (B.31).

$$K_f = \frac{\tau_f}{\gamma_f} \text{ where } \gamma_f = \frac{\delta}{L_{in}} = \frac{1}{L_{in}} \int_0^{l_{12}} x \phi dx \tag{B.31}$$

Where δ was drift and x was the distance variable from the inflection point, and Φ was the curvature function of x. The next step was to determine the pullout deformations by using equations given in Figure B.2, and pullout stiffness K_{pul} by solving Eq. (B.32).

$$K_{pul} = \frac{\tau_f}{\gamma_{pul}} \tag{B.32}$$

By applying MCFT flexibility matrix in Eq. (B.20) was obtained. Then the modified flexibility matrix was obtained from Eq. (B.21). After that, shear spring stiffness K_s was computed utilizing Eq. (B.33) where shear stress τ_s and shear drift $\gamma_s$were determined by solving Eq. (B.20).

$$K_s = \frac{\tau_s}{\gamma_s} \tag{B.33}$$

As a result, total stiffness K_γ corresponding to the total drift ratio γ was determined by Eq. (B.34).

$$\frac{1}{K\gamma} = \frac{1}{K_f} + \frac{1}{K_s} + \frac{1}{K_{pul}} \qquad \tau = K_\gamma \gamma \tag{B.34}$$

Where $\gamma = \gamma_f + \gamma_s + \gamma_p$.

In the ASFI method, inflection point was considered in the mid-height of the column. Therefore, L_{in} is taken as $L/2$ for the columns tested in double curvature and L for the columns tested in single curvature.

APPENDIX C

CONSTITUTIVE MODELS PROPOSED BY MAEKAWA FOR LONGITUDINAL BARS IN COMPRESSION

Stress-strain relationships of the compression bars were calculated using following equations. (Units are in N, mm.)

$$\sigma_{sc} = E_s \varepsilon_{sc} \text{ , for } \varepsilon_{sc} \le \varepsilon_y \tag{C.1}$$

$$\frac{\sigma_{sc}}{\sigma_t} = 1 - \left(1 - \frac{f_i}{f_{it}}\right)\left(\frac{\varepsilon_{sc} - \varepsilon_y}{\varepsilon_i - \varepsilon_y}\right) \text{, for } \varepsilon_y < \varepsilon_{sc} \le \varepsilon_i \tag{C.2}$$

$$\sigma_{sc} = f_i - 0.02E_s\left(\varepsilon_{sc} - \varepsilon_i\right);\ \sigma_{sc} \ge 0.2 f_y \text{, for } \varepsilon_{sc} > \varepsilon_i \tag{C.3}$$

Where σ_t and f_{it} were the stresses in tension envelope corresponding to the ε_{sc} (current strain) and ε_i (strain at the intermediate point), respectively, ε_y is the yield strain E_s is the modulus of elasticity, and f_y is the yield strength of the reinforcing steel. Intermediate strain ε_i was derived from Eq. (C.4).

$$\frac{\varepsilon_i}{\varepsilon_y} = 55 - 2.3\sqrt{\frac{f_y}{100}}\frac{L}{D} \text{, and } \frac{\varepsilon_i}{\varepsilon_y} \ge 7 \tag{C.4}$$

Where $\frac{L}{D}$ was slenderness of the compression bar. L was the length of the bar that was able to buckle. $\frac{f_i}{f_{it}}$ was obtained using Eq. (C.5).

$$\frac{f_i}{f_{it}} = \alpha\left(1.1 - 0.016\sqrt{\frac{f_y}{100}}\frac{L}{D}\right);\ \frac{f_i}{f_y} \ge 0.2 \tag{C.5}$$

Where α was a coefficient related to the nature of the strain hardening and taken as 0.75 for elastic-perfectly plastic bars. For other type of bars Eq. (C.6) was suggested by Maekawa [26] to compute α.

$$\alpha = 0.75 + \frac{\varepsilon_u - \varepsilon_{sh}}{300\varepsilon_y};\ \alpha \le \frac{f_u}{1.5 f_y};\ 0.75 \le \alpha \le 1.0 \tag{C.6}$$

Where ε_u is the ultimate strain, ε_{sh} is the strain at the onset of hardening, and f_u is the ultimate strength of the reinforcing bars.

Stress-strain relationship proposed by Maekawa is presented in Figure C.1.Stress-strain relationship for reinforcing bars used in the section analysis is presented in Figure C.2.

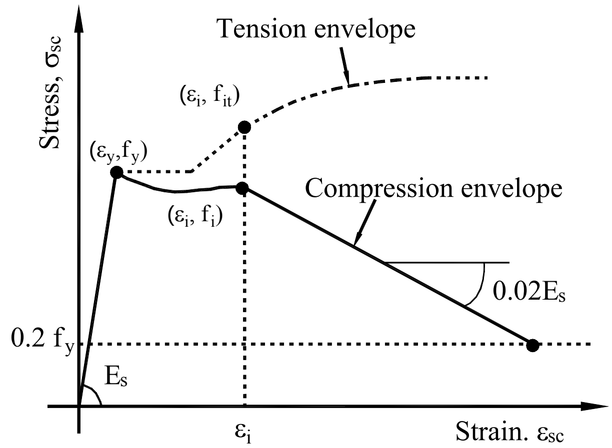

Figure C.1 Representation of Monotonic Compression Envelope for the Reinforcing Bars [26]

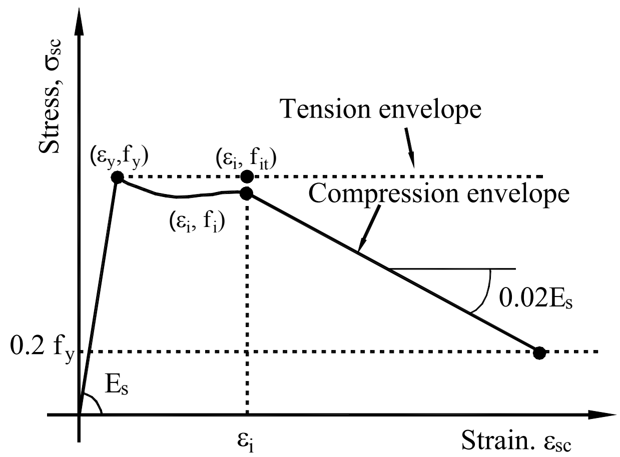

Figure C.2 Compression and Tension Envelope used in ASFI (M), ELWOOD and HSU(M) model for Reinforcing Bars [26]

APPENDIX D

CONSTITUTIVE MODELS PROPOSED BY THOMAS HSU

Model for the concrete in compression;

$$\sigma_2 = \zeta f_c' \left(2\left(\frac{\varepsilon_2}{\zeta\varepsilon_0} \right) - \left(\frac{\varepsilon_2}{\zeta\varepsilon_0} \right)^2 \right) \text{ for } \varepsilon_2/\zeta\varepsilon_0 \leq 1 \qquad \textbf{(D.1)}$$

$$\sigma_2 = \zeta f_c' \left(1 - \left(\frac{\varepsilon_2/\zeta\varepsilon_0 - 1}{4/\zeta - 1} \right)^2 \right) \text{for } \varepsilon_2/\zeta\varepsilon_0 > 1 \qquad \textbf{(D.2)}$$

Where f_c' is the cylinder compressive strength of concrete, ε_0 is the concrete strain at maximum compressive stress, and ζ is the softened coefficient. ε_0 was taken as 0.002 in equations (D.1) and (D.2).

Softened coefficient ζ in Eq. (D.1) and Eq. (D.2) is

$$\zeta = \frac{5.8}{\sqrt{f_c'}} \frac{1}{\sqrt{1 + \frac{400\varepsilon_1}{\eta'}}} \leq 0.9 \qquad \text{(MPa)} \qquad \textbf{(D.3)}$$

$$\eta = \frac{\rho_y f_{yy} - \sigma_y}{\rho_x f_{xx} - \sigma_x} \qquad \textbf{(D.4)}$$

where ρ_x, ρ_y are reinforcement ratios in x and y directions, respectively; f_{xx}, f_{yy}, yield stress of steel in the x and y directions, respectively; and σ_x, σ_y, applied stresses in the x and y directions, respectively. The symbol η' in Eq. (D.3) is expressed by η in Eq. (D.4) or its reciprocal, whichever is less than unity. The η' values are limited to a range of $0.2 \leq \eta' \leq 1.0$. in the descending portion of the concrete stress-strain curve (Eq. (D.2)) the lowest stress value was taken as $0.2\zeta f_c'$ to avoid the potential numerical errors in calculation. The softened compressive stress-strain curve of concrete proposed by Hsu is presented in Figure D.1.

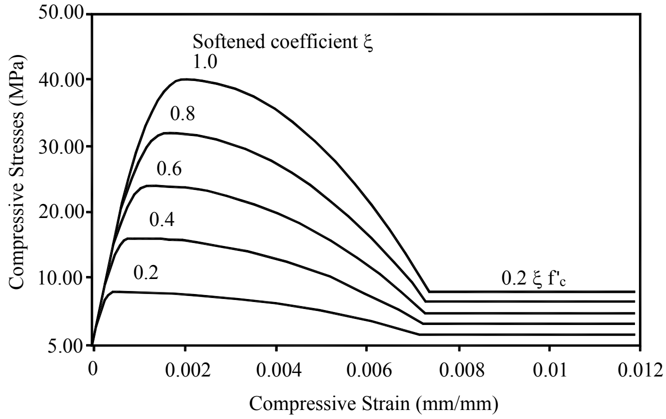

Figure D.1 Softened Compressive Stress-Strain Curve of Concrete For Concrete in Compression [28]

Model for the concrete in tension;

$$\sigma_1 = E_c \varepsilon_1 \text{ for } \varepsilon_1 \le \varepsilon_{cr} \tag{D.5}$$

$$\sigma_1 = f_{cr} \left(\frac{\varepsilon_{cr}}{\varepsilon_1} \right)^{0.4} \text{ for } \varepsilon_1 > \varepsilon_{cr} \tag{D.6}$$

Where E_c is modulus of elasticity of concrete; f_{cr} is cracking stress of concrete; and ε_1 is the cracking strain of concrete. Stress-strain curve of concrete in tension was presented in Figure D.2.

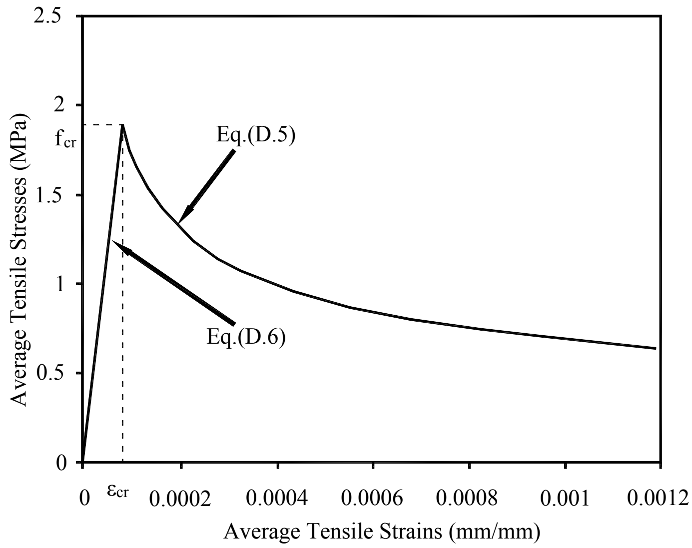

Figure D.2 Average Tensile Stress-Strain Curve of Concrete [28]

Average stress-strain relationship of steel embedded in concrete is represented by two straight line equations given in equation (D.7) and (D.8):

$$f_s = E_s \varepsilon_s \qquad \text{for} \quad \varepsilon_s \le \varepsilon_n \tag{D.7}$$

$$f_s = f_y \left[\left(0.91 - 2B\right) + \left(0.02 + 0.25B \frac{\varepsilon_s}{\varepsilon_y} \right) \right] \qquad \text{for} \quad \varepsilon_s > \varepsilon_n \tag{D.8}$$

Where f_s and ε_s are the average stress and strain of the steel bars, respectively; f_y and ε_y are the yield stress and strain of the bare steel bars, respectively; E_s is the modulus of elasticity of steel bars $\varepsilon_n = \varepsilon_y(0.93 - 2B)$. The parameter B is given by $B = \left(f_{cr}/f_y\right)^{1.5}/\rho$, where ρ is the reinforcement steel ratio and $\rho \ge 0.5\%$. f_{cr} is the cracking strain of the concrete given by $f_{cr} = 0.31\sqrt{f_c'}$ (MPa). Average stress-strain relationship of the reinforcement steel is shown in Figure D.3. It was intended by the use of average (or smeared) stress-strain relationships given in Eq. (2.13) and (2.14), in combination with the concrete average stress-strain relationship given in Eq. (2.9) to Eq. (2.12) that tension stiffening effect of steel bars by concrete was considered and the deformations of steel-concrete composites were evaluated correctly.

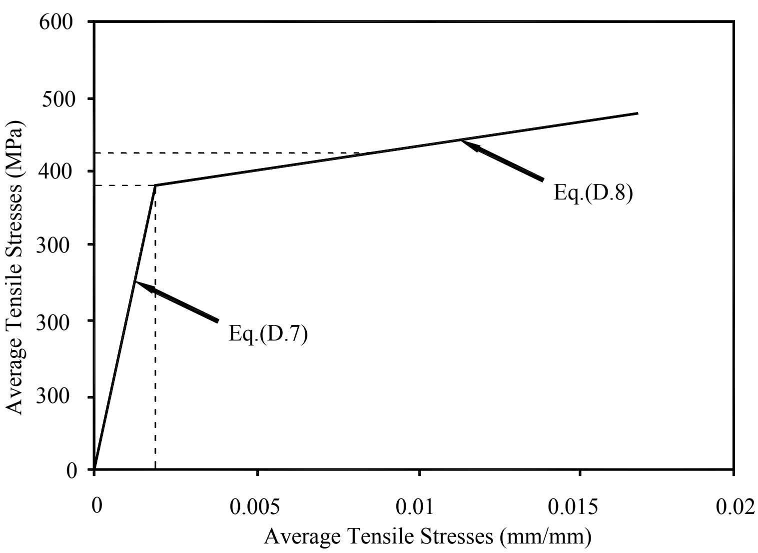

Figure D.3 Average Stress-Strain Curve of Steel Bars Embedded in Concrete [28]

APPENDIX E

ESTIMATION OF FAILURE MODE ACCORDING TO TEC2007 LINEAR PROCEDURE

For linear analysis, shear strength is calculated by formulation given in TS500 [31], which is defined below:

Shear strength of the member is calculated from the Eq. (E.1) presented in TS500 [31]. In shear strength calculation, material strengths are taken as in-situ measured values adjusted according to the building information levels.

$$V_r = V_c + V_w \tag{E.1}$$

$$V_c = 0.8 V_{cr} \tag{E.2}$$

$$V_c = 0.65 f_{ctk} b_w d \left(1 + \gamma \frac{N_d}{A_c} \right) \tag{E.3}$$

$$V_w = \frac{A_{sw}}{s} f_{ywk} d \tag{E.4}$$

Where, V_r is shear strength of the section, V_c is concrete contribution to the shear strength and calculated from Eq. (E.2) where, V_{cr} is diagonal cracking strength and calculated from Eq. (E.3), V_w is transverse reinforcement contribution to shear strength and calculated from Eq. (E.4). In Eq. (E.3), f_{ctk} is the tensile strength of the concrete and equal to $0.35\sqrt{f_{ck}}$ (Mpa), where, f_{ck} is the concrete compressive strength adjusted according to building information levels, b_w is the width of the section perpendicular to shear force, d is the effective depth of the section, γ is a factor reflecting effect of axial force on cracking strength and in case of axial compression it is taken as 0.07, in case of axial tension it is taken as -0.3, and if axial tensile stress is less than 0.5 Mpa it is taken equal to zero, N_d is applied axial load, and A_c is cross sectional area. In Eq. (E.4), A_{sw} is area of transverse reinforcement, f_{ywk} is the yield stress of transverse reinforcement adjusted according to building information level, s is spacing of transverse reinforcement, and d is effective depth of the section.

Shear demand on critical section is calculated according Eq. (E.5).

$$V_e = \frac{M_a + M_{ü}}{l_n} \quad \textbf{(E.5)}$$

Where, V_e is the shear force, M_a and $M_{ü}$ are moments at two ends of the column and l_n is the clear length of the column. M_a and $M_{ü}$ are calculated according to the expected plastic mechanism. If columns are stronger than beams, then total moment capacity at the end sections of beams at the joint are calculated from Eq. (E.6) and distributed to columns according to the stiffness of columns.

$$\sum M_p = M_{pi} + M_{pj} \quad \textbf{(E.6)}$$

Where, M_{pi} and M_{pj} can be calculated definitely or approximately as, $M_{pi} = 1.4M_{ri}$ and $M_{pj} = 1.4M_{rj}$, M_{ri} and M_{rj} are the ultimate moment capacities of beams at the ends and calculated using design strengths of the materials without consideration of strain hardening effect of reinforcement steel. In the study, a definite solution is also used to calculate moment capacities of the sections considering strain hardening affect and compression bar buckling. In addition, approximate solution was also applied to observe the difference between definite and approximate solution. On the other hand, if the columns at a joint are weaker than the beams at that joint, M_a and $M_{ü}$ will be calculated as column moment capacities at the considered critical section using definite and approximate solutions.

Therefore,

$M_a = M_{pa} = 1.4\ M_{ra}\ (or\ \ moment\ capacity\ calculated\ with\ definite\ solution)$

$M_{ü} = M_{pü} = 1.4\ M_{rü}\ (or\ \ moment\ capacity\ calculated\ with\ definite\ solution)$

In the calculation of M_{ra} and $M_{rü}$, strain hardening effect of reinforcement steel is neglected and design material strengths were utilized.

- If shear force that was calculated from combination of gravity loads and earthquake loading for which response modification factor is taken as unity (elastic earthquake loading) is smaller than calculated force V_e, it is taken as shear force instead of V_e.
- If there are short columns in the system, in the formulation of the Eq. (E.5), l_n is taken as column length as it is.
- Finally, obtained V_e and V_r are compared, If V_r is greater than V_e than member is taken as a “ductile member”, otherwise it is considered as “brittle member”.

APPENDIX F

CALCULATIONS ACCORDING TO THE NONLINEAR PROCEDURE DEFINED IN TEC2007

Deformations of the specimens were calculated for immediate occupancy (IO), life safety (LS) and collapse prevention (CP) performance levels for the ductile specimens and results are tabulated. Table F.1 summarizes the load deformation properties calculated according to the nonlinear procedure defined in TEC2007 for the ductile specimens. Table F.2 presents plastic curvature, plastic rotation and displacement limits for different performance levels for ductile members.

Notations:

N: Axial load (N)

$f_c^{'}$: Concrete compressive strength (Mpa)

A_g: Cross sectional area (mm^2)

EI_e: Effective Flexural Rigidity of the column section ($KN.m^2$)

V_e: Flexural shear strength demand (KN)

V_n: Shear strength (KN)

ρ_s: Volumetric ratio of transverse reinforcement

ρ_{sm}: Volumetric ratio of transverse reinforcement that shall be provided to section according to the TEC2007

Φ_y: Yield curvature (rad/mm)

Φ_u: Ultimate curvature limit for determined performance level (rad/mm)

ε_{cg}: Ultimate crushing strain of concrete for determined performance level

ε_s: Ultimate steel strain for reinforcement steel for determined performance level

θ_p: Plastic rotation limit for determined performance level (radians)

δ: Lateral displacement limit for determined performance level (mm)

L: Length of the column from the inflection point to the end (m)

Table F.1 Load-Deformation Properties for Ductile Specimens (TEC2007 Nonlinear procedure)

Specimen	$N/f_c'A_g$	$EI_e(KN.m^2)$	V_e	V_n	V_n/V_e	ρ_s	ρ_{sm}	$(\varepsilon_{cg})_{IO}$	$(\varepsilon_{cg})_{LS}$	$(\varepsilon_{cg})_{CP}$	$(\varepsilon_s)_{IO}$	$(\varepsilon_s)_{LS}$	$(\varepsilon_s)_{CP}$
2CLH18	0.07	47624	227.1	272.8	1.20	0.0016	0.0175	0.0035	0.0044	0.0053	0.01	0.04	0.06
2CMH18	0.28	73085	277.6	302.0	1.09	0.0016	0.0202	0.0035	0.0043	0.0051	0.01	0.04	0.06
3SMD12	0.28	73085	341.4	371.6	1.09	0.0057	0.0202	0.0035	0.0063	0.0080	0.01	0.04	0.06
NO:1	0.15	56881	262.0	308.4	1.18	0.0061	0.0237	0.0035	0.0061	0.0076	0.01	0.04	0.06
NO:2	0.61	84268	254.5	402.8	1.58	0.0062	0.0355	0.0035	0.0052	0.0064	0.01	0.04	0.06
NO:4	0.15	56302	264.1	311.3	1.18	0.0061	0.0245	0.0035	0.0060	0.0075	0.01	0.04	0.06
3CMD12	0.26	73545	353.0	381.6	1.08	0.0024	0.0219	0.0035	0.0046	0.0056	0.01	0.04	0.06
HPRC10-63	0.17	2173	90.0	119.9	1.33	0.0154	0.0083	0.0035	0.0135	0.0180	0.01	0.04	0.06
40.048(East)	0.15	5829	103.8	112.2	1.08	0.0112	0.0432	0.0035	0.0061	0.0076	0.01	0.04	0.06
223.09	0.90	1264	62.5	264.7	4.23	0.0345	0.0109	0.0035	0.0135	0.0180	0.01	0.04	0.06

Table F.2 Plastic Deformations and Displacement Limits for Different Performance Levels for Ductile Members (TEC2007 Nonlinear Procedure)

Specimen	Φy	$(\Phi u)_{IO}$	$\Phi u_{(LS)}$	$\Phi u_{(CP)}$	$\theta p_{(IO)}$	$\theta p_{(LS)}$	$\theta p_{(CP)}$	$\delta_{(IO)}$	$\delta_{(LS)}$	$\delta_{(CP)}$
2CLH18	6.23E-06	3.40E-05	5.30E-05	5.63E-05	7.59E-03	1.07E-02	1.14E-02	14.8	19.0	20.1
2CMH18	1.07E-05	1.79E-05	2.44E-05	2.73E-05	1.65E-03	3.13E-03	3.79E-03	10.0	12.0	12.9
3SMD12	1.10E-05	1.79E-05	3.55E-05	4.35E-05	1.58E-03	5.60E-03	7.43E-03	10.1	15.6	18.1
NO:1	1.15E-05	2.05E-05	4.56E-05	5.42E-05	2.06E-03	7.80E-03	9.76E-03	11.1	18.9	21.6
NO:2	1.05E-05	1.23E-05	2.16E-05	2.56E-05	4.11E-04	2.54E-03	3.45E-03	8.2	11.0	12.3
NO:4	1.12E-05	2.07E-05	4.60E-05	5.40E-05	2.18E-03	7.95E-03	9.79E-03	11.0	18.9	21.4
3CMD12	9.95E-06	1.85E-05	2.77E-05	3.30E-05	1.95E-03	4.06E-03	5.27E-03	9.9	12.7	14.4
HPRC10-63	2.05E-05	7.61E-05	3.08E-04	3.09E-04	5.56E-03	2.88E-02	2.89E-02	2.0	7.8	7.8
40.048(East)	1.38E-05	4.45E-05	1.09E-04	1.13E-04	4.68E-03	1.45E-02	1.51E-02	7.3	15.2	15.6
223.09	1.86E-05	2.96E-05	1.50E-04	1.95E-04	8.76E-04	1.05E-02	1.41E-02	0.9	3.6	4.6

For brittle members displacement at failure was calculated elastically. Lateral displacement at lateral load capacity (shear strength calculated according to the TS500) is calculated by Eq. (F.1).

$$\delta_{(CP)} = \frac{VL}{GA} + \frac{VL^3}{3EI_e} \quad \textbf{(F.1)}$$

Calculations are performed and results are summarized in Table F.3 for brittle members.

Table F.3 Load-Deformation Properties for Brittle Members

Specimen	$N/f_c'A_g$	**EIe(KN.m^2)**	**Ve**	V_n	V_n/V_e	$\delta_{(CP)}$
3CLH18	0.09	44941	298.7	248.9	0.83	6.0
3CMH18	0.26	73545	351.6	309.7	0.88	4.6
3SLH18	0.09	44941	298.7	248.9	0.83	6.0
CUW	0.16	7591	309.9	216.4	0.70	1.0
25.033	0.07	4721	105.0	95.2	0.91	4.6
40.033a(East)	0.12	5479	108.4	101.1	0.93	4.2